ARCHIVES OF ACOUSTICS
8, 1, 3-10 (1983)

TRANSMISSION AND REFLECTION OF A SURFACE WAVE AT A CORNER OF TWO PLANES ON AN ISOTROPIC BODY

W. PAJEWSKI, M. SZALEWSKI

Institute of Fundamental Technological Research, Polish Academy of Sciences
(00-049 Warsaw, ul.Świętokrzyska 21)

This paper reports on an experimental investigation of the diffraction of a Rayleigh wave at a corner of an isotropic solid bounded by two planes forming a dihedral angle with respect to each other.

Application of piezoelectric transducers and their appropriate setting on samples permitted the determination of the coefficient of reflection and transmission of Rayleigh waves at a corner and the directional characteristics of transverse waves, with polarisation in a plane perpendicular to the surface of R propagation, radiated at that time by the corner. The results were compared with the results of papers published in the world literature.

1. Introduction

The problem of reflection and transmission of Rayleigh waves at a corner of a dihedral angle is not easy to be solved theoretically even in the case of an isotropic body. Satisfaction of the complex boundary conditions requires the assumption of a reflected wave which passes onto the other plane and the conversion of part of the energy of a surface wave into that of a bulk wave propagating into the material. Several theoretical and experimental papers [1-4] were devoted to this problem.

In paper [4] HUDSON and KNOPOFF presented a theory of the transmission of a Rayleigh wave from one plane of the dihedral angle θ onto the other in the case of an isotropic body, making a number of simplifying assumptions. As a result of this theory they obtained relations permitting calculation of the coefficients of reflection and transmission of a surface wave as a function of the angle θ and the Poisson ratio σ (Fig. 1). They attempted to confirm the theoretical results experimentally [5]; the values of the coefficients differed greatly from those calculated theoretically. Their investigations were not precise

enough, in view, it seems, of the shape of samples and the manner of generating and detecting surface waves. In paper [1] the authors took into account in acoustooptical measurements only surface waves, while bulk waves were accounted for as a complementation of energy balance. These methods did permit more detailed examination of the phenomenon of the transformation of surface waves into bulk ones.

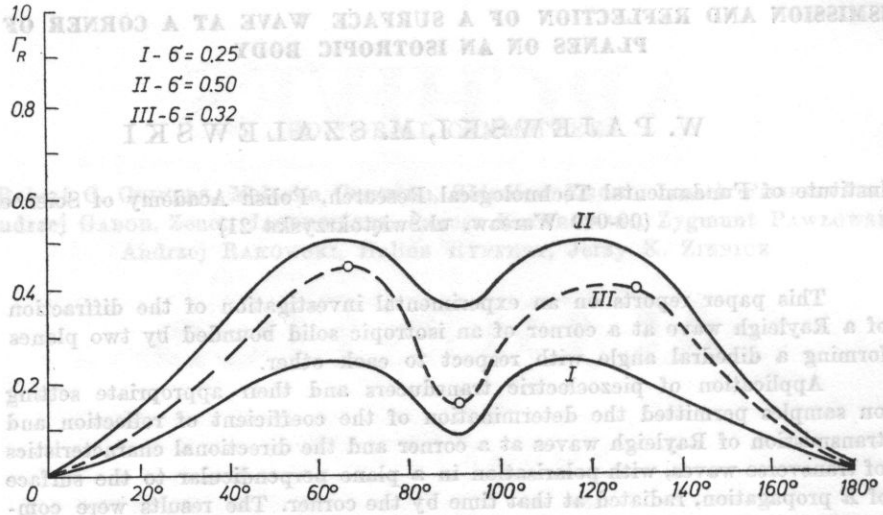

Fig. 1. The reflection coefficient of Rayleigh wave from the edge as a function of the Poisson ratio σ and the dihedral angle θ between the propagation planes [4]. Measurement points are marked on curve *III* $\sigma = 0.32$

In paper [3] GORUK and STEGEMAN investigated experimentally bulk waves arising at a corner after the passage of Rayleigh waves. Their method can only be used in the case of a transparent body; there are also additional difficulties in visualizing transverse components in optically little active crystals.

The method which permits the measurement of surface and bulk waves, both transverse and longitudinal near the corner, is the method which consists in using piezoelectric transducers with transverse or longitudinal vibration as sources of surface waves and as detectors of surface and bulk waves on samples with appropriate shape.

2. Investigation of the reflection of Rayleigh waves from the corner

The investigations used piezoelectric ceramic material which permitted experiments both with transverse surface waves and Rayleigh waves. The sample used in the investigations had the shape of cylinder sections, with the

angle θ being 90, 125, and 65° (Fig. 2). The planes of the dihedral angle of each section were polished so as to obtain minimum attenuation of Rayleigh waves. The Rayleigh wave was excited by a piezoelectric transducer of transverse vibration polarised perpendicularly to the propagation plane. The transducer was set with hardenable resin at the corner of the plane and the cylindrical surface. Thus, the wave propagating along the surface was incident onto the edge of the dihedral angle and subsequently passed onto the other plane or, when reflected, returned to the transmitting transducer. In order to observe transverse waves generated at that time by the edge of the dihedral angle, identical transducers fixed with epoxy resin were set on the cylindrical surface of the section (Fig. 3). Signals detected by transducers were registered using

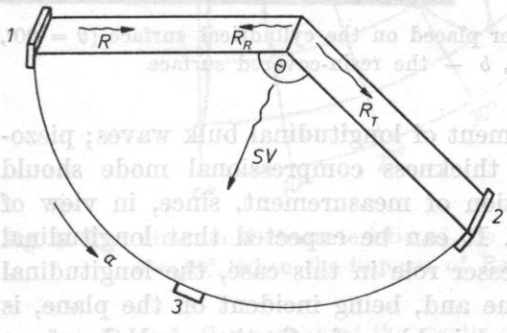

Fig. 2. The transmission of Rayleigh wave at a corner of the dihedral angle θ

1 – the transducer generating the Rayleigh wave and registering the reflected wave; *2-3* – the transducers registering the transmitted wave and the bulk wave SV, R – the incident wave, R_R – the reflected wave, R_T – the transmitted wave, SV – the transverse bulk wave

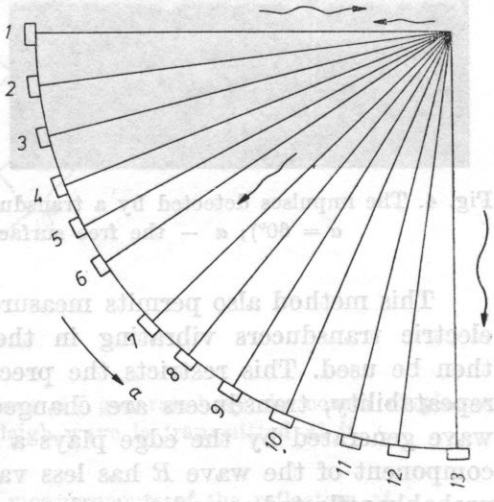

Fig. 3. The position of piezoelectric plate transducers (1-13) for generation and detection of waves in order to observe the phenomenon of the transmission of Rayleigh wave at a corner

an oscilloscope. In this case, the electric signal was proportional to the amplitude of an acoustic impulse. A whole series of oscillograms were thus obtained, on the basis of which it was possible to compare the amplitudes of the impulses of respective waves. It appeared to be quite easy to determine the paths of the impulses, taking into consideration their passage time and the velocity of surface or, alternatively, bulk waves. In the case when a surface wave converts in to a bulk one, part of the path of the impulse is the path over the surface from the transducer to the edge and part is the radius from the edge to the

surface of the cylinder. Consideration of different paths and different velocities permits relatively easy identification of the impulses and determination of their amplitude (Fig. 4).

The investigations covered transmitted and reflected surface waves and a transverse bulk wave polarised in the plane perpendicular to the propagation surface.

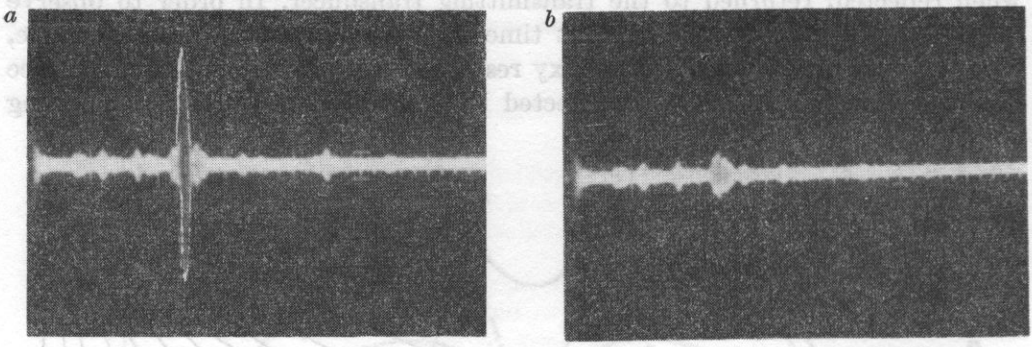

Fig. 4. The impulses detected by a transducer placed on the cylindrical surface ($\theta = 90°$, $\alpha = 60°$); a — the free surface, b — the resin-covered surface

This method also permits measurement of longitudinal bulk waves; piezoelectric transducers vibrating in the thickness compressional mode should then be used. This restricts the precision of measurement, since, in view of repeatability, transducers are changed. It can be expected that longitudinal wave generated by the edge plays a lesser role in this case, the longitudinal component of the wave R has less value and, being incident on the plane, is probably reflected according to the geometrical law of reflection; and, therefore, it should be sought in the respective direction. In the case of the transverse component of displacement of the wave R the reflection conditions are more complicated and geometrical relations are not valid. This problem is not yet clear and requires investigation.

The directional characteristics of the propagation of the bulk wave SV inside the sample (Figs. 5-7) were obtained from measurements. It is interesting to note that in Fig. 5 there are two maxima close to the angles $\alpha \cong 60°$ and $\alpha \cong 30°$ (see Fig. 2), which is in agreement with the results of paper [3] obtained by an acoustooptical method. The results of the investigations were compared with the results in world literature which were obtained using optical methods [1, 3]. The latter results apply to a $LiNbO_3$ crystal with Y-cut and propagation direction z, and to a quartz crystal with X-cut and propagation direction z. In the case of an isotropic body, the results of the reflection of the wave R were obtained by modelling the behaviour of the wave using a computer [2].

The piezoelectric ceramic material can be regarded as an isotropic body, since it was polarised parallel to the propagation surface. It can be seen from

Tables 1 and 2 that the results obtained are quite significantly different from those published in the papers mentioned above. They agree, however, with the results represented by the curve $\sigma = 0.32$ in Fig. 1 (*III*).

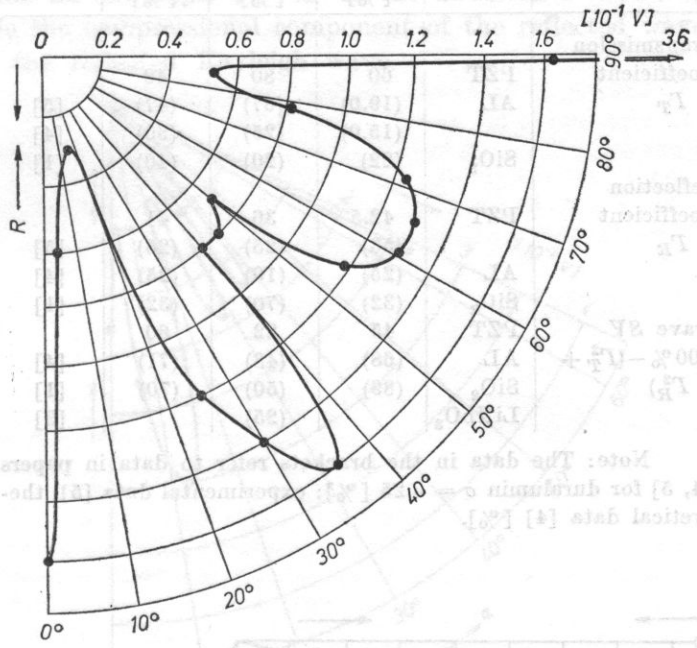

Fig. 5. The directional characteristic of the wave *SV* generated by the corner of planes $\theta = 90°$, when the impulse of Rayleigh wave is transmitted at it

Table 1. Comparison of the results of measurements of the reflection of Rayleigh wave from the corner of a quarter — space ($\theta = 90°$) (power coefficient)

Material kind	Reflected wave [%]	Transmitted surface wave [%]	Bulk wave (*SV*) [%]	Paper
SiO_2 ($y \to x$)	30	50	20	[1]
$LiNbO_3$ ($y \to z$)	23	39	25	[3]
isotropic body	13	41	46	[2]
PZT (isotropic)	13	65	22	

Table 2 confirms the presence of a minimum reflection for the angle $\theta = 90°$ and of maxima corresponding to the angles $\theta = 65°$ and $\theta = 125°$.

These results were obtained applying the conservation rule of energy for the impulses of the waves whose origin is at the corner. However, the energy of longitudinal wave was omitted. A component of this type can readily be found using acoustooptic methods. A closer analysis of the characteristics

Table 2. Comparison of the reflection coefficients of Rayleigh waves from the edge of the angle θ in the case of piezoelectric ceramic material ($\sigma = 0.32$) and other materials

Angle θ		65° [%]	90° [%]	125° [%]	Paper
transmission coefficient Γ_T	PZT	60	80	48	
	AL	(19.0)	(67)	(47)	[5]
		(15.0)	(25)	(50)	[4]
	SiO_2	(22)	(20)	(40)	[1]
reflection coefficient Γ_R	PZT	42.5	36	41	
		(53)	(25)	(26)	[5]
	AL	(25)	(10)	(25)	[4]
	SiO_2	(32)	(70)	(32)	[1]
wave SV $100\% - (\Gamma_T^2 + \Gamma_R^2)$	PZT	45	22	60	
	AL	(68)	(48)	(71)	[4]
	SiO_2	(89)	(50)	(70)	[1]
	$LiNbO_3$		(25)		[3]

Note: The data in the brackets refer to data in papers [4, 5] for duralumin $\sigma = 0.25$ [%]: experimental data [5], theoretical data [4] [%].

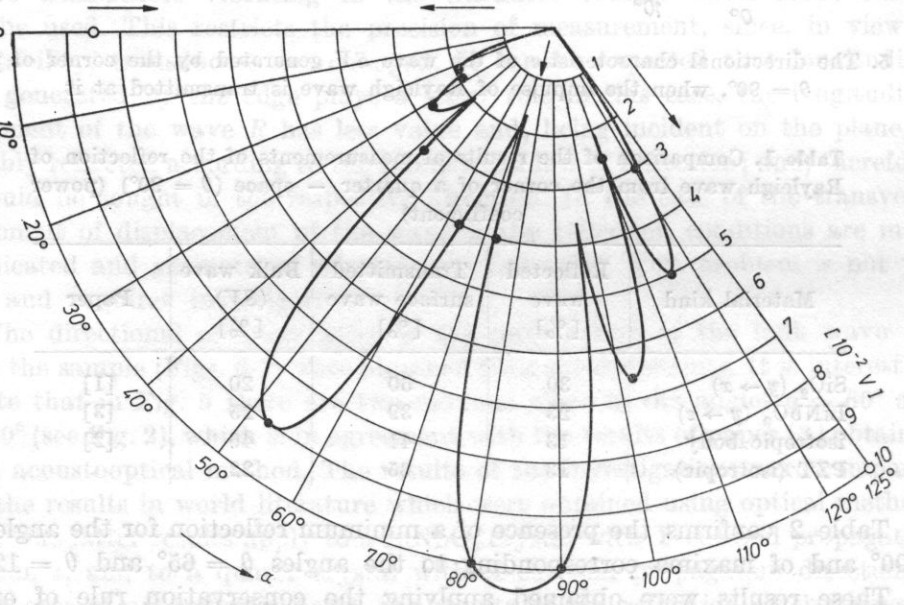

Fig. 6. The directional characteristic of the transverse wave SV for the transmission of Rayleigh wave at the corner $\theta = 125°$

of wave radiation from the edge (Figs. 5-7) and the existing lobes indicates that minima of the amplitude of a transverse bulk wave can be observed in the directions where a reflected longitudinal wave might occur. E.g. for the angle $\theta = 125°$ the lobe of the longitudinal wave should be in the direction $\alpha = 70°$, while for the angle $\theta = 65°$ in the direction $\alpha = 55°$. In the case of a right angle the compressional component of the reflected wave is probably included in the reflected Rayleigh wave.

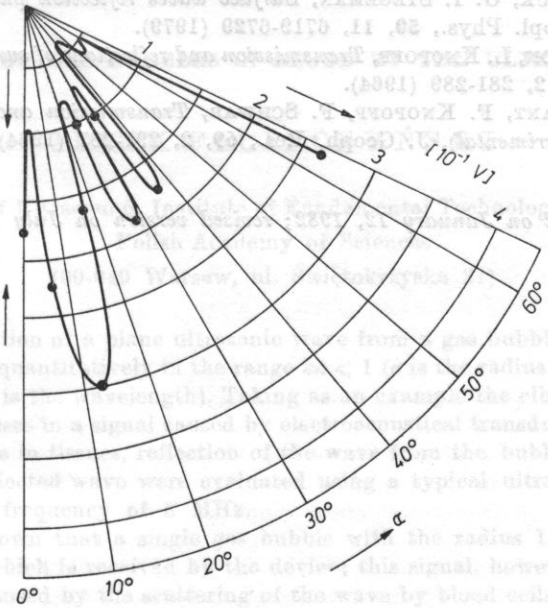

Fig. 7. The directional characteristic of the transverse wave SV for the transmission of Rayleigh wave at the corner $\theta = 65°$

3. Conclusions

The present method for the investigation of the phenomenon of the reflection of waves from the corner gives interesting results and can complement other methods, e.g. optical ones, where these cannot be used. Moreover, it can facilitate the solution of the theoretically difficult problem of the reflection of Rayleigh wave from plane edges, since it permits the determination of the contribution of respective waves to the phenomenon and indicates therefore the possibility of their being neglected in calculation. Finally, the results obtained here contribute to a better understanding of the phenomena involved.

The results obtained also indicate the possibility of using acoustoelectric waves in the construction of piezoelectric resonators — the more convenient reflection of waves can permit greater quality to be obtained in the resonators, without the use of complex reflecting structures.

References

[1] J. I. Burow, Nguen c. Thank, Anastazova, *Reflection, transmision and conversion of acoustic surface waves incident normally onto a quartz wedge with plane Y, X-cut*, Appl. Phys., **20**, 189-191 (1979).

[2] C. W. Farnel, *Types and properties of surface waves*, Springer Verlag, Berlin – Heidelberg – New York 1978, pp. 49-53.

[3] W. S. Goruk, G. I. Stegeman, *Surface waves reflection phenomena at interfaces on yz $LiNbO_3$*, J. Appl. Phys., **50**, 11, 6719-6729 (1979).

[4] I. A. Hudson, L. Knopoff, *Transmission and reflections of surface waves at a corner*, J. Geoph. Res., **69**, 2, 281-289 (1964).

[5] W. L. Pilant, F. Knopoff, F. Schwab, *Transmission and reflection of surface waves at corner (experimental)*, J. Geoph. Res., **69**, 2, 291-297 (1964).

Received on January 12, 1982; revised version on July 1, 1982.

ARCHIVES OF ACOUSTICS
8, 1, 11-30 (1983)

DETECTABILITY OF GAS BUBBLES IN BLOOD BY THE ULTRASONIC METHOD

LESZEK FILIPCZYŃSKI

Department of Ultrasound, Institute of Fundamental Technological Research,
Polish Academy of Sciences
(00-049 Warsaw, ul. Świętokrzyska 21)

The reflection of a plane ultrasonic wave from a gas bubble in the blood was considered quantitatively in the range $ka \leqslant 1$ (a is the radius of the bubble, $k = 2\pi/\lambda$ and λ is the wavelength). Taking as an example the elbow vein (vena basilica), the losses in a signal caused by electroacoustical transducing, attenuation of the wave in tissues, reflection of the wave from the bubble and divergence of the reflected wave were evaluated using a typical ultrasonic Doppler device with a frequency of 8 MHz.

It was shown that a single gas bubble with the radius 1.6 μm already gives a signal which is received by the device; this signal, however, is masked by the signal caused by the scattering of the wave by blood cells and, in addition, this bubble is instable. Determination of the level of signals scattered in blood indicated that in the case investigated it is possible to detect in the vein a single gas bubble with its radius greater than 16 μm or gas bubbles with a radius of 11 μm lying at the stability limit provided that their density exceeds 35 cm^{-3}.

The present calculation procedure permits the determination in a specific anatomic case of the level of signals scattered by blood, the level of electronic noise and also the determination of the detectability of gas bubbles in blood caused, for example, by the decompression of divers or by the caisson disease. In the case of the pulmonary artery, using a frequency of 5 MHz, minimum radii of detectable gas bubbles greater than 70 μm were obtained.

Notation

A — surface area of the transducer
A_l — attenuation loss
a — radius of the gas bubble
a_d — radius of the gas bubble lying at the detectability limit
a_0 — limiting radius of the gas bubble
a_m — expansion coefficient of the wave reflected from the gas bubble
$\bar{a}_m$ — expansion coefficient of the wave penetrating into the gas bubble

a_t — radius of the transducer
B — level of the signal scattered by blood cells
c — wave velocity in blood
$\bar{c}$ — wave velocity in gas
$\bar{c}_0$ — wave velocity in gas under normal conditions
c^D — wave velocity in the transducer with constant electric induction
c_A — wave velocity in the medium loading the back surface of the transducer
c_B — wave velocity in the medium loading the front surface of the transducer
D — loss caused by the divergence of the ultrasonic beam
d — internal diameter of the blood vessel
d_t — thickness of the transducer
e — base of natural logarithms
f — frequency
f_e — frequency of electromechanical resonance in the transducer
f_m — frequency of mechanical resonance in the transducer
f_{res} — resonance frequency of the gas bubble
$h_m^{(2)}$ — spherical Hankel function of the second kind of order m
$h_m^{(2)\prime}$ — see formula (5a)
I_0 — intensity of the plane incident wave
I_s — intensity of the scattered spherical wave
$J_{m+1/2}$ — Bessel function of order $m+1/2$
j — $\sqrt{-1}$
j_m — a spherical Bessel function of order m
j_m' — see formula (5b)
k — wave number in blood
$\bar{k}$ — wave number in gas
k_t — coefficient of electromechanical coupling
l — distance of the blood vessel from the transducer
M_s — scattering power
M_A — power emitted at the back loading of the transducer
M_B — power emitted at the front loading of the transducer (biological medium)
m — natural number
$N_{m+1/2}$ — Neuman function of order $m+1/2$
n_m — spherical Neuman function of the order m
n — density of blood cells (erythrocytes)
n_0 — density of gas bubbles
P_m — Legendre polynomial (spherical function)
P_a — static pressure of air
P_l — static pressure in liquid
P_i — static pressure in a gas bubble
P_δ — static pressure caused by the surface tension
p_i — static pressure of the incident wave
p_0 — acoustic pressure amplitude of the incident wave
p_s — acoustic pressure of the reflected (scattered) wave
R — reflection loss
r — radial coordinate of the polar system
S — loss caused by scattering in blood
T — loss caused by piezoelectric transducing
t — time
W — ratio of the maximum to the minimum electric signal
V — blood volume in the ultrasonic beam

v_A – velocity of the back surface of the transducer
v_B – velocity of the front surface of the transducer
x – relative frequency (see formula (19))
x_e – relative frequency of the electric resonance of the transducer
α_m – the scattering (intensity) coefficient in muscle tissue
α_b – the scattering (intensity) coefficient blood
Γ_ϑ – function of far field reflection
δ – equivalent cross-section of scattering by blood cells
η – coefficient of backscattering
θ – inclination angle of the ultrasonic beam
ϑ – angular coordinate of the polar system
λ – wavelength in blood
ϱ – density of blood
$\bar{\varrho}$ – density of gas
ϱ_0 – density of gas under normal conditions
ϱ_t – density of the transducer
ϱ_A – density of the medium loading the back surface of the transducer
ϱ_B – density of the biological medium loading the front surface of the transducer
Σ – equivalent cross-section of scattering of the gas bubble
Σ_0 – equivalent cross-section of scattering of a gas bubble with the limiting radius
σ – surface tension at the blood-air interface
ω – angular frequency

1. Introduction

Ultrasonic diagnostic methods permit the possibility of detecting such structures in the human body whose acoustic specific impedance is different from the impedance of the surrounding tissues. These are, for example, gas bubbles in divers' blood during decompresion (divers' or caisson disease) or in persons staying at high altitudes. An ultrasonic method permits detection of the presence of gas bubbles in blood even before distinct, clinical symptoms of this disease occur [20]. Gas bubbles in blood are also detected ultrasonically in the blood circulation system in the artificial kidney.

Gas bubbles in blood are detected by means of the ultrasonic Doppler technique [19, 20] and, in some applications, by means of the conventional pulse technique. In some of our investigations [15] performed in cooperation with the Central Institute of Occupational Safety, the Doppler technique was used at a frequency of 5 MHz to observe the appearance of gas bubbles in the pulmonary artery. SPENCER *et al.* [20], who were the first to use the method, showed that it was also possible to detect gas bubbles in the veins of the peripheral circulation system, e.g. in the elbow vein (vena basilica).

The principal aim of this investigation is to evaluate the minimum size of a single, spherical gas bubble to be detectable in blood using ultrasonic, Doppler or pulse, methods. The author found no answer to this problem in papers related to this subject [2, 10, 12, 19, 20]. A quantitative analysis of the

problem will be performed in the case of detection of gas bubbles in the elbow vein (vena basilica) using a Doppler method under the conditions shown in Fig. 1.

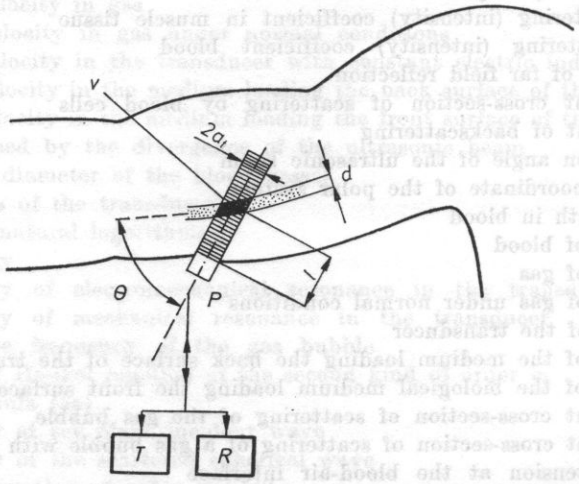

Fig. 1. The system for detection of gas bubbles in the elbow vein (vena basilica) P – the ultrasonic probe with a piezoelectric transducer, T – the transmitter of electric signals, R – the receiver of electric signals, d – the diameter of the vein, V – the volume of blood covered by the ultrasonic beam, l – the depth at which the vein lies, θ – the inclination angle of the ultrasonic beam with respect to the vein, $2\,a_t$ – the diameter of the ultrasonic beam

2. Assumptions of the analysis

It can be assumed that an ultrasonic beam of longitudinal waves at a frequency of 8 MHz is radiated by a piezoelectric transducer with the diameter $2a_t = 5$ mm. The mean wave velocity in soft tissues is approximately equal to the wave velocity in blood ($c = 1.57$ km/s). Thus the radiated wavelength is $\lambda = 0.2$ mm. The boundary between the near and the for field is then $a_t^2/\lambda = 31$ mm. Considering typical anatomic conditions, it can be assumed that the vein of interest with its internal diameter $d = 3$ mm lies at the depth $l = 15$ mm from the body surface on which the piezoelectric transducer was placed (Fig. 1). It can then be recognized that at this distance the ultrasonic beam is cylindrical. The mean (in the cross-section of the beam) wave intensity is, as a result of diffraction loss, lower by only about 1.5 dB at the distance l than at the body surface [3].

An ultrasonic Doppler device [5] will be used to detect gas bubbles. The output voltage of the transmitter is $U_T = 4$ V when matched to the impedance of the ultrasonic probe, i.e. 50 Ω. The voltage sensitivity of the receiver limited by electronic noise is $U_R = 4$ μV. Under these conditions the ratio of the maximum to the minimum electronic signal is $W = U_T/U_R = 10^6 \doteq 120$ dB.

3. Reflection of a plane ultrasonic wave from a gas bubble in blood

A further step of calculations here will be the determination of the acoustic pressure of the wave reflected from a spherical gas bubble with the radius a. It can be assumed additionally that the wave of the acoustic pressure incident on the gas bubble is plane. The reflection of the plane wave from a sphere filled with a fluid medium (liquid or gas) was considered in detail by RSHEVKIN in his monograph [16] and subsequently by MORSE and INGARD [11]. The further part of this paper is based on the former of these references.

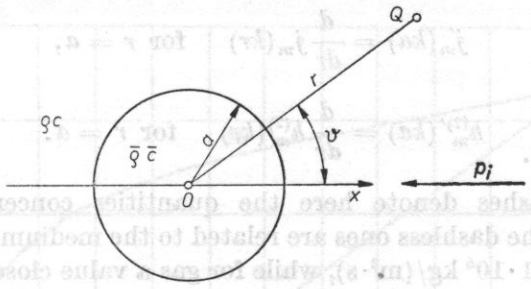

Fig. 2. The polar coordinate system (r, ϑ) with a gas bubble in the shape of a sphere with radius a and with a plane acoustic pressure wave p_i incident in the direction $-X$
ϱc, $\bar{\varrho} c$ are the acoustic specific impedance of the media, respectively, outside and inside the sphere

In a threedimensional polar coordinate system a plane continuous wave with the acoustic pressure p_i, incident in the negative direction of the x axis (Fig. 2) on a sphere placed at the origin of the system, can be represented as an infinite series of spherical waves of the form [16]

$$p_i = p_0 \exp(j\omega t) \sum_{m=0}^{\infty} j^m (2m+1) P_m(\cos\vartheta) j_m(kr). \tag{1}$$

The wave reflected from the sphere can, in turn, be expressed in the form of an infinite series of spherical waves propagating in the medium surrounding the sphere in the direction of the increasing radius r

$$p_s = \exp(j\omega t) \sum_{m=0}^{\infty} a_m P_m(\cos\vartheta) h_m^{(2)}(kr). \tag{2}$$

The wave penetrating into the sphere can be described by the expression

$$p_t = \exp(j\omega t) \sum_{m=0}^{\infty} \bar{a}_m P_m(\cos\vartheta) j_m(\bar{k}r). \tag{3}$$

The coefficients a_m and $\bar{a}_m$ are determined from the boundary conditions satisfied on the surface of the sphere $(r = a)$ which are the continuity of the acoustic pressure and of the radial component of the acoustic velocity on the

surface of the sphere. RSHEVKIN gives the following expression for the expansion coefficients [16]

$$a_m = -p_0 j^m (2m+1) \frac{j'_m(ka) - \frac{\varrho c}{\bar{\varrho}\bar{c}} \frac{j'_m(\bar{k}a)}{j_m(\bar{k}a)} j_m(ka)}{h_m^{(2)\prime}(ka) - \frac{\varrho c}{\bar{\varrho}\bar{c}} \frac{j_m(\bar{k}a)}{j'_m(\bar{k}a)} h_m^{(2)}(ka)}, \tag{4}$$

where

$$j'_m(ka) = \frac{d}{dr} j_m(kr) \quad \text{for } r = a, \tag{5a}$$

$$h_m^{(2)\prime}(ka) = \frac{d}{dr} h_m^{(2)}(kr) \quad \text{for } r = a. \tag{5b}$$

Horizontal dashes denote here the quantities concerning the medium inside the sphere, the dashless ones are related to the medium outside the sphere. For blood $\varrho c = 1.61 \cdot 10^6$ kg/(m^2·s), while for gas a value close to that for air can be assumed, $\varrho c = 0.0004 \cdot 10^6$ kg/(m^2·s).

MORSE and INGARD [11] give analogous formulae in a slightly different form, which, it can readily be verified, are the same as RSHEVKIN's formulae.

The point of interest here is the wave reflected at the point Q (Fig. 2) at a distance so far from the centre of the sphere that the following condition is satisfied

$$r \gg \lambda \quad \text{or} \quad kr \gg 1. \tag{6}$$

Thus the Hankel function $h_m^{(2)}$ can be approximated by the expression

$$h_m^2(z) \underset{z\to\infty}{\to} \frac{1}{z} \exp\left[-j\left(kr - \frac{m+1}{2}\pi\right)\right]. \tag{7}$$

Considering formula (7) expression (2) becomes

$$p_s = p_0 \frac{\exp(-jkr)}{kr} \Gamma_\vartheta(ka), \tag{8a}$$

where

$$\Gamma_\vartheta(ka) = \sum_0^\infty a_m P_m(\cos\vartheta) \exp[j(m+1)\pi/2]. \tag{8b}$$

The quantity $\Gamma_\vartheta(ka)$ will be called the function of far field reflection. This function depends on the argument ka and on the angle ϑ (Fig. 2). However, in the ultrasonic technique used for detection of gas bubbles in blood one common piezoelectric transducer is used for transmission and detection of ultrasonic waves or two transducers placed in one probe close to each other. In

such a case only the value of the function $\Gamma_\vartheta(ka)$ in the direction of the wave radiation, i.e. for the angle $\vartheta = 0$, is of interest here. This simplifies further calculations, since for $\vartheta = 0$, $P_m(1) = 1$. Hence the function

$$\Gamma_{\vartheta=0}(ka) = \sum_0^\infty a_m \exp[j(m+1)\pi/2] \tag{9}$$

is only dependent on the argument ka. Fig. 3 shows this function calculated in the dB scale for low values of $ka = 0.05$-1.4. The values of the spherical

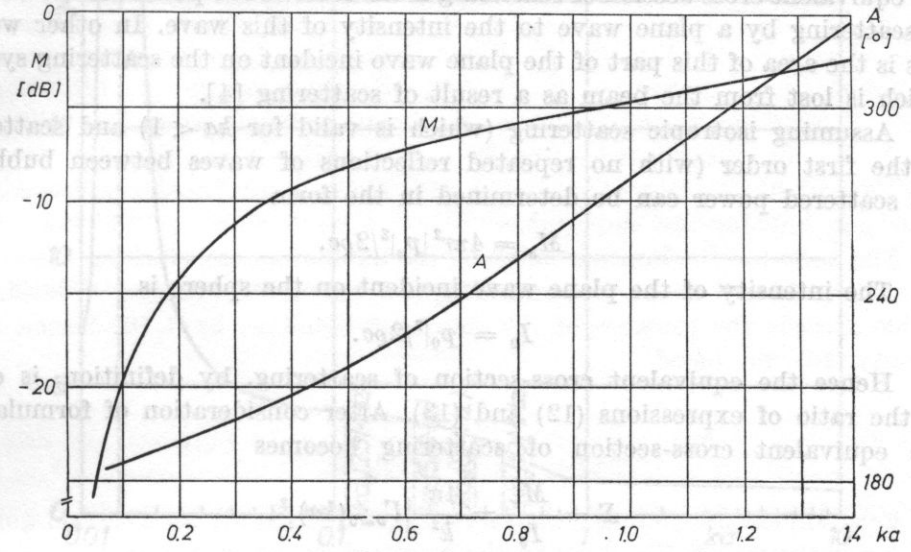

Fig. 3. The function of far field reflection $\Gamma_{\vartheta=0}$ (ka) from the gas bubble in blood ($\vartheta = 0$, $kr \gg 1$)

M – the mode $\Gamma_{\vartheta=0}$ (ka), A – arg $\Gamma_{\vartheta=0}$ (ka), a – the radius of the bubble, $k = 2\pi/\lambda$

functions necessary for the determination of the values of coefficients (4) were calculated from the following relations between these functions and the Bessel and Neuman functions of order 1/2

$$j_m(z) = \sqrt{\frac{\pi}{2z}}\, J_{m+\frac{1}{2}}(z), \tag{10a}$$

$$n_m(z) \sqrt{\frac{\pi}{2z}}\, N_{m+\frac{1}{2}}(z), \tag{10b}$$

$$h_m^{(2)}(z) = j_m(z) - j n_m(z). \tag{10c}$$

In turn, the values of the function $J_{m+1/2}(z)$ and $N_{m+1/2}(z)$ were calculated using the library of subprogrammes of a CYBER 70 IBM computer.

On the basis of the curve of the function $\Gamma_{\vartheta=0}(ka)$ and formula (8a), the pressure p_s of the wave reflected from a single gas bubble can be determined. The quantity

$$R = 20 \log \operatorname{mod} \Gamma_{\vartheta=0}(ka) \tag{11}$$

represents the loss in the signal caused by the reflection of the wave from the gas bubble.

In the case of a large number of bubbles it becomes practical to introduce the notion of the equivalent cross-section of scattering [4, 9]. By definition the equivalent cross-section of scattering is the ratio of the power lost as a result of scattering by a plane wave to the intensity of this wave. In other words, this is the area of this part of the plane wave incident on the scattering system which is lost from the beam as a result of scattering [4].

Assuming isotropic scattering (which is valid for $ka < 1$) and scattering of the first order (with no repeated reflections of waves between bubbles), the scattered power can be determined in the form

$$M_s = 4\pi r^2 |p_s|^2 / 2\varrho c. \tag{12}$$

The intensity of the plane wave incident on the sphere is

$$I_0 = |p_0|^2 / 2\varrho c. \tag{13}$$

Hence the equivalent cross-section of scattering, by definition, is equal to the ratio of expressions (12) and (13). After consideration of formula (8), the equivalent cross-section of scattering becomes

$$\Sigma = \frac{M_s}{I_0} = \frac{4\pi}{k^2} |\Gamma_{\vartheta=0}(ka)|^2. \tag{14}$$

The function $\Gamma_\vartheta(ka)$ was determined only for the value of the angle $\vartheta = 0$ and therefore expression (14) is valid strictly for consideration of backscattered signals in the incidence direction of the plane wave. For $\vartheta \neq 0$ this formula becomes approximate, to be used when $ka < 1$.

It is interesting to note the ratio of the equivalent cross-section of scattering Σ to the cross-section area of the bubble πa^2, shown as a function of ka in a broad range of this product in Fig. 4. The curve calculated shows a maximum for the value $ka_{\text{res}} \approx 0.014$, which corresponds to resonance vibrations of the bubble; these vibrations are of the zeroth order. The value of this maximum depends on the magnitude of energy of the reflected wave, viscosity of the surrounding liquid and on the thermal conduction of the liquid [10].

Neglecting in first approximation the viscosity of the liquid and also the surface tension, the resonance frequency of the bubble can be determined from the formula [16]

$$f_{\text{res}} = \frac{1}{2\pi a} \sqrt{\frac{3\bar{\varrho}\bar{c}_0^2}{\varrho} \frac{P_l}{P_0}}, \tag{15}$$

where ϱ_0 and c_0 denote respectively the density and wave velocity in gas under normal conditions (temperature 0°C, normal pressure $P_0 = 750$ mm Hg $= 1000$ hPa).

The above formula assumes an adiabatic transition of gas in the bubble. In the case of very small bubbles, as a result of low gas volume and high thermal conduction of the liquid, the phenomenon is isothermal and the above formulae require some modification [10]. This, however, does not cause any greater change in the resonance frequency.

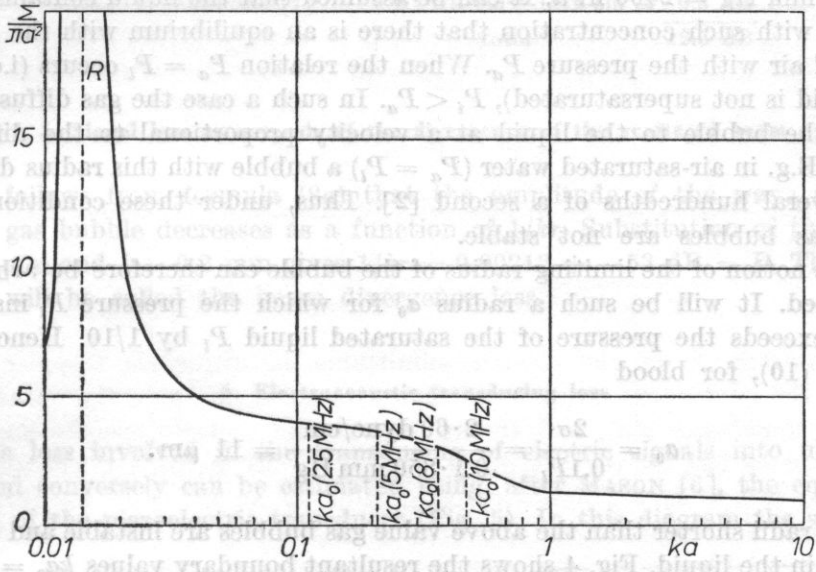

Fig. 4. The relative equivalent cross-section of backscattering of the gas bubble in blood calculated in relation to ka from formulae (14), (9) and (4)

Σ – the absolute equivalent cross-section of backscattering; a, a_0 and a_{res} – respectively, the radius, the limiting radius and the resonance radius of the gas bubble, R – the vibration resonance of the bubble

Attention should be drawn to the phenomenon of the surface tension occurring on the surface of the gas bubble. It causes the appearance of additional pressure directed from the liquid to the surface of the bubble. This pressure has the value [8]

$$P = \frac{2\sigma}{a}. \tag{16}$$

The surface tension of blood has the value $\sigma = 60$ dyne/cm [12]. For a bubble radius longer than 10 μm, from formula (16), the pressure P_σ caused by this is lower by almost one order of magnitude than the mean blood pressure in man which is taken as 850 mm Hg $= 1.13 \cdot 10^5$ dyne/cm^2 $= 1130$ hPa.

In the case of gas bubbles with shorter diameters the pressure within the bubble becomes greater than that of the surrounding liquid, since the following equation occurs [2],

$$P_i = P_1 + \frac{2\sigma}{a}, \tag{17}$$

where P_i is the gas pressure inside the bubble and P_l is the static pressure in the liquid. For $a = 0.5$ μm the excessive value of this pressure is $P_i - P_l = 1800$ mm Hg $= 2400$ hPa. It can be assumed that the liquid contains dissolved gas with such concentration that there is an equilibrium with the gaseous phase of air with the pressure P_a. When the relation $P_a = P_l$ occurs (i.e. when the liquid is not supersaturated), $P_i < P_a$. In such a case the gas diffuses from within the bubble to the liquid at a velocity proportional to the difference $P_i - P_a$. E.g. in air-saturated water ($P_a = P_l$) a bubble with this radius dissolves over several hundredths of a second [2]. Thus, under these conditions very small gas bubbles are not stable.

The notion of the limiting radius of the bubble can therefore be arbitrarily introduced. It will be such a radius a_0 for which the pressure P_i inside the bubble exceeds the pressure of the saturated liquid P_l by 1/10. Hence, from formula (10), for blood

$$a_0 = \frac{2\sigma}{0.1P_l} = \frac{2 \cdot 60 \text{ dyne/cm}}{0.1 \cdot 850 \text{ mm Hg}} = 11 \text{ μm}. \tag{18}$$

For radii shorter than the above value gas bubbles are instable and quickly dissolve in the liquid. Fig. 4 shows the resultant boundary values $ka_0 = 2\pi f a_0/c$ for frequencies $f = 2.5$, 5, 8 and 10 MHz. It follows therefore that no practical possibility exists for resonance to occur when bubbles are detected using frequencies equal to or higher than 2.5 MHz.

It follows from Fig. 4 that in the range $ka = 0.11\text{-}10$ the equivalent cross-section of scattering is from 4 to 1 times as large as the area of the equatorial cross-section of the gas bubble.

4. Signal loss as a result of wave attenuation in the biological medium

Evaluation of the attenuation of ultrasonic waves on their way from the body surface through the skin, muscle and the wall of a blood vessel to its interior can only be approximate. Table 1 presents such an evaluation. Considering the path of an ultrasonic wave in both directions, attenuation loss can be taken as $A_l = -25$ dB.

Table 1. Estimation of ultrasonic wave attenuation on the path from the transducer to the vessel (vena basilica) (extrapolated for the frequency $f = 8$ MHz)

1. Muscle (including skin) (acc. to HOETER [7])	9.0 dB cm^{-1} · 1.3 cm =	11.7 dB
2. Vessel wall (acc. to GREENLEAF [7])	4.8 dB cm^{-1} · 0.1 cm =	0.5 dB
3. Blood (acc. to KIKUCHI [7]	2.2 dB cm^{-1} · 0.15 cm =	0.3 dB
	total	12.5 dB

5. Signal loss as a result of the divergence of the scattered beam

It follows from formula (8*a*) that the amplitude of the wave reflected from a gas bubble decreases as a function of $1/kr$. Substitution of the values $r = 15$ mm and $\lambda = 0.2$ mm gives $1/kr = 0.00212 \doteq -53$ dB $= D$. The quantity D will be called the beam divergence loss.

6. Electroacoustic transducing loss

The loss involved in the transducing of electric signals into ultrasonic ones and conversely can be estimated using, after MASON [6], the equivalent system of the piezoelectric transducer (Fig. 5). In this diagram the symbol x

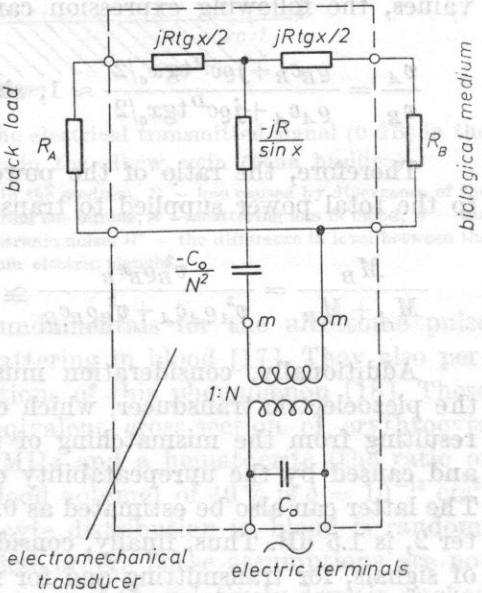

Fig. 5. The equivalent electromechanical system of the piezoelectric transducer with thickness vibration, according to MASON

$R_A = A\varrho_A c_A$, $R_B = A\varrho_B c_B$, $R = A\varrho_t c^D$, A – the surface area of the transducer, C_0 – the static capacity of the transducer, N – the "turn" ratio of the electromechanical transformer, x – the relative frequency

denotes the relative frequency equal to

$$x = \pi f/f_m = \omega d/c^D. \tag{19}$$

With good enough approximation it can be assumed that [6]

$$f_e/f_m = \sqrt{1-k_t^2}\,. \tag{20}$$

Taking for the ceramic material CERAD used here the value of the coefficient of electromechanical coupling for thickness vibration $k_t = 0.5$ and the frequency of electromechanical resonance $f_e = 8$ MHz, the following value can be obtained from formulae (19) and (20),

$$x_e = \pi\sqrt{1-k_t^2} = 2.72. \tag{21}$$

On the basis of the equivalent diagram (Fig. 5), the simple relation can be written

$$v_A(\varrho_A c_A + j\varrho c^D \operatorname{tg} x_e/2) = v_B(\varrho_B c_B + j\varrho c^D \operatorname{tg} x_e/2). \tag{22}$$

Measurements of the electric admittance of ultrasonic Doppler probes used in the continuous wave blood flow measurements give the value of the acoustic impedance $\varrho_A c_A = 3\cdot 10^6$ kg/(m^2·s). The acoustic specific impedance of soft tissues has the average value $\varrho_B c_B = 1.6\cdot 10^6$ kg/(m^2·s). The analogous value for piezoelectric transducers is greater by an order of magnitude and varies within the limits $\varrho c^D = (25\text{-}35)\cdot 10^6$ kg/(m^2·s). Considering the above values, the following expression can be derived from formula (22),

$$\frac{v_A}{v_B} = \frac{\varrho_B c_B + j\varrho c^D \operatorname{tg} x_e/2}{\varrho_A c_A + j\varrho c^D \operatorname{tg} x_e/2} \approx 1, \text{ since } \quad \varrho_B c_B < \varrho_A c_A \ll \varrho c^D \operatorname{tg} x_e/2. \tag{23}$$

Therefore, the ratio of the power M_B emitted in the biological medium to the total power supplied to transducer is

$$\frac{M_B}{M_A + M_B} = \frac{v_B^2 \varrho_B c_B}{v_A^2 \varrho_A c_A + v_B^2 \varrho_B c_B} \cong \frac{\varrho_B c_B}{\varrho_A c_A + \varrho_B c_B} = 0.35 \doteqdot -4.6 \text{ dB}. \tag{24}$$

Additionally, consideration must be given to the loss occurring inside the piezoelectric transducer, which can be estimated as 0.75 dB, and the loss resulting from the mismatching of the transducers to the electronic systems and caused by the unrepeatability of the parameters of ceramic transducers. The latter can also be estimated as 0.75 dB. The diffraction loss, given in chapter 2, is 1.5 dB. Thus, finally, considering the double piezoelectric transducing of signals, for transmitting and for receiving of signals, the total transducing loss $T = -15$ dB can be determined.

7. Wave scattering in blood

Fig. 6 shows all the signal losses which have been calculated so far. Under the measurement conditions assumed the smallest gas bubble at the detectability limit would be a bubble for which $ka = 0.05$. This corresponds to the radius $a = 0.05\lambda/2\pi = 1.6$ μm; since then the signal received would be equal to the level of electronic noise N. It can be noted, however, that red blood cells (erythrocytes) have dimensions Ø 8.5 ×2.5 μm. Moreover, aggregates of blood cells up to 6-10 cells, or sometines up to hundreds of cells, form in large blood vessels [5]. Accordingly, it is essential to explain to what extent the wave scattering, mostly by erythrocytes, masks the signal from a single gas bubble.

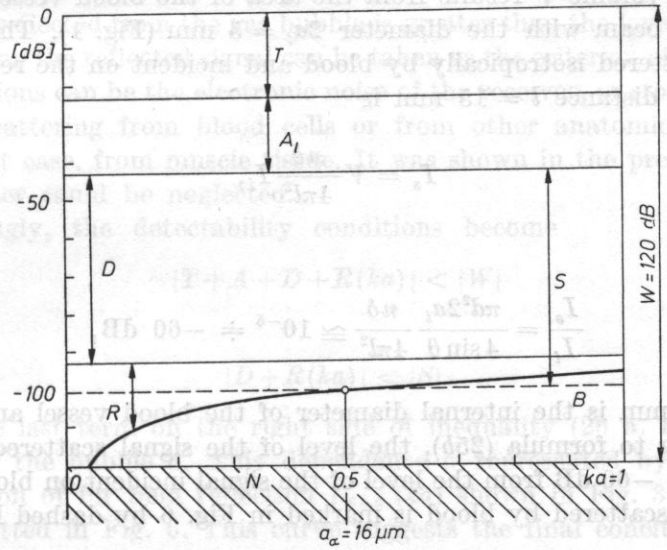

Fig. 6. The level of the signals with respect to the electrical transmitted signal (0 dB) in the course of the detection of a gas bubble in the elbow vein (vena basilica)

T – piezoelectric transducing loss, A_l – attenuation loss in the medium, D – loss caused by divergence of the beam scattered by bubbles, R – loss caused by reflection from the bubble, S – scattering loss in blood, B – the level of the signal scattered in blood, N – the level of electronic noise, W – the difference in level between the maximum and minimum electric signals

Reid *et al.* developed theoretical fundamentals for the ultrasonic pulse method for the measurement of wave scattering in blood [17]. They also performed extensive experimental investigations of this phenomenon [18]. These authors determined the value of the eqivalent cross-section of erythrocyte scattering which for a frequency of 8.5 MHz and a hematocrite (the ratio of the volume of erythrocytes to the total blood volume) of 40 % is $\delta = 10^{-13}$ cm^2.

It can be assumed that the erythrocyte distribution in blood is random, while the reflection is isotropic, of the first order. These assumptions are not strictly satisfied in blood, for example, because of the relatively densely packed

erythrocytes. As the packing density of erythrocytes (increasing hematocrite) increases, the equivalent cross-section of scattering decreases [17]. Multiple reflection might occur then or the erythrocyte distribution might cease to be random. The scattering phenomenon becomes more complicated; despite this, a single model of scattering can be used, taking the above assumptions for satisfied. The argument for this assumption is the fact that the amplitude of each successive wave reflected from an erythrocyte is lower by at least 23 dB than the amplitude of the previous reflected wave. This results from the hardly distinct difference in acoustic specific impedance between erythrocyte and blood plasma [5].

The erythrocyte density $n = 5 \cdot 10^6$ mm^{-3} can now be assumed. The scattering blood volume V results from the area of the blood vessels covered by an ultrasonic beam with the diameter $2a_t = 5$ mm (Fig. 1). The intensity of the wave scattered isotropically by blood and incident on the receiving transducer at the distance $l = 15$ mm is

$$I_s = V \frac{n\delta}{4\pi l^2} I_i, \tag{25a}$$

hence

$$\frac{I_s}{I_i} = \frac{\pi d^2 2a_t}{4 \sin\theta} \frac{n\delta}{4\pi l^2} \cong 10^{-6} \doteq -60 \text{ dB}, \tag{25b}$$

where $d = 3$ mm is the internal diameter of the blood vessel and $\theta = 45°$.

According to formula (25*b*), the level of the signal scattered by blood is lower by $S = -60$ dB from the level of the signal incident on blood. The level of the signal scattered by blood is marked in Fig. 6 by dashed line *B*.

8. Wave scattering in muscle tissue

The scattering of ultrasonic waves in muscle tissue is much greater than that in blood. This can be shown on the basis of the results of experimental investigations performed on the muscles of dog's hearts by O'DONNOLL *et al.* [14]. At a frequency of 8 MHz they determined the value of the differential coefficient of backscattering $\eta = 2.5 \cdot 10^{-2}$ cm$^{-1} \cdot$sr^{-1}. Therefore, assuming isotropic scattering, the (intensity) coefficient of scattering [4] is $a_m = 4\pi\eta$ cm^{-1} $= 0.32$ cm^{-1}. In turn, the analogous scattering coefficient for blood is $a_b = \delta n = 5 \cdot 10^{-4}$ cm^{-1}. Thus, when the scattering volumes of muscle and blood, placed at the same distance from the transmit-receive transducer, are assumed to be the same, the power of the signal scattered in muscle is greater by $a_m/a_b = 640 \doteq 28$ dB than that of the signal scattered in blood.

However, in contrast to blood, muscle tissue or, alternatively, other tissues penetrated by ultrasonic wave is stationary. Accordingly, the wave scattered by this tissue does not change its frequency with respect to the incident wave; the Doppler phenomenon is absent. In view of this, the signals of these waves can be eliminated electronically, e.g. by filtration or the technique of stationary echo cancellation [13].

9. Detectability of gas bubbles

The radius of the gas bubble detectable by means of the present method can be determined directly from Fig. 6. The condition for which the magnitude of the signal reflected from the gas bubble is greater than the level of disturbing signals masking the reflected signal can be taken as the criterion of detectability. These distortions can be the electronic noise of the receiver, or stochastic signals caused by scattering from blood cells or from other anatomical structures; in the present case, from muscle tissue. It was shown in the preceding section that the latter could be neglected.

Accordingly, the detectability conditions become

$$|T+A+D+R(ka)| < |W| \tag{26a}$$

and

$$|D+R(ka)| < |S|. \tag{26b}$$

Only the last term on the right side of inequality (26 a, b) depends on the radius of the bubble a. This dependence is represented by the modulus of the function of far field reflection $\Gamma_{\vartheta=0}(ka)$ shown in Fig. 3 (see formula (11)) and plotted in Fig. 6. This curve suggests the final conclusion that the detectability condition (26) is satisfied for a single gas bubble for which $ka > 0.5$. For a frequency of 8 MHz used here this signifies that the radius of the bubble detectable under the present conditions must satisfy the condition

$$a > a_d = 0.5\frac{\lambda}{2\pi} = 16\mu\text{m}. \tag{27}$$

In the case of a larger number of gas bubbles in blood the situation becomes complicated insomuch as the distribution of the size of bubbles with different radii is not known. Therefore, the least convenient detectability conditions are taken, under the assumption that only gas bubbles with limiting radii (lying at the stability limit) whose radius was determined by formula (18), occur in blood.

The density n_0 [cm^{-3}] of such bubbles, necessary for their detection, can then be found. At a frequency of 8 MHz the equivalent cross-section of scattering of a bubble with the boundary radius $a_0 = 11$ μm is $\Sigma_0 = 3\pi a_0^2$ (see Fig. 4),

while for a single bubble lying at the detectability limit, with the radius $a_d = 16\ \mu m$ ($ka = 0.5$), this value is $\Sigma = 2.5\pi a_d^2$. The power of the signal reflected from $n_0 V$ bubbles with the radius a_0, equal to $I_i \Sigma_0 n_0 V$, can be equated to the power of the signal reflected from a single gas bubble with the radius a_d, equal to $I_i \Sigma$. Hence, the desired density of bubbles follows,

$$n_0 = \frac{\Sigma}{\Sigma_0 V} = \frac{2.5\pi a_d^2}{3\pi a_0^2} \frac{4 \sin\theta}{\pi d^2 2a_t} \cong 35\ \text{cm}^{-3}. \tag{28}$$

The analysis performed indicates that the sensitivity of the method for detection of gas bubbles is very large, since they are detectable with density as low as 35 cm^{-3}. Calculations were made for air bubbles, while divers' work involves nitrogen bubbles. The wave velocity and the density of nitrogen and air differ from each other by only a few percent [1, 8]; and therefore the results obtained can be extended to the case of nitrogen bubbles.

The above procedure for the calculation of the detectability of bubbles can be used with success in the case of other blood vessels. As an example, the detectability of bubbles in the pulmonary artery can now be calculated. This is an important case from the practical point of view, because of the fact that all the blood in the circulation system flows through this artery, when one neglects the slight bronchial flow. By covering the entire cross-section of the pulmonary artery with the ultrasonic beam, it is possible to control fully the circulation.

A disadvantage of this measurement system is the higher attenuation of signals in view of the greater depth of the pulmonary artery, compared to the case of the veins in the peripheral system, and also in view of the movements of the heart which make examination more difficult.

It is now possible to take an ultrasonic beam and a pulmonary artery with diameters of 1.3 cm and the centre of the artery at the depth $l = 4$ cm. Table 2 shows the estimation of loss as a result of attenuation in the penetrated tissue. It follows from this table that attenuation on the path from the transducer to the centre of the pulmonary artery and back is $A = -48$ dB.

Table 2. Estimation of ultrasonic wave attenuation on the path from the transducer to the pulmonary artery (extrapolated for the frequency $f = 8$ MHz)

1. Muscle (including skin)	9.0 dB $cm^{-1} \cdot 1$ cm = 9 dB
2. Adipose and connective tissue	6 dB $cm^{-1} \cdot 2$ cm = 12 dB
3. Vessel wall	5 dB $cm^{-1} \cdot 0.2$ cm = 1 dB
4. Blood (to the centre of the artery)	2.2 dB $cm^{-1} \cdot 0.8$ cm = 1.8 dB
	total 23.8 dB $\cong$ 24 dB

The loss resulting from the divergence of the scattered ultrasonic beam is, according to formula (8a), $D = 20 \log 0.2 \text{ mm}/2\pi \cdot 40 \text{ mm} = -62$ dB (see section 5). The total loss $T+A+D = -125$ dB is so great that, even when neglecting the reflection loss $R(ka)$, the signal received would be lower than the level of electronic noise of the device, and thus undetectable. For this reason it is necessary to eliminate the frequency of 8 MHz from further consideration and to use instead a frequency of 5 MHz, also typical of Polish-made Doppler equipment.

Since attenuation in soft tissue is directly proportional to frequency, attenuation loss then decreases to the value $A = 30$ dB. The loss caused by the divergence of the scattered beam is $D = 20 \log 0.32 \text{ mm}/2\pi \cdot 40 \text{ mm} = -58$ dB.

The level of the signal scattered by blood also changes to become

$$S = I_s/I_i = V \frac{n\delta}{4\pi l^2} = -60 \text{ dB},$$

where $V = 2.2$ cm^3 is the blood volume in the artery covered by the ultrasonic beam ($a_t = 7.5$ mm) and $\delta = 2 \cdot 10^{-14}$ cm^2 is the equivalent cross-section of scattering of erythrocyte for a frequency of 5 MHz [18]. The detectability condition (26b) becomes $|-58 \text{ dB} + R(ka)| < |-60 \text{ dB}|$, hence the inequality $R(ka) > -2$ dB results. Considering relation (11), the value $ka = 1.4$ can be found for $R(ka) = -2$ dB from the curve in Fig. 3. It follows therefore that at a frequency of 5 MHz single gas bubbles with a radius greater than $a_d = 70$ μm can be detected.

10. Conclusions

The analysis and calculations performed here show that in the anatomical case considered (elbow vein – vena basilica), when a typical ultrasonic Doppler device is used at a frequency of 8 MHz, even a single gas bubble with a radius greater than 1.6 μm gives a signal received by an electronic device. This signal, however, is masked by signals caused by wave scattering in blood. Moreover, the bubble with so small a radius is unstable. The level of the signals scattered in blood (B in Fig. 6) is equal to the level of the signal from a single gas bubble with a radius of 16 μm ($ka = 0.5$). Thus single gas bubbles with a radius greater than 16 μm are detectable. Bubbles with a minimum radius of 11 μm lying at the stability limit are detectable when their density exceeds 35 cm^{-3}.

In the case of the pulmonary artery the frequency of the ultrasonic wave should be decreased in view of the overlarge attenuation in tissue. It was shown that when a frequency of 5 MHz is used, single gas bubbles with radii greater than 70 μm are detectable.

It is interesting to note that this is the necessary but not sufficient detectability condition, since detection of a signal above the level of distortions requires some difference between these levels and the probability of detection of gas bubbles increases as this difference increases.

The values of the radius and density of detectable gas bubbles obtained here depend on dimensions and position of the blood vessel in which measurements are taken, on the kind of tissue penetrated by the ultrasonic beam and on the electronic and acoustic parameters of the ultrasonic equipment used.

For simplification it was assumed in the present analysis that the acoustic pressure distribution in the near field of the ultrasonic beam was uniform and equal to the mean value for the beam cross-section. In practice local minima and maxima of the acoustic pressure occur in the beam; these maxima being theoretically twice as large as the mean value mentioned. This value can cause variations in the signal received from the gas bubbles as it crosses with the blood flow the successive minima and maxima in the beam.

The present calculation procedure permits the estimation in a specific case of the detectability of gas bubbles in blood and also the estimation of the level of signals received from blood with respect to electronic noise of the device. This makes possible the optimization of the technological conditions of electronic and acoustic devices for investigations of blood flows and for detection of gas bubbles in blood.

The present calculations have to a large extent the nature of an estimation and therefore the results should be regarded as approximate. Although these results apply to continuous wave Doppler equipment, their extension to pulse equipment does not offer difficulties.

References

[1] J. BLITZ, *Fundamentals of ultrasonic*, Butterworths, London 1967.

[2] W. COAKLEY, W. NYBORG, *Cavitation; Dynamics of gas bubbles; Applications*, (Ultrasound, F. FRY, ed.), Part I, Chapter II, Elsevier, Amsterdam 1978, p. 79.

[3] B. FAY, *Numerische Berechung der Beugungsversluste im Schallfeld von Ultraschallwandlern*, Acustica, **36**, 209-213 (1976/77).

[4] L. FILIPCZYŃSKI, *Ultrasonic characterization of tissues in cardiology*, Archives of Acoustics, **8**, 1, 83-93 (1983).

[5] L. FILIPCZYŃSKI, R. HERCZYŃSKI, A. NOWICKI, T. POWAŁOWSKI, *Blood flows — hemodynamics and ultrasonic Doppler measurement methods* (in Polish), PWN, Warsaw 1980.

[6] L. FILIPCZYŃSKI, G. ŁYPACEWICZ, *Dependence between the Q-value of piezoelectric transducers loaded acoustically and the electromechanical coupling coefficient*, Proceedings of Vibration Problems, Warsaw, **10**, 2, 213-229 (1969).

[7] S. GOSS, E. JOHNSTON, F. DUNN, *Comprehensive compilation of empirical ultrasonic properties of mammalian tissues*, J. Acoust. Soc. Am., **64**, 2, 423-457 (1978).

[8] GRIMSEHL TOMASCHEK, *Lehrbuch der Physik*, Band I. Teubner, Leipzig 1942, p. 269.

[9] I. MALECKI, *Theory of waves and acoustic systems*, PWN, Warsaw 1964.

[10] H. MEDWIN, *Counting bubbles acoustically: a review*, Ultrasonics, **15**, 1, 7-13 (1977).

[11] P. MORSE, K. INGARD, *Theoretical acoustics*, McGraw Hill, New York 1968, p. 425.

[12] R. NISHI, *Ultrasonic detection of bubbles with Doppler flow transducers*, Ultrasonics, 173-179 (July 1972).

[13] A. NOWICKI, J. REID, *Dynamic ultrasonic visualization of blood vessels and flows*, Archives of Acoustics, **7**, 3-4, 225-245 (1983).

[14] M. O'DONNOLL, J. MIMBS, J. MILLER, *Relationship between collagen and ultrasonic backscatter in myocardial tissue*, J. Acoust. Soc. Am., **69**, 2, 580-588 (1981).

[15] P. RUSZCZEWSKI, J. ETIENNE, A. NOWICKI, *A method for detection of gas bubbles in blood* (in Polish), Bezpieczeństwo Pracy, CIOP, Warsaw, **10**, 14-18 (1981).

[16] S. N. RSHEVKIN, *Lectures on theory of sound* (in Russian), Moscow 1960, p. 272.

[17] R. SIGELMANN, J. REID, *Analysis and measurement of ultrasound backscattering from an ensemble of scatterers excited by sinewave bursts*, J. Acoust. Soc. Am., **53**, 1351-1355 (1973).

[18] K. SHUNG, R. SIGELMANN, J. REID, *Scattering of ultrasound by blood*, IEEE Transactions on Biomedical Eng., **23**, 460-467 (1976).

[19] M. SPENCER, *Decompression limits for compressed air determined by ultrasonically detected blood bubbles*, J. Appl. Physiology, **40**, 2, 229-235 (1976).

[20] M. SPENCER, H. CLARKE, *Precordial monitoring of pulmonary gas embolism and decompression bubbles*, Aerospace Medicine, **43**, 7, 762-767 (1972).

Received on September 17, 1981; revised version on July 1, 1982.

ARCHIVES OF ACOUSTICS
8, 1, 31-40 (1983)

THE EFFECT OF THE MODULATION TRANSFER FUNCTION ON THE IMAGE IN AN ACOUSTIC MICROSCOPE

JERZY LITNIEWSKI

Department of Ultrasound, Institute of Fundamental
Technological Research, Polish Academy of Sciences
(00-049 Warsaw, ul. Świętokrzyska 21)

This paper considers the effect of the diffraction phenomenon and of errors in the geometry of the system on the quality of images obtained using a scanning acoustic microscope working in transmission. An analysis of image formation is presented, permitting the derivation of the formula for the modulation transfer function (MTF). The effect of nonaxial and out-of-parallel elements of the system on the symmetry of this function with respect to zero frequency is determined. The paper also shows microscopic images obtained from numerical simulation for two selected objects with different magnitude of deviation from the symmetry of the function MTF.

The shape of the function MTF for a system working at a relatively low frequency of 3 MHz was also determined experimentally and compared with the shape expected according to the theoretical formula derived in this paper. Satisfactory agreement was observed.

1. Introduction

The development of the acoustic microscope significantly extended the possibility of using ultrasonic waves for investigation of small biological objects, surfaces of materials and integrated elements. Taking advantage of the relatively large transmittivity of ultrasonic waves even at very high frequencies, it is now possible to construct visualization devices with resolution comparable to that of light microscopes (1 μm).

Interpretation of acoustic images is to a large extent related to their quality described by the modulation transfer function for a given acoustic system. This function describes how the process of image formation affects changes in the amplitude of spatial frequencies involved in the functions describing

the object. The shape of the MTF gives an insight into the fidelity with which information contained in the image is reproduced. It depends on diffraction effects, lens transmission, aberration, irregular attenuation and on the geometry of the acoustic system.

The aim of the present paper is to describe theoretically the formation of an image in an acoustic microscope working in transmission and to discuss the effect of the frequency transmission function on the resultant image.

2. Image formation in an acoustic scanning microscope

The acoustical part of the scanning microscope can with good approximation be regarded as a system of two thin lenses working in a confocal setting (Fig. 1). The lenses can be assumed to be thin (which, as a matter of fact, they are not), since this only neglects spherical aberration. In practice this aberration is very low, since it depends not only on the numerical aperture of the lens but also on the inverse of the square of the refraction coefficient [4] which is very large ($n = 7.4$) in the case of materials used in this imaging technique.

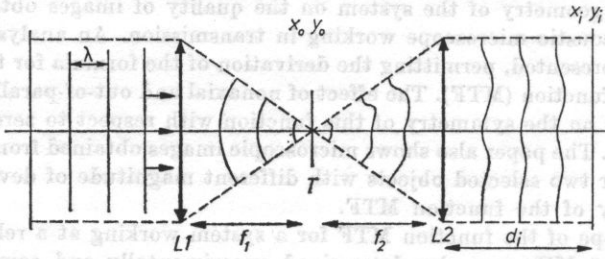

Fig. 1. A schematic diagram of the system of the acoustic scanning microscope

It can be assumed that a plane continuous ultrasonic wave with the length λ is incident on the lens L_1 and is focussed in the plane of the object. The object is scanned in the plane X_0Y_0. The origin of the coordinate system related to the plane lies in the focus of two lenses. Let the function $T(x_0, y_0)$ describe the effect of the object on the ultrasonic wave propagating through it, determining the transmittivity of the amplitude by the object. When the pressure distribution preceding the passage of the wave through the object is defined as $U(x_0y_0)$, the wave leaving the object can be written as [1]

$$U_p(x_0, x_0) = U(x_0, y_0)\, T(x_0, y_0). \tag{1}$$

The independence of transmission from the incidence angle of the wave is assumed here.

The wave U_p is subsequently collected by the lens L_2 and as a pseudo-plane wave falls onto the receiver, a transducer placed in the plane X_iY_i. The

response of the transducer is proportional to an integral over its surface of the pressure field of the wave multiplied by the response function of the transducer. The response function of the transducer corresponds to the pressure distribution on the surface of the transducer caused by supplying to its electrodes a voltage with unitary amplitude. The voltage collected from the transducer serves in controlling the brightness of the corresponding points on the screen of the receiver. The position of these points should correspond to the values of the coordinates $(\bar{x}, \bar{y})$ which the centre of the system X_0Y_0 has in the coordinates XY related to the object being scanned (Fig. 2).

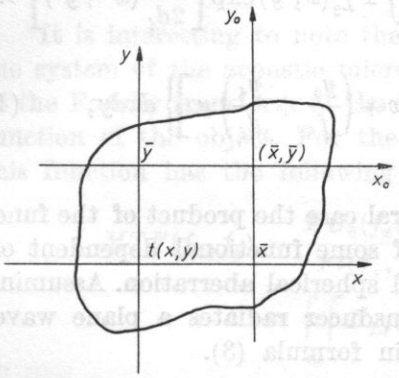

Fig. 2. Coordinate systems related to the object being scanned and to the axis of symmetry of the acoustic system

$\bar{x}, \bar{y}$ – the coordinates of the centre of the system related to the axis in coordinates related to the object, $t(x, y)$ – the object in coordinates related to the object, $T(x_0, y_0) = t(\bar{x}+x_0, \bar{y}+y_0)$ – the object in coordinates related to the axis of the system

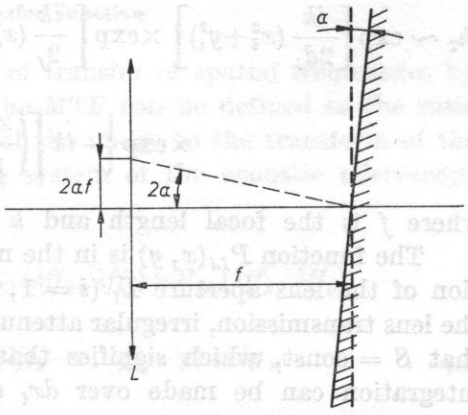

Fig. 3. A schematic diagram of the system fo measurement of the MTF

Using the known principle of image formation [1], the introduction of the function $h_3(x_0, y_0)$ permits the formulation of the following integral expression for the spatial distribution of voltage which constitutes an image of the object

$$U_0(\bar{x}, \bar{y}) = \iint_{\infty} h_3(x_0 y_0)\, U(x_0, y_0)\, t(\bar{x}+x_0, \bar{y}+y_0)\, dx_0 dy_0,$$
$$t(\bar{x}+x_0, \bar{y}+y_0) := T(x_0, y_0), \tag{2}$$

where the function $h_3(x_0, y_0)$ defines the magnitude of the voltage appearing on the transducer caused by the placing of the point source of the wave in the point (x_0, y_0). The function $h_3(x_0, y_0)$ can be found to be

$$h_3(x_0, y_0) = \iint_{\infty} h_2(x_i, y_i, x_0, y_0)\, P_p(x_i, y_i)\, S(x_i, y_i)\, dx_i dy_i, \tag{3}$$

where h_2 describes the pressure distribution in the plane of the transducer, P_p defines the aperture of the transducer and S is its response function. It seems justified to assume that the beam of the incident energy is completely focussed on the surface of the transducer, which permits it to take $P_p(x_i, y_i) = 1$. The function h_2 can be found by placing the point source in a point with the coordinates x_0, y_0. Consideration of the phase shift caused by the lens and the use of the Fresnel diffraction formulae permit the determination of the pressure distribution from this source in the plane of the transducer [1]. For the present system this distribution is given by the formula

$$h_2 \sim \exp\left[\frac{ik}{2d_i}(x_i^2+y_i^2)\right] \times \exp\left[\frac{ik}{2_f}(x_0^2+y_0^2)\right] \int\int_{\infty} P_{L_2}(x, y) \exp\left[\frac{ik}{2d_i}(x^2+y^2)\right] \times$$

$$\times \exp\left\{-ik\left[\left(\frac{x_0}{f}+\frac{x_i}{d_i}\right)x+\left(\frac{y_0}{f}+\frac{y_i}{d_i}\right)y\right]\right\} dxdy, \qquad (4)$$

where f is the focal length and $k = 2\pi/\lambda$.

The function $P_{Li}(x, y)$ is in the most general case the product of the function of the lens aperture L_i $(i = 1, 2)$ and of some functional dependent on the lens transmission, irregular attenuation and spherical aberration. Assuming that $S = \text{const}$, which signifies that the transducer radiates a plane wave, integration can be made over dx_i and dy_i in formula (3).

This gives in effect

$$h_3(x_0, y_0) \sim \exp\left[\frac{ik}{2f}(x_0^2+y_0^2)\right] FP_{L_2}\left(\frac{x_0}{\lambda_f}, \frac{y_0}{\lambda_f}\right), \qquad (5)$$

where $FP(x, y)$ corresponds to a Fourier transform of the function P made at a point with the coordinates (x, y). The smallness of the area of non-zero value of FP_{L2} [1] permits one to take the oscillating factor as constant.

In a way analogous to (4) it is possible to determine the quantity $U(x_0, y_0)$, i.e. the pressure distribution from the transmitting transducer determined just before the scanning plane. It can be assumed that a plane wave is incident on L_1, which is equivalent to the placement of the point source in infinity $(f \to \infty)$. Adequate substitution in formula (4) $(d_i = f, P_{L2} = P_{L1})$ gives

$$U(x_0, y_0) \sim \exp\left[\frac{ik}{2f}(x_0^2+y_0^2)\right] FP_{L1}\left(\frac{x_0}{\lambda f}, \frac{y_0}{\lambda f}\right). \qquad (6)$$

For the same reasons as in (5) the oscillating factor before FP_{L1} in (6) can be regarded as constant. Insertion of (5) and (6) into (2) now gives an expression describing an image of the object $t(x, y)$, i.e. the voltage distribution taken from the transducer, depending on the position of the object with respect to

the focus of the system.

$$U_0(\bar{x}, \bar{y}) \sim \iint_{\infty} FP_{L1}\left(\frac{x_0}{\lambda f}, \frac{y_0}{\lambda f}\right) FP_{L2}\left(\frac{x_0}{\lambda f}, \frac{y_0}{\lambda f}\right) t(\bar{x}+x_0, \bar{y}+y_0)\, dx_0 dy_0$$

$$\Leftrightarrow U_0(\bar{x}, \bar{y}) \sim t(\bar{x}, \bar{y}) * \left(FP_{L1} \cdot FP_{L2}\left(\frac{\bar{x}}{\lambda f}, \frac{\bar{y}}{\lambda f}\right)\right), \tag{7}$$

where $*$ signifies the operation of correlation of the function.

3. Modulation transfer function

It is interesting to note the manner of transfer of spatial frequencies by the system of the acoustic microscope. The MTF can be defined as the ratio of the Fourier transform of the function of the image to the transform of the function of the object. For the scanning system of the acoustic microscope this function has the following form

$$MTF(f_x, f_y) = \frac{FU_0(f_x, f_y)}{Ft(f_x, f_y)} \sim P_{L1}(\lambda f f_x, \lambda f f_y) \times P_{L2}(\lambda f f_x, \lambda f f_y)$$

$$= \iint_{\infty} P_{L1}(x, y) P_{L2}(\lambda f f_x - x, \lambda f f_y - y)\, dx dy, \tag{8}$$

where $\times$ signifies convolution and f_x, f_y are spatial frequencies.

It is particularly easy to determine an explicit form of the MTF in the case of two identical lenses with a circular aperture, without aberration and transmission independent of the incidence angle. In this case the MTF is a convolution of two identical functions of the form

$$\operatorname{circ}\left(\frac{\sqrt{f_x^2+f_y^2}}{l/2\lambda f}\right) := \begin{cases} 1 & \text{for } f_x^2+f_y^2 \leqslant (l/2\lambda f)^2; \\ 0 & \text{for } f_x^2+f_x^2 > (l/2\lambda f)^2, \end{cases}$$

where l is the diameter of the lens, λ is the wavelength in the medium surrounding the lens and f is the focal length of the lens.

The operation of convolution gives

$$\mathrm{MTF}(\varrho) = \begin{cases} \dfrac{2}{\pi}\left[\arccos\left(\dfrac{\varrho\lambda f}{l}\right) - \dfrac{\varrho\lambda f}{l}\left(1-\dfrac{\varrho\lambda f}{l}\right)^{1/2}\right] & \text{for } \varrho \leqslant \dfrac{1}{\lambda f}, \\ 0 \quad \text{for } \varrho > \dfrac{l}{\lambda f}, \end{cases} \tag{9}$$

$\varrho = (f_x^2+f_y^2)^{1/2}$ is the radius in the frequency space. Thus, in an ideal case, considering only the diffraction phenomena, the maximum frequency carried by the microscope system is equal to $l/\lambda f$.

4. Measurement of the modulation transfer function

The value of the MTF resulting from formula (8) derived here will now be compared with the values obtained experimentally using the method proposed in paper [5]. This method takes advantage of the fact that theoretically the system in Fig. 1 is equivalent to a system in which a reflecting plate would be placed in the focal plane of the lenses and in which the transducer 1 and the lens L_1 would work in a transmit-receive arrangement (Fig. 3). Under the assumption of non-dependence of the reflected amplitude on the incidence angle, this plate can be described as $t(x, y) = \text{const}$.

The use of formula (7) defining the relation between the image and the object gives the following expression for the image of the plate

$$U_0(\bar{x}, \bar{y}) = \iint_{\infty} FP_{L1}\left(\frac{x_0}{\lambda f}, \frac{y_0}{\lambda f}\right) FP_{L2}\left(\frac{x_0}{\lambda f}\frac{y_0}{\lambda f}\right) \text{const}\, dx_0 dy_0. \tag{10}$$

Since this quantity is not dependent on the coordinates $\bar{x}, \bar{y}$, only one point of the image can be considered further. The Parseval equation [2] permits the transformation of expression (10) to the form

$$U_0 \sim \iint_{\infty} P_{l1}(x, y) P_{L1}(-x, -y)\, dxdy. \tag{11}$$

It can now be assumed that the plate was deflected from the X axis by a small angle α_x. This causes a change in the path of the reflected beam by $2\alpha_x$. It can be assumed for small deflections that the pressure field of the beam reflected before the lens L_1 is shifted along the X axis by $2\alpha_x f$ with respect to the field for $\alpha_x = 0$. This is equivalent to a shift of the lens L_1 working in the collecting mode by the same value.

In such a case

$$U_0(\alpha_x, \alpha_y = 0) \sim \iint_{\infty} P_{L1}(x, y) P_{L1}(2\alpha_x f - x, -y)\, dxdy. \tag{12}$$

When formula (8) is written for $f_y = 0$ and compared with (12), it becomes evident that [5]

$$\text{MTF}(f_x, 0) \sim U_0(\alpha_x, 0), \quad f\lambda f_x = 2\alpha_x f.$$

It follows therefore that the spatial frequency $f_x = 2\alpha_x/\lambda$ corresponds to the angle α_x. Obviously, an analogous case occurs with deflection from the Y axis and with the frequency f_y. This provides a simple method for the measurement of the MTF of a given system of the acoustic microscope.

MTF measurements using the above method were carried out for a microscope system working at low frequency (3 MHz). A highly damped ceramic transducer gave an almost plane ultrasonic wave which was incident on a poly-

styrene lens with a focal length in water equal to 210 mm. An aluminium plate whose inclination with respect to the axis of the system could be changed was placed in the focus. A defectoscope was used as a transmit-receive system. Fig. 4 shows the experimentally determined transfer function of spatial frequencies in this system. Fig. 4 also shows the theoretical curve calculated from formula (9) which accounts only for the diffraction effects. A circle with its diameter equal to that of the transducer, $l = 47$ mm, was taken as the active aperture of the lens. The length of the wave at a frequency of 3 MHz in water is 0.5 mm.

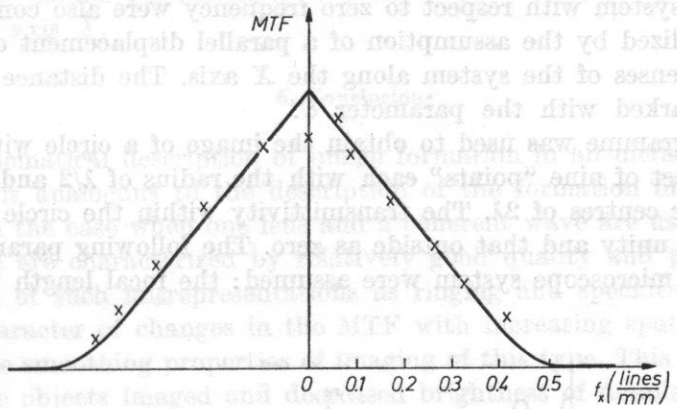

Fig. 4. The curve of MTF for the system of the acoustic microscope working at a frequency of 3 MHz

solid line – theoretical curve, points * correspond to experimentally determined MTF

These curves are only proportional to the measured and calculated MTF functions. Therefore, their comparison with each other is useful only when the comparison involves their total bandwith of the frequency carried and the ratio of amplitudes at different frequencies for the same curve. The measured function MTF is shifted with respect to the origin of the system. This was probably caused by some imprecision in the setting of $\alpha_x = 0$.

In the case of the acoustic microscope working in transmission this effect can be caused by errors in the technology of preparing the lens material and by imprecision in the geometry of the system.

A parallel shift of the axis of the transmitting lens by the distance R with respect to the axis of the receiving lens causes the field incident on this lens to be shifted with respect to it by R from the axial arrangement. Using the expression for the MTF (8) it is possible to calculate that this gives a shift of this function by $R/\lambda f$ in the spatial frequency domain.

A similar case occurs when the transmitting transducer is set so that it radiates a wave at the angle α to the axis of the lens. In this case the use of (8)

permits the determination of the shift of MTF by the quantity $2a/\lambda$. Obviously, these relations can only be valid for small deflections, so small that it can be assumed that the field distributions are only shifted.

5. The effect of the function MTF on the image

In order to evaluate the effect of the function MTF on the image a computer programme was developed, which using formula (7) permitted a simulation of the imaging process occurring in the acoustic microscope with a circular aperture. The diffraction phenomenon and the possibility of a shift of the MTF of the system with respect to zero frequency were also considered. This shift was realized by the assumption of a parallel displacement of the optical axes of the lenses of the system along the X axis. The distance between the axes was marked with the parameter C.

The programme was used to obtain the image of a circle with the radius of 7λ and a set of nine "points" each with the radius of $\lambda/2$ and the distance between their centres of 2λ. The transmittivity within the circle or the point was taken as unity and that outside as zero. The following parameters of the lenses of the microscope system were assumed: the focal length 75 λ and the

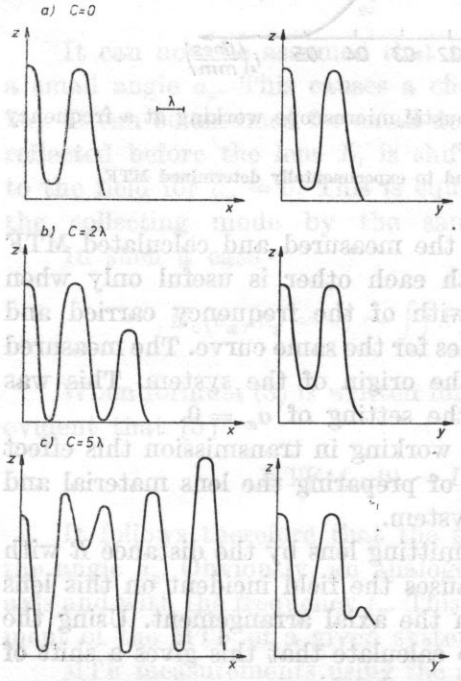

Fig. 5. Sections of the image of a circle obtained for different values of the parameter C

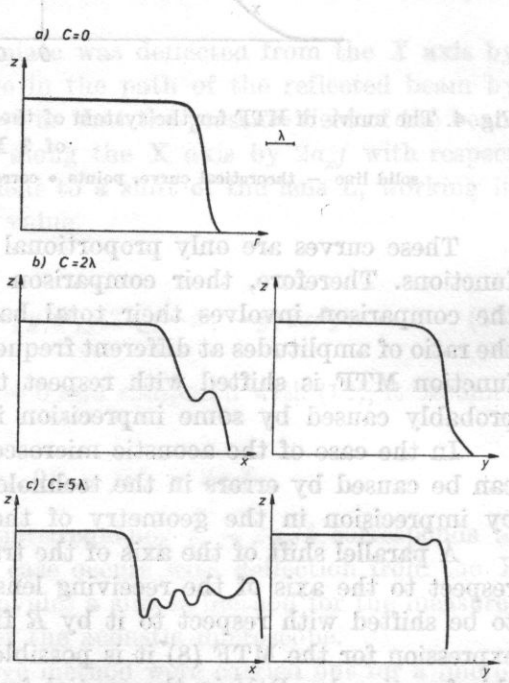

Fig. 6. Sections of images of a system of points obtained for different values of the parameter C

lens diameter 100 λ. Figs. 5 and 6 shows sections of the objects and their images along the axes X and Y. The centre of the coordinate system XY is placed in the centre of symmetry of the image. The sections are symmetrical with respect to the axis Z.

The diffraction effect ($C = 0$) causes blurred edges of the images of the order of the wavelength. Displacement of the lenses causes this blur to extend along the shift axis. The resolution of the system depends on the axis along which it is measured. A circular object gives an elliptic image with irregular brightness. In the case of points the displacement of the axes of the lenses causes additional brightenings to appear in the image, which will be interpreted as additional points. An increased number of points appears in the direction of the shift axis X.

6. Conclusions

A mathematical description of image formation in an ultrasonic scanning microscope is analogous to the description of the formation of the image of an object in the case when one lens and a coherent wave are used [1]. Images of this type are characterized by relatively good quality and particularly by the absence of such misrepresentations as ringing and speckles.

The character of changes in the MTF with increasing spatial frequencies indicates the smoothing properties of imaging of this type. This causes blurred edges of the objects imaged and decreased brightness of details.

In view of errors in the geometry of the acoustic microscope system, its MTF can be nonsymmetrical with respect to the zero spatial frequency. This is a source of numerous misrepresentations in the image. In such cases objects with constant distribution of acoustical parameters show irregular brightness and their edges are differently blurred. This causes a distortion of the image, introduces misinformation and worsens resolution. It seems that the nonsymmetricity of MTF accounts well enough for unexpected darkenings which often occur in images obtained using the acoustic microscope.

The function of the pulse response of the transducer, S, has a large effect on the image. In real systems it is not constant on the surface of the transducer, which was assumed in the present calculations. This can be another source of distortions in the image.

The images obtained numerically for cases of different geometry of the system of the acoustic microscope permit the determination of admissible geometry errors. Coaxiality of the lenses better than the wavelength and out-of-parallelness of the axes of the lenses below $1/3°$ should eliminate one of the major reasons for distortions in the image. Interpretation of acoustical images using the acoustic microscope requires the use of the MTF. It seems that for this purpose it is possible to use an MTF with a shape determined experimentally by means of such a simple and approximate method as the present one.

References

[1] J. W. GOODMAN, *Introduction to fourier optics*, McGraw Hill, New York 1968.

[2] Hwej P. HSU, *Fourier analysis*, Simon and Schuster, New York 1970.

[3] H. K. WICKRAMASINGHE, *Contrast and imaging performance in the scanning acoustic microscopy*, Journal of Applied Pfysics, **50**, 2, 664-672 (1979).

[4] R. A. LEMONS, *Acoustic microscopy by mechanical scaning*, Internal Memorandum, The J. A. Hartford Foundation, Stanford 1975.

[5] A. ATALAR, *Modulation transfer function for the acoustic microscopy*, Electronic Letters, **15**, 11, 321-323 (1979).

Received on July 27, 1981; revised version on September 2, 1982.

ARCHIVES OF ACOUSTICS
8, 1, 41-54 (1983)

THE COEFFICIENT OF REFLECTION OF ULTRASONIC WAVES FROM AN ADHESIVE BOND INTERFACE

ALEKSANDER PILARSKI

Institute of Fundamental Technological Research, Polish Academy of Sciences
(00-049 Warszawa, ul. Świętokrzyska 21)

This paper reports on an attempt to explain the existence of a relation between the reflection coefficient and mechanical strength of an adhesive bond, based on a model of a bond with finite rigidity. On the basis of formulae derived, a correlation relation was determined from experimental results between the modulus of the pressure reflection coefficient of a plane ultrasonic wave incident normal to the interface of an adhesive bond of lucite with epoxy resin, and the tensile strength of the bond.

Notation

A_p, A_0, B – displacement amplitudes, respectively, of incident, reflected and transmitted waves
c_i – propagation velocity of ultrasonic waves in the ith medium
f – frequency of ultrasonic wave
g – thickness
K – bond rigidity
$\bar{r}_{21}$ – complex pressure reflection coefficient
$(r_{21})_0$ – pressure reflection coefficient for $K = \infty$
R_0 – tensile strength
t – time
u_i – displacement in the direction of the x axis in the $i$the medium
x – attenuation over one wavelength
Z_i – characteristic acoustic impedance in the ith medium
$\bar{Z}_i$ – complex characteristic acoustic impedance in the ith medium
α – attenuation coefficient
σ_i – stress in the ith medium
σ_g – stress at the interface
λ_i, μ_i – Lamé constants
ω – angular frequency
ϱ_i – density of the ith medium

1. Introduction

One of the possible ways of evaluating adhesive strength (degree of adhesion) of layered joints by ultrasonic methods consists in measurement of the pressure coefficient of the reflection of a plane ultrasonic wave incident normal to the bond interface [1]. The results of a number of papers [2-4] indicate the presence of a relation between the reflection coefficient and mechanical strength of a bond developed using different techniques (explosive welding, rolling, gluing etc.). The authors of these papers give correlations for specific bonds obtained from results of strength (destructive) tests and ultrasonic investigations. The present paper reports on an attempt to explain changes in the reflection coefficient accompanying changes in adhesive bond quality, based on a model of a bond with finite rigidity.

2. Complex reflection coefficient

Acoustically, adhesive bonds are characterized by a boundary surface on which a step-like change occurs in characteristic acoustic impedance (Fig. 1a). In practice, this class of bonds also includes, in addition to those with a distinct boundary such as e.g. some bimetals or glue-and-metal bonds, those involving a thin intermediate layer, caused, for example, by diffusion processes,

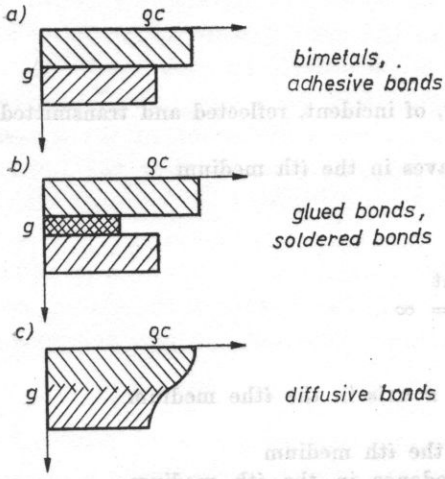

Fig. 1. A division of layered bonds from the acoustical point of view

whose thickness, however, is much less than the length of the ultrasonic wave incident on the boundary. Another group of layered bonds consists of those which involve a layer with thickness comparable to the length of the wave used and with characteristic acoustic impedance distinctly different from that of the materials bound (Fig. 1b). This group includes, for example, glued or

soldered bonds. In investigations of these bonds, a distinction is made between problems related to cohesive strength, i.e. the strength of the binding layer itself, and adhesive strength, which is a measure of the degree of adhesion of elements bound to a binder. The other problem corresponds to the first group of bonds, the so-called adhesive bonds. Finally, a third group consists of diffusive bonds which involve a smooth change in acoustic properties at a thickness comparable to the wavelength.

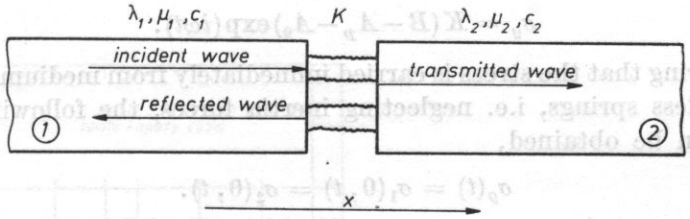

Fig. 2. A model of the interface of an adhesive bond
ϱ_i – density, c_i – ultrasonic wave propagation velocity, λ_i and μ_i – Lamé constants

Fig. 2 shows schematically the model of an adhesive bond interface in which vibration are carried from medium 1 to medium 2 by weightless springs with equivalent rigidity K [N/m³] per unit area. The assumption of a finite value of the rigidity K permits a modification in boundary conditions, allowing a displacement jump Δu caused by the current stress σ_g at the interface of the media [9]

$$\sigma_g = K\Delta u. \tag{1}$$

When the displacements u_1 and u_2 (in the direction of the x axis) in the two media for a plane wave propagating in the positive direction of the x axis are expressed with the formulae

$$u_1 = A_p \exp[i\omega(t-x/c_1)] + A_0 \exp[i\omega(t+x/c_1)],$$
$$u_2 = B\exp[i\omega(t-x/c_2)], \tag{2}$$

where A_p, A_0 and B are displacement amplitudes, respectively, of incident, reflected and transmitted waves; and are subsequently related to the stresses σ_1 and σ_2 by the relations

$$\sigma_i = (\lambda_i + 2\mu_i)\frac{\partial u_i}{\partial x}, \quad i = 1, 2, \tag{3}$$

and considering that

$$Z_i = (\lambda_i + 2\mu_i)/c_i;$$

the displacement jump Δu at the interface ($x = 0$) can be given by

$$\Delta u = u_2(0, t) - u_1(0, t) = (B - A_p - A_0)\exp[i\omega t], \tag{4}$$

while the stresses in media 1 and 2 can be expressed in the following way

$$\sigma_1 = -i\omega Z_1 A_p \exp\left[i\omega\left(t-\frac{x}{c_1}\right)\right] + i\omega Z_1 A_0 \exp\left[i\omega\left(t+\frac{x}{c_1}\right)\right],$$

$$\sigma_2 = -i\omega Z_2 B \exp\left[i\omega\left(t-\frac{x}{c_2}\right)\right]. \tag{5}$$

According to formula (1), the stress at the interface is

$$\sigma_g = K(B-A_p-A_0)\exp(i\omega t). \tag{6}$$

Considering that the stress is carried immediately from medium 1 to medium 2 by weightless springs, i.e. neglecting inertia forces, the following boundary condition can be obtained,

$$\sigma_g(t) = \sigma_1(0,t) = \sigma_2(0,t). \tag{7}$$

The satisfaction of this condition leads to a system of equations

$$-i\omega Z_1 A_p + i\omega Z_1 A_0 = -i\omega Z_2 B = K(B-A_p-A_0). \tag{8}$$

The pressure reflection coefficient $\bar{r}_{21}$ can be determined from the system of equations (8). This coefficient is the ratio of the pressure amplitude of the reflected wave to the pressure amplitude of the incident wave,

$$\bar{r}_{21} = \frac{Z_2-Z_1-i(\omega Z_1 Z_2/K)}{Z_2+Z_1+i(\omega Z_1 Z_2/K)}. \tag{9}$$

It is a complex form of the reflection coefficient, neglecting wave attenuation in the two media, which is a result, in contrast to classical solutions, of the assumption of discontinuous displacement at the interface. The introduction of the rigidity K with finite value permits consideration of imperfection of a bond. Similar reasoning led the authors of papers [6-8] to the same relation between the reflection coefficient and the rigidity or compliance of a bond.

Transformation of formula (9) gives a relation between the rigidity K and the modulus of the reflection coefficient, $|\bar{r}_{21}|$,

$$K = \omega\left[A+\frac{B}{|\bar{r}_{21}|^2-C}\right]^{1/2}, \tag{10}$$

where

$$A = -[Z_1 Z_2/(Z_1+Z_2)]^2, \quad B = -A[1-(r_{21})_0^2],$$

$$C = (r_{21})_0^2 = [(Z_2-Z_1)/(Z_2+Z_1)]^2, \quad \omega = 2\pi f, \quad f - \text{frequency}.$$

It can be noted that without adhesion ($K = 0$) the modulus of the reflection coefficient is 1, while for $K = \infty$ (an ideal bond)

$$|\bar{r}_{21}| = (r_{21})_0 = (Z_2-Z_1)(Z_2+Z_1).$$

Fig. 3 gives a frequency relation between the bond rigidity K and the modulus of the reflection coefficient $|\bar{r}_{21}|$ calculated from formula (10) for an adhesive bond of epoxy resin ($\varrho = 1.189 \cdot 10^3$ kg/m^3, $c_L = 2650$ m/s) and lucite ($\varrho = 1.182 \cdot 10^3$ kg/m^3, $c_L = 2740$ m/s). It can be seen that at higher frequency a weaking of the bond with respect to an ideal one causes a greater change in the modulus of the pressure reflection coefficient. Moreover, changes in the reflection coefficient, which correspond to frequency changes, are greater for mean values of bond stiffness than for bonds which are either extremely "good" or "bad".

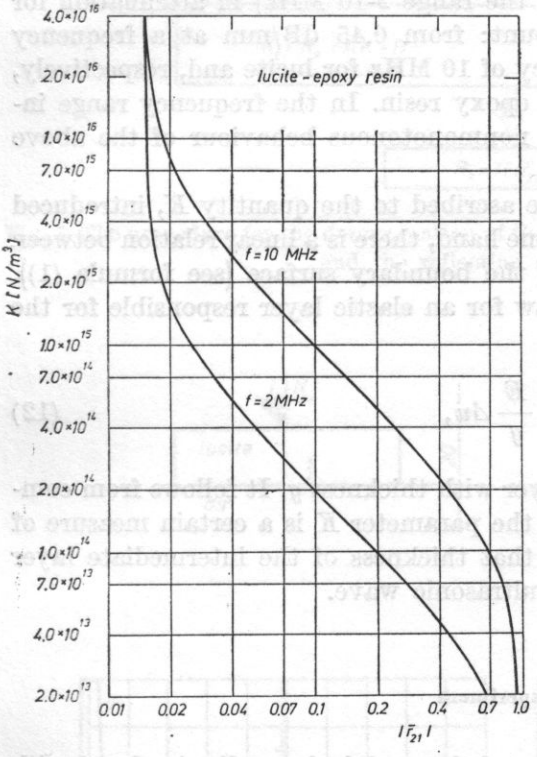

Fig. 3. The frequency relation between bond rigidity and the modulus of the reflection coefficient

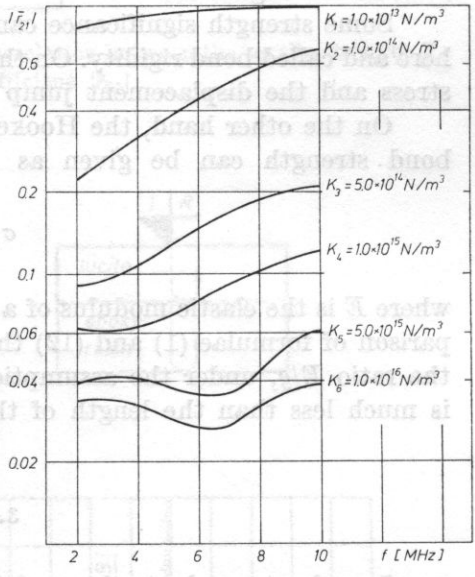

Fig. 4. The frequency dependence of the modulus of the reflection coefficient for different rigidity of a lucite — epoxy resin bond, with consideration of attenuation in materials bound

In terms of the measurement resolution of the coefficient $|\bar{r}_{21}|$ the combination of materials bound is also significant. From this point of view, pairs of materials with close values of characteristic acoustic impedance $(r_{21})_0 \to 0$ are most convenient. Yet, particularly in such cases, additional changes in the value of the reflection coefficient, caused by attenuation changes in the two materials bound as frequency changes, must be expected. These can be noticed

particularly with materials which differ greatly in the attenuation coefficient (by a few orders). These changes can be evaluated by introducing into formula (9) the complex characteristic wave impedances

$$\bar{Z}_i = Z_i/(1+x_i)^2 - ix_1 Z_i/(1+x_i)^2, \quad i = 1, 2; \tag{11}$$

where $x_i = c_i a_i/\omega$ is the attenuation over one wavelength, c_i the propagation velocity of the ultrasonic wave, and a_i is the attenuation coefficient.

Fig. 4 shows results of calculations of the modulus of the reflection coefficient as a function of frequency for some values of the rigidity K of a lucite-epoxy resin bond. Linear changes (in the range 2-10 MHz) in attenuation for both materials were taken into account: from 0.45 dB/mm at a frequency of 2 MHz to 1.0 dB/mm at a frequency of 10 MHz for lucite and, respectively, from 0.88 dB/mm to 2.0 dB/mm for epoxy resin. In the frequency range investigated it is interesting to note a nonmonotonous behaviour of the above relation for higher K.

Some strength significance can be ascribed to the quantity K, introduced here and called bond rigidity. On the one hand, there is a linear relation between stress and the displacement jump at the boundary surface (see formula (1)).

On the other hand, the Hooke law for an elastic layer responsible for the bond strength can be given as

$$\sigma = \frac{E}{g} \Delta u, \tag{12}$$

where E is the elastic modulus of a layer with thickness g. It follows from comparison of formulae (1) and (12) that the parameter K is a certain measure of the ratio E/g, under the assumption that thickness of the intermediate layer is much less than the length of the ultrasonic wave.

3. Experiment

In order to evaluate the usefulness of the model of an adhesive bond with finite rigidity for explanation of the relation between the modulus of the pressure reflection coefficient of an ultrasonic wave incident normal to the interface of two bodies and the strength of their bond, experiments were performed according to the following procedure (Fig. 5):

– Different (mechanical and chemical) preparation of the surface of lucite yielded 29 samples of the adhesive lucite – epoxy resin bond with different degree of adhesion. The shape of the samples is shown in Fig. 7.

– Ultrasonic investigations were performed to determine the modulus of the pressure reflection coefficient of a wave at a frequency of 10 MHz, according to the procedure shown in Fig. 6.

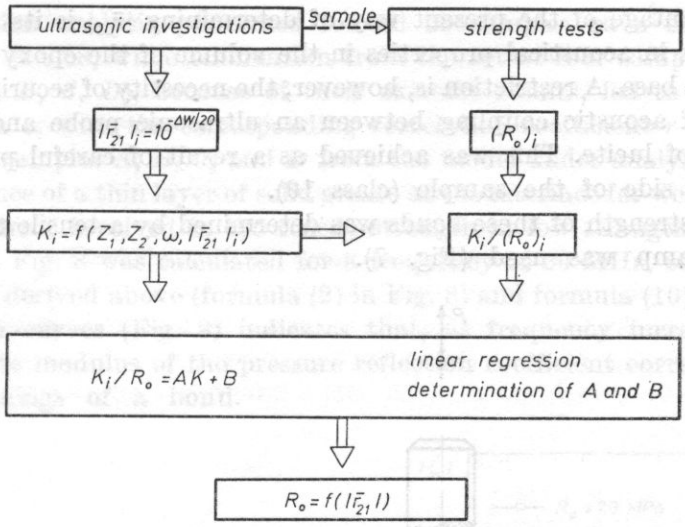

Fig. 5. The procedure for the determination of the correlation between the tensile strength R_0 and the reflection coefficient $|\bar{r}_{21}|$

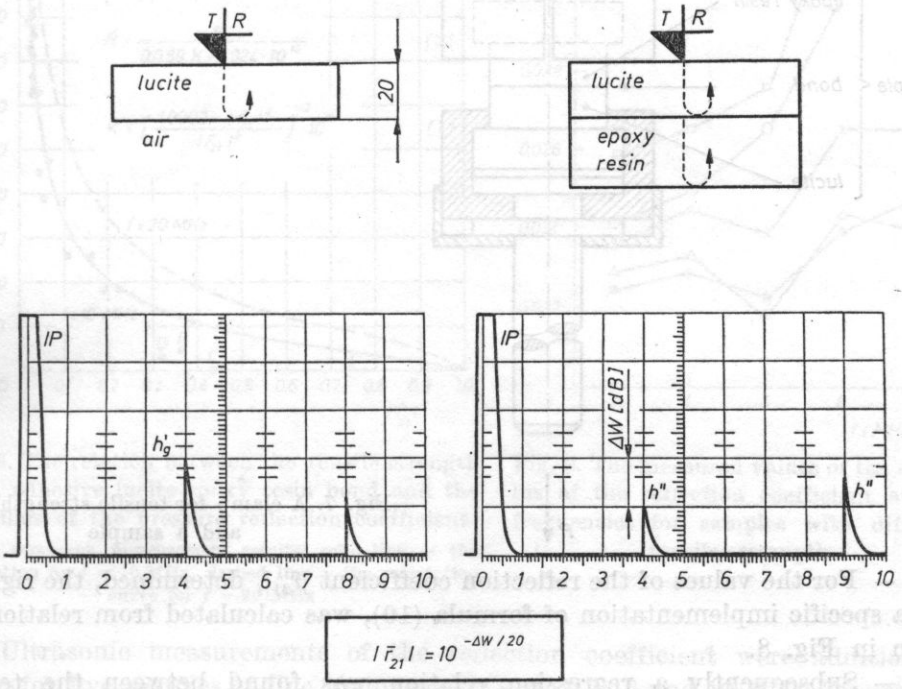

Fig. 6. The procedure for the determination of the modulus of the pressure reflection coefficient of ultrasonic waves $|\bar{r}_{21}|$

An advantage of the present way of determining $|\bar{r}_{21}|$ is its independence from changes in acoustical properties in the volume of the epoxy resin poured on to a lucite base. A restriction is, however, the necessity of securing repeatable conditions of acoustic coupling between an ultrasonic probe and the sample on the side of lucite. This was achieved as a result of careful preparation of the external side of the sample (class 10).

— The strength of these bonds was determined by a tensile test, in which a special clamp was used (Fig. 7).

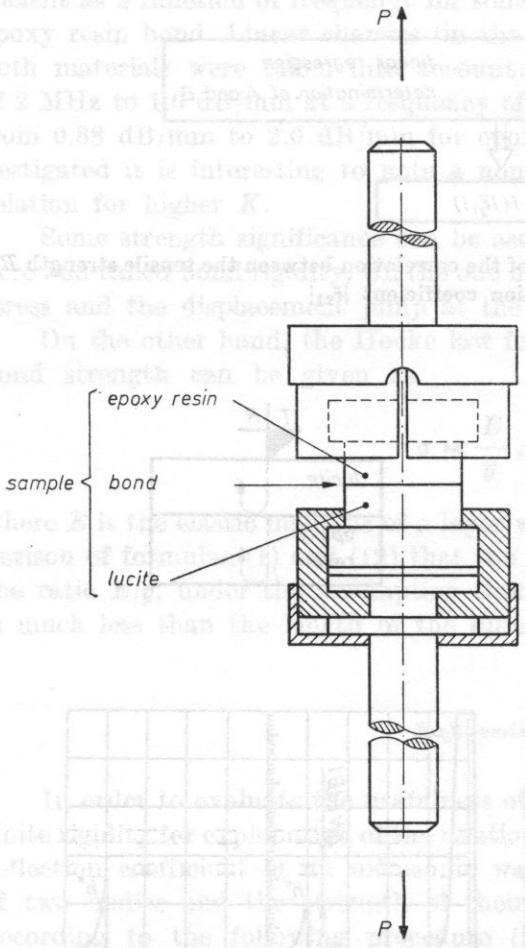

Fig. 7. A clamp for tensile strength tests and a sample

— For the values of the reflection coefficient $|\bar{r}_{21}|_i$ determined, the rigidity K_i, a specific implementation of formula (10), was calculated from relation (1) given in Fig. 8.

— Subsequently a regression relation was found between the tensile strength R_0 and the bond rigidity K, under the assumption of a homographic functional relation between R_0 and K.

Correlation analysis performed for all 29 samples gave the correlation coefficient $r = 0.68$, while elimination from the set of four samples with least strength (A, B, C, D), because of their extreme results, led to the equation given in Fig. 8, with the corresponding correlation coefficient $r = 0.998$. The deviation of samples A, B, C, and D from the model under analysis is justified by the presence of a thin layer of solid grease at the interface for weakest samples and by the error involved in the tensile strength at low strength. The dashed line curve in Fig. 8 was calculated for a frequency of 20 MHz, on the basis of a correlation derived above (formula (2) in Fig. 8) and formula (10). Comparison of these two curves (Fig. 8) indicates that, as frequency increases, greater changes of the modulus of the pressure reflection coefficient correspond to the same weakenings of a bond.

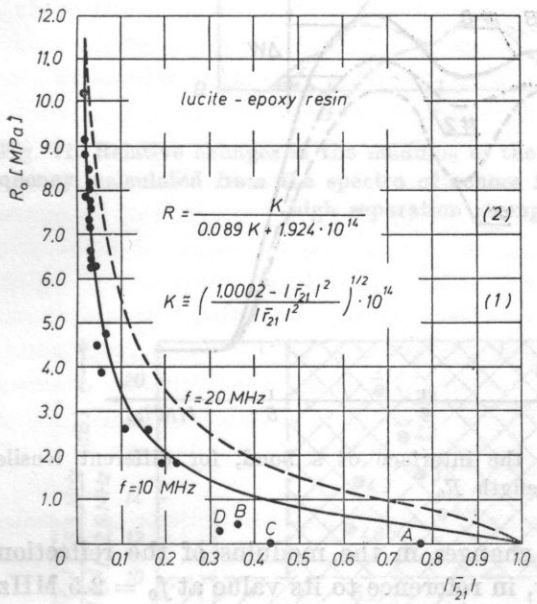

Fig. 8. The relation between the tensile strength of an adhesive lucite-epoxy resin bond and the modulus of the pressure reflection coefficient

points represent measurement results; solid line – the correlation for $f = 10$ MHz, dashed line – the calculation curve for $f = 20$ MHz

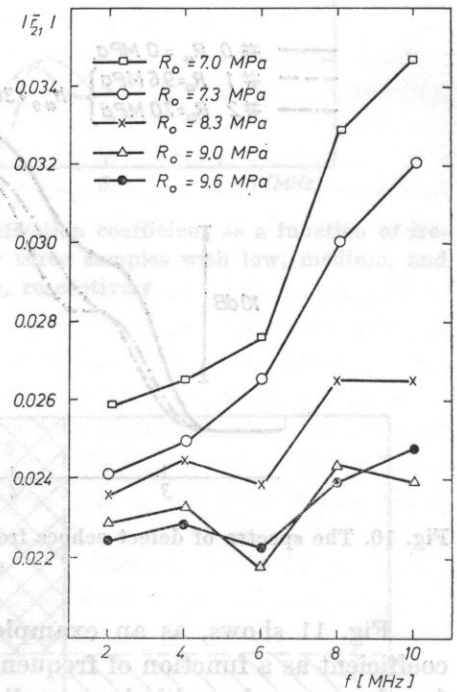

Fig. 9. The measured values of the modulus of the reflection coefficient at five frequencies for samples with different tensile strength

Ultrasonic measurements of the reflection coefficient were additionally taken for five samples at five frequencies, i.e. 2, 4, 6, 8 and 10 MHz. The results of the measurements are given in Fig. 9. Its similarity with Fig. 4 is noteworthy. These results also confirm the thesis that measurement sensitivity increases

as frequency increases. It is also possible to see the nonmonotonous character of changes in the reflection coefficient, depending on frequency for "good" bonds, with corresponding larger K.

In order to investigate the frequency dependence more precisely, on ultrasonic spectral analysis was used. At the Nondestructive Testing Laboratory of the Institute of Machinery Construction (SVUSS) in Prague (Czechoslovakia), measurements were taken on 20 samples of a lucite — epoxy resin bond using an analogue spectral analyzer manufactures by Hewlett Packard. Fig. 10 shows some examples of echoes from interface for two samples with different tensile strength against the background of the spectrum for a "zero" sample, i.e. without connection. On the basis of the spectra obtained, the moduli of the reflection coefficient were calculated at 0.25 MHz intervals over the frequency range 2.5-6 MHz.

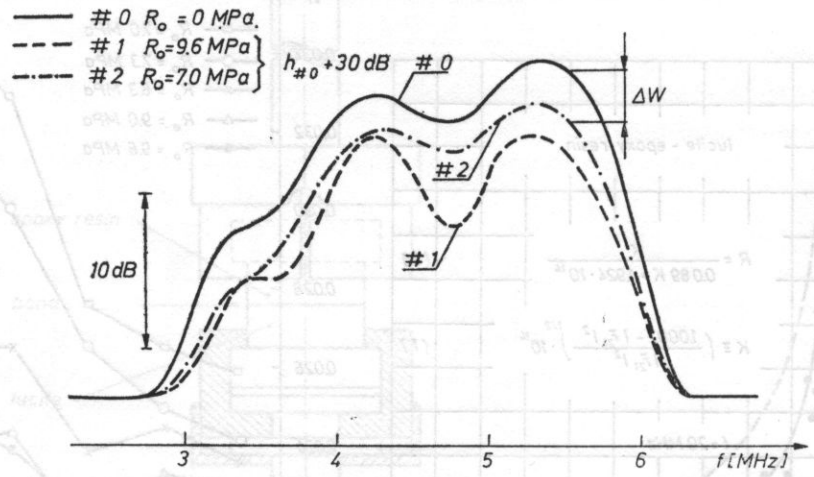

Fig. 10. The spectra of defect echoes from the interface of a bond, for different tensile strength R_0

Fig. 11 shows, as an example, changes in the modulus of the reflection coefficient as a function of frequency, in reference to its value at $f_0 = 2.5$ MHz for three samples with low, medium and high tensile strength, respectively.

Fig. 12, in turn, shows collectively results obtained for all samples in the system: the horizontal axis — the values of the moduli of the reflection coefficient at a frequency of 5.5 MHz, the vertical axis — the difference, in dB, between the values of the reflection coefficient at frequencies of 5.5 MHz, and 2.5 MHz. Respective strength determined in a tensile test was assigned to each point on the curve. Accordingly, three groups of results can be distinguished. The first group consists of high-strength bond samples, with corresponding low values of the moduli of the reflection coefficient and small changes as a function of frequency. The second group is composed of medium-strength

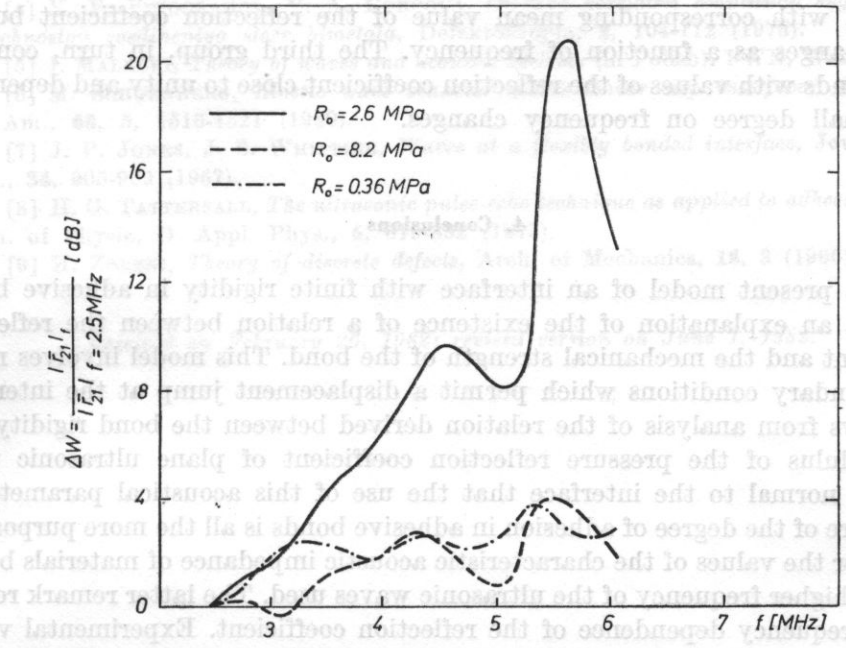

Fig. 11. Relative changes in the modulus of the reflection coefficient as a function of frequency, calculated from the spectra of echoes for three samples with low, medium, and high separation strength, respectively

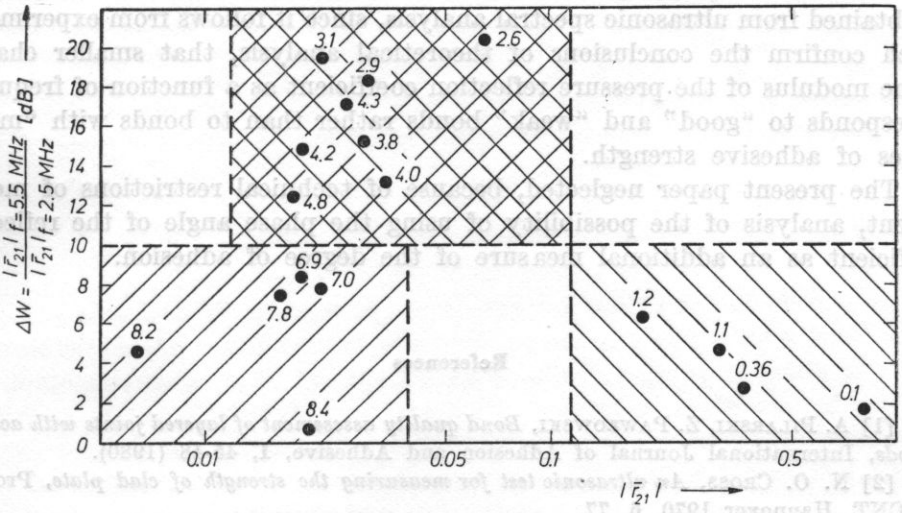

Fig. 12. Moduli of the reflection coefficient $|\bar{r}_{21}|$ at the frequency $f = 5.5$ MHz and the ratio of the moduli $|\bar{r}_{21}|$ at $f = 5.5$ MHz and 2.5 MHz. The figure also shows numerical values of bond tensile strength

samples, with corresponding mean value of the reflection coefficient but its large changes as a function of frequency. The third group, in turn, contains weak bonds with values of the reflection coefficient close to unity and dependent to a small degree on frequency changes.

4. Conclusions

The present model of an interface with finite rigidity in adhesive bonds provides an explanation of the existence of a relation between the reflection coefficient and the mechanical strength of the bond. This model involves modified boundary conditions which permit a displacement jump at the interface. It follows from analysis of the relation derived between the bond rigidity and the modulus of the pressure reflection coefficient of plane ultrasonic wave incident normal to the interface that the use of this acoustical parameter as a measure of the degree of adhesion in adhesive bonds is all the more purposeful, the closer the values of the characteristic acoustic impedance of materials bound and the higher frequency of the ultrasonic waves used. The latter remark relates to the frequency dependence of the reflection coefficient. Experimental verification showed the usefulness of relation (10) derived here for the search for a relationship between the rigidity of a bond and its strength. The advantages of this approach include the possibility of diminishing the number of standard samples necessary for correlation analysis, by the performance of ultrasonic measurements for some different frequencies. Additional information, which facilitates a distinguishing of adhesive bonds in terms of their strength, can be obtained from ultrasonic spectral analysis, since it follows from experiments, which confirm the conclusions of theoretical analysis, that smaller changes in the modulus of the pressure reflection coefficient as a function of frequency corresponds to "good" and "weak" bonds rather than to bonds with "mean" values of adhesive strength.

The present paper neglected, because of technical restrictions of measurement, analysis of the possibility of using the phase angle of the reflection coefficient as an additional measure of the degree of adhesion.

References

[1] A. PILARSKI, Z. PAWŁOWSKI, *Bond quality assessment of layered joints with acoustic methods*, International Journal of Adhesion and Adhesive, **1**, 45-48 (1980).

[2] N. O. CROSS, *An ultrasonic test for measuring the strength of clad plate*, Proc. of VI ICNT, Hannover 1970, 6, 77.

[3] L. CHLADEK, *Evaluation of the strength of cooper-steel explosive welds by means of ultrasonic test*, Proc. of III Int. Symp. "Explosive Welding of Metals", Marianske Laznie 1973, 305.

[4] N. V. VINOGRADOV, V. A. BOBROVA, *Otsenka korelatsii amplitudy sygnalu ultr. z prochnostyu soedineniya sloev bimetala*, Defektoskopia, **3**, 104-112 (1973).

[5] I. MALECKI, *Theory of waves and acoustic systems* (in Polish), PWN, Warsaw 1964.

[6] M. SCHOENBERG, *Elastic wave behavior across linear slip interfaces*, J. Acoust. Soc. Am., **68**, 5, 1516-1521 (1980).

[7] J. P. JONES, J. S. WHITTIER, *Waves at a flexibly bonded interface*, Journ. Appl. Mech., **34**, 905-909 (1967).

[8] H. G. TATTERSALL, *The ultrasonic pulse-echo technique as applied to adhesion testing*, Journ. of Physic, D. Appl. Phys., **6**, 819-832 (1973).

[9] H. ZORSKI, *Theory of discrete defects*, Arch. of Mechanics, **18**, 3 (1966).

Received on February 26, 1982; revised version on June 1, 1982.

ARCHIVES OF ACOUSTICS
8, 1, 55-68 (1983)

ULTRASONIC AND HYPERSONIC INVESTIGATIONS OF STRUCTURAL RELAXATION IN AQUEOUS SOLUTIONS OF HEXAMETHYLPHOSPHORTRIAMIDE

PIOTR MIECZNIK

Chair of Acoustics, Mickiewicz University
(60-769 Poznań, ul. Matejki 48/49)

Measurements of the absorption coefficient of ultrasonic waves in the frequency range 10-100 MHz and of the propagation velocity of ultra- and hypersonic waves in aqueous solutions of hexamethylphosphortriamide (HMPT) were carried out. In addition the density of the solutions and the coefficient of shear viscosity was measured. On the basis of the quantities measured, the coefficient of bulk viscosity, relaxation parameters of the process observed and, on the basis of the theory of compressibility relaxation, change in free energy and volume between two structural states were measured.

The analysis of the results of measurements of the absorption coefficient of ultrasonic waves, depending on the frequency, temperature, and composition of solutions, shows the presence in aqueous solutions of HMPT of a relaxation process related to the formation and disintegration of clathrate structures with the composition HMPT·17 H_2O. On the basis of compressibility relaxation theory, it was shown that the process of structural relaxation is related to a change in volume ΔV and in free energy ΔF between two structural states.

1. Introduction

The character of changes in the absorption coefficient of ultrasonic waves depending on the concentration of a solution varies greatly for a great number of liquid mixtures [1, 6, 11, 10, 3]. An interesting group is made of aqueous solutions of non-electrolytes for which the absorption coefficient of ultrasonic waves reaches a maximum for a strictly defined composition [2, 5, 11-14]. The occurring maximum of the absorption coefficient of ultrasound indicates the presence in the solution of a relaxation process related to the formation and disintegration of strictly defined structures (molecular complexes) between water molecules and the molecules of the medium dissolved.

The most systematic investigations which gave most insight into the problem of the character of relaxation occurring in aqueous solutions of non-electrolytes were performed by ANDREAE, EDMONDS, and MCKELLAR [2]. They formulated theses on the ultrasonic relaxation for non-electrolytes dissolved in water, under the assumption that the processes observed in aqueous solutions of some amines consist in the formation and disintegration of free complexes, in which a strictly defined number of water molecules corresponds to one non-electrolyte molecule. Accordingly, these authors relate the additional absorption of acoustic waves to the interaction of the type solvent – dissolved substance. In turn, NISHIKAWA, YASUNAGA, and TAKAHASHI [9] explain the additional absorption of ultrasonic waves in aqueous solutions of amyloamine and butyloamine on the basis of the reaction of association – dissociation of molecules and hydrolysis.

It is also significant whether the relaxation process observed in aqueous solutions of non-electrolytes is mainly conditioned by a change in the volume of the system (structural relaxation) or a process dependent on temperature changes (thermal relaxation). ANDREAE, EDMONDS, and MCKELLAR assume that the relaxation observed in aqueous solutions of non-electrolytes is thermal in character; in theoretical considerations, however, they also assume that the process of sound propagation in aqueous solutions of non-electrolytes is isothermal, obtaining as a result the equation for the maximum coefficient of sound absorption, μ_{max}, dependent on the change in volume of the system ΔV, in the course of the reaction. The question remains as to whether the relaxation process observed in aqueous solutions of non-electrolytes is in fact a thermal process or a process of structural (compressibility) relaxation.

The present paper attempts, on the basis of the results of measurements of the absorption coefficient of ultrasonic waves and the velocity of the propagation of hypersonic waves, to determine what sort of relaxation processes occur in aqueous solutions of HMPT.

The previous data on the structure and interactions in aqueous solutions of HMPT [7] permit the conclusion that within the temperature range ($-30°C$ – $+50°C$) and the concentration of solutions (0-1 molar fraction HMPT), the occurrence of the effect of molecular relaxation process on the absorption of ultrasonic waves can be expected.

2. Properties of aqueous solutions of HMPT

On the basis of both the measurements of the propagation velocity of an ultrasonic wave at a frequency of 15 MHz and of density in aqeous solutions of HMPT ($[(CH_3)_2N]_3OP$), depending on temperature and concentration, and on the calculated values of adiabatic compressibility of solutions, partial molar volumes, and partial molar compressibilities of components in the solution,

it was concluded that within the concentration range 0.04 (−30°C) - 0.08 (+50°C) molar fraction of HMPT a stabilization of the structure of a solution occurs as a result of the formation of clathrate structures with the composition HMPT · ·17 H_2O [7]. This phenomenon should become clear in measurements of the absorption coefficient of ultrasonic waves, depending on the frequency of the waves and the concentration of solutions investigated.

3. Method

The measurements of the absorption coefficient of ultrasonic waves were made using an ultrasonic high-frequency system type US-4 manufactured by the Institute of Fundamental Technological Research, which permitted measurements at frequencies of 10, 13.3, 16.6, 20, 30 and 47 MHz and using a modified high-frequency ultrasonic system which permitted measurements at frequencies of 60 and 100 MHz. The measurements of the absorption coefficient of ultrasonic waves in the range 10-47 MHz were taken using broadband transducers, and at frequencies of 60 and 100 MHz using resonance transducers at a fundamental frequency of 20 MHz. In the detective channel of the signal at frequencies of 60 and 100 MHz attachments, which functioned as preamplifiers of high-frequency signals and transformed frequencies of 60 and 100 MHz to 10 MHz, were additionally used. As a result, detection and amplification in the receiver occurred as low as a frequency of 10 MHz. The high-frequency ultrasonic system was modified at the Chair of Acoustics, Adam Mickiewicz University. The relative error of measurements of the absorption coefficient of ultrasonic waves did not exceed 10 percent.

The measurements of the propagation velocity of hypersonic waves were taken using the Mandelsztam-Brillouin light scattering method. The measurement system used was described in paper [8].

Moreover, additional measurements of the coefficients of shear viscosity, density, and propagation velocity of ultrasonic waves were taken. The coefficient of shear viscosity was measured using a type BH2 Hoeppler viscosimeter, while density was measured by a method using the Archimedes law (of the submerged float) with relative accuracies of 0.5 and 0.02 percent. The measurements of the propagation velocity of ultrasonic waves were taken using an impulse-phase interferometer at a frequency of 12 Mz, with error not exceeding 0.1 percent. The medium investigated was thermostated with an accuracy of up to 0.05°C and controlled using a copper – constantan thermocouple. The investigations used HMPT with purity degree recognized by the producer (E. Merck, Darmstadt) as "pure for analysis" and double distilled water.

The measurements of the frequency of ultrasonic waves were taken using a type CZE-30 numerical frequency meter with an accuracy of 100 Hz over the range 10-100 MHz.

4. Experimental results and their analysis

The measurements of the absorption coefficient of ultrasonic waves for $T = +15°C$ were taken over the frequency range 10-100 MHz and showed the stability of the quantity α/f^2 over the whole range investigated. In turn, the character of changes in the quantity $(\alpha/f^2)_{exp}$ relative to concentration (Fig. 1) shows the presence of a sharp maximum for a strictly defined concentration $k_{mo} \cong 0.1$. Fig. 1 also shows the plot of the dependence $(\alpha/f^2)_{cl}$ on concentration [11], which defines the contribution of the compressible viscosity to the total absorption of acoustic waves. The maximum in the dependence $(\alpha/f^2)_{ad} = (\alpha/f^2)_{exp} - (\alpha/f^2)_{cl}$ on concentration which occurs for the concentration $k_{mo} = 0.1$ shows in turn that in aqueous solutions of HMPT there is some relaxation process related to volume viscosity relaxation. In order to investigate this process the absorption coefficient of ultrasonic waves was measured in the temperature range $-30°C$ - $+15°C$ and in the frequency range 10-100 MHz. Fig. 2 shows the experimental results of the measurement of the absorption coefficient depending on the concentration k_{mo} (as an example, for $T = -30°C$). A sharp maximum occurs for a strictly defined composition and the value of the maximum decreases as the frequency of ultrasonic waves increases which shows that in aqueous solutions of HMPT a relaxation process occurs in the frequency range 10-100 MHz. The maximum of the absorption coefficient corresponds to a concentration close to 0.1 molar faction of HMPT.

The relation $(\alpha/f^2)_{cl} = f(k_{mo})$ also shows a maximum for a strictly defined concentration (Fig. 3), which indicates that in aqueous solutions of HMPT both the process of volume relaxation and that of shear viscosity occur. However, since the experiment reveals a single relaxation process, it can be expected that both processes have similar values of the relaxation time and cannot be distinguished in the range of measurement error. The calculations of the absorption coefficient related to the so-called classical absorption used the quantities listed in Table 1 (the values of the propagation velocity of ultrasonic waves c, the shear viscosity η_s and the density of the medium ϱ).

The concentration dependencies of the absorption coefficient of ultrasonic waves (Fig. 2) show that a relaxation process also occurs in media investigated. However, only the dependence of the quantity α/f^2 on frequency permits the determination of the relaxation time of the above process. The dependencies of α/f^2 on frequency for specific concentration and temperature of the medium are given in Figs. 4-8.

It can be noted that for temperatures below $-20°C$ and in the investigated frequency range of ultrasonic waves and in the concentration range of the solution there is the dependence of the quantity α/f^2 on frequency, indicating the presence of a single relaxation process. In order to determine accurately the relaxation frequency, the numerical method proposed by Boch [4] was used. On the basis of knowledge of the relaxation frequencies f_r and

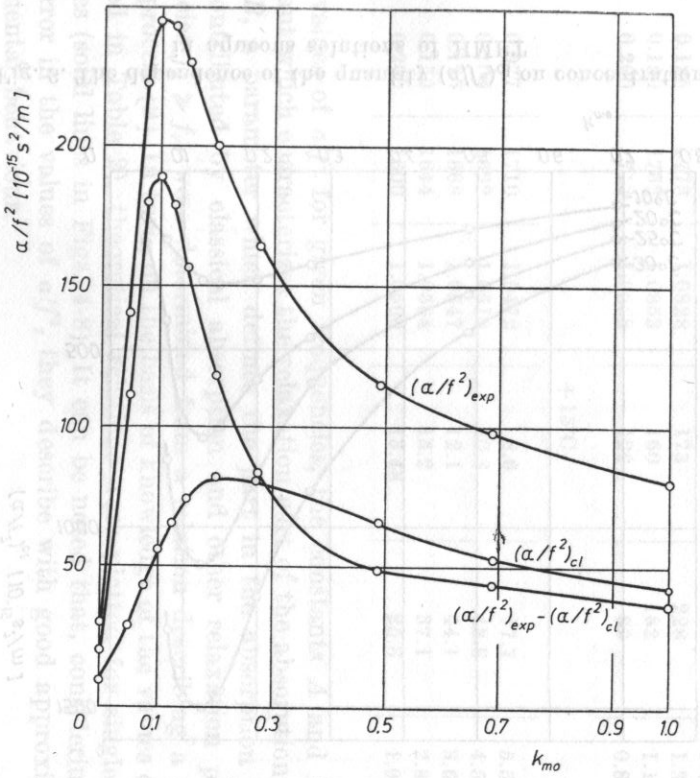

Fig. 1. The dependence of the quantity α/f^2 on concentration in aqueous solutions of HMPT for $T = +15°C$

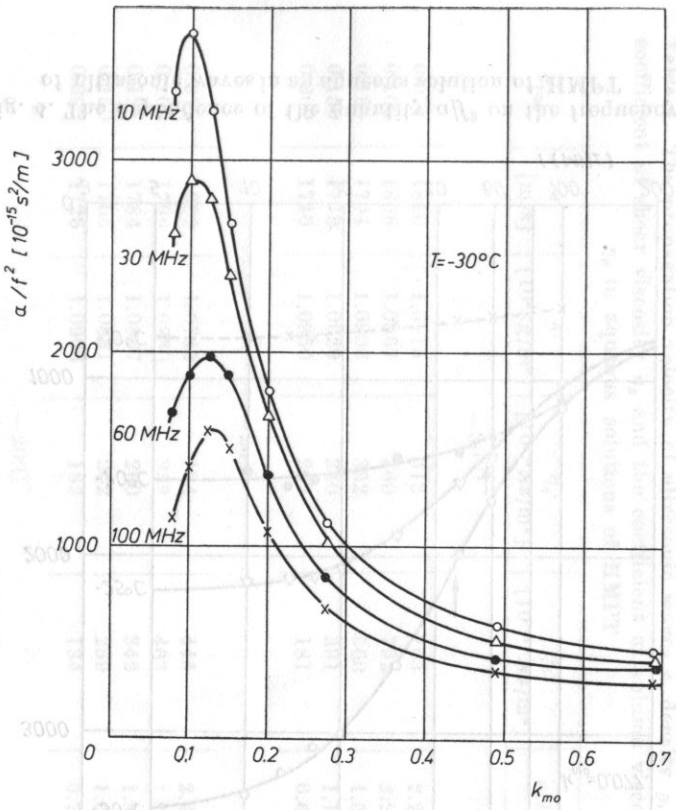

Fig. 2. The dependence of the quantity α/f^2 on concentration in aqueous solutions of HMPT

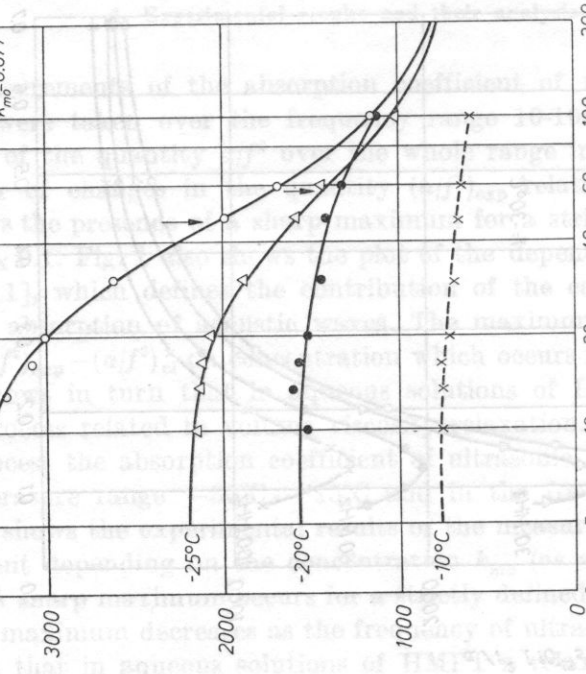

Fig. 4. The dependence of the quantity a/f^2 on the frequency of ultrasonic waves in an aqueous solution of HMPT

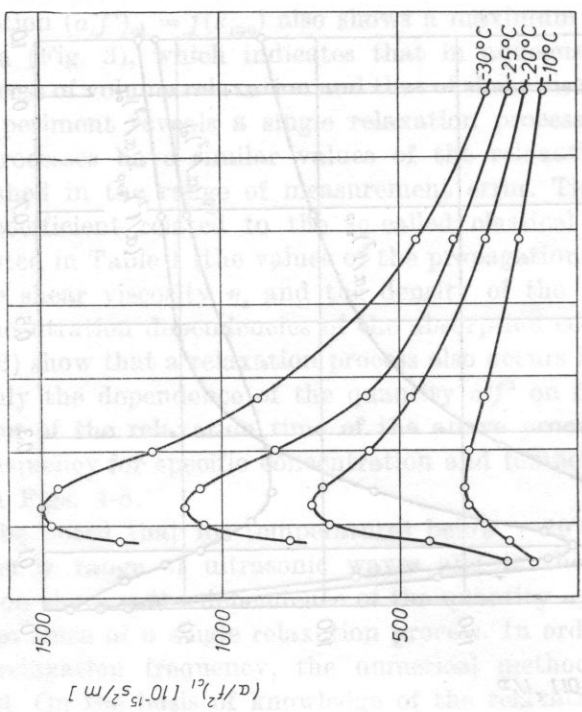

Fig. 3. The dependence of the quantity $(a/f^2)_{el}$ on concentration in aqueous solutions of HMPT

Table 1. The propagation velocity of ultrasonic waves c, density ϱ, the coefficient of shear viscosity η_s and the coefficient of volume viscosity η_v in aqueous solutions of HMPT

k_{mo}	c [m/s]	ϱ [10^3kg/m^3]	η_s [10^{-3}Ns/m^2]	η_v [10^{-3} Ns/m^2]	η_v/η_s
			−30°C		
0.077	1810	1.0775	313	703	2.25
0.100	1806	1.0867	360	792	2.20
0.125	1794	1.0906	362	560	1.55
0.150	1778	1.0929	340	391	1.15
0.200	1740	1.0950	262	181	0.69
			−25°C		
0.077	1802	1.0743	194	445	2.29
0.100	1796	1.0830	252	463	1.83
0.125	1784	1.0867	260	342	1.32
0.150	1765	1.0891	242	259	1.07
0.200	1726	1.0908	183	134	0.73
			−20°C		
0.077	1794	1.0711	103	348	3.39
0.100	1786	1.0792	165	561	3.40
0.125	1773	1.0828	173	228	1.32
0.150	1752	1.0853	160	182	1.14
0.200	1713	1.0868	122	99	0.81
			+15°C		
0.077	1710	1.0472	8.6	47.7	5.58
0.100	1692	1.0519	10.8	48.8	4.50
0.125	1668	1.0547	12.1	44.1	3.65
0.150	1644	1.0564	13.2	37.1	2.80
0.200	1600	1.0560	13.48	25.8	1.92

of the values of α/f^2 for given frequencies, the constants A and B (A being a constant which characterizes the relaxation part of the absorption of acoustic wave; B, a parameter which defines the part in the absorption of acoustic wave contributed by classical absorption and other relaxation processes at frequencies $f_r' \gg f_r$) were determined from a relation describing a single relaxation process [2]. In turn, on the basis of knowledge of the values of f_r, A and B (listed in Table 2), theoretical relations were plotted for single relaxation processes (solid lines in Figs. 4-8). It can be noted that, considering measurement error in the values of α/f^2, they describe with good approximation the experimental behaviour.

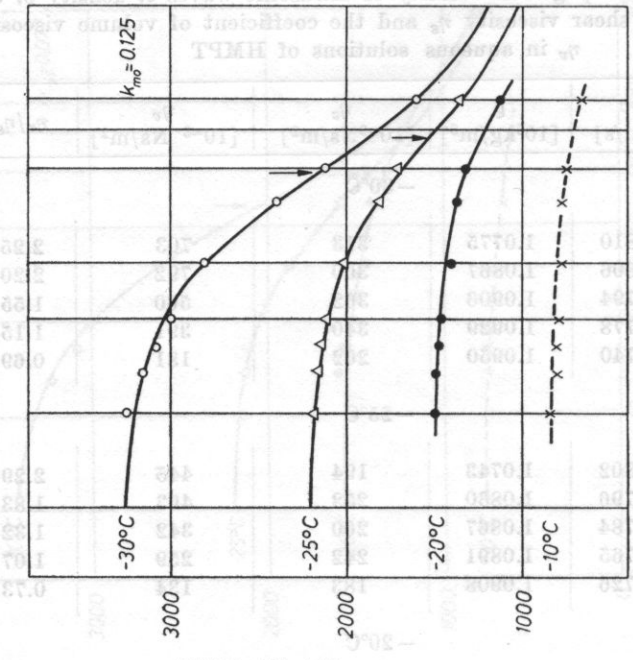

Fig. 6. The dependence of the quantity α/f^2 on the frequency of ultrasonic waves in an aqueous solution of HMPT

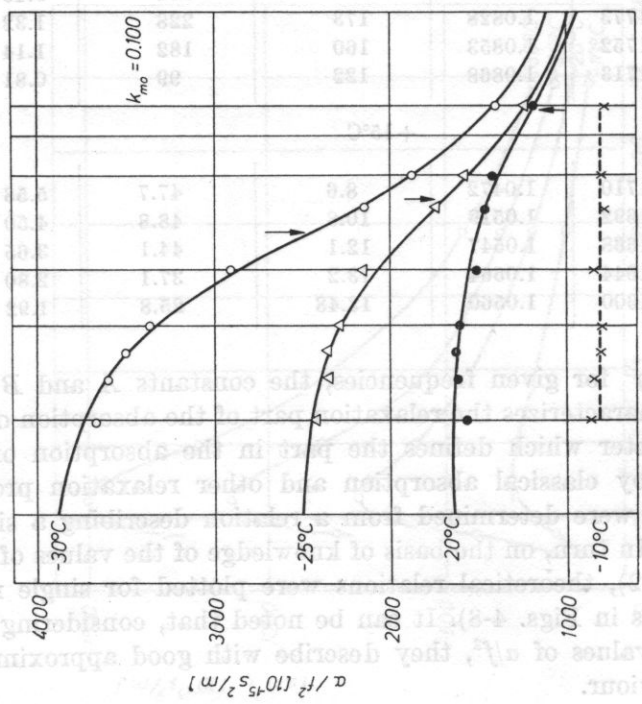

Fig. 5. The dependence of the quantity α/f^2 on the frequency of ultrasonic waves in an aqueous solution of HMPT

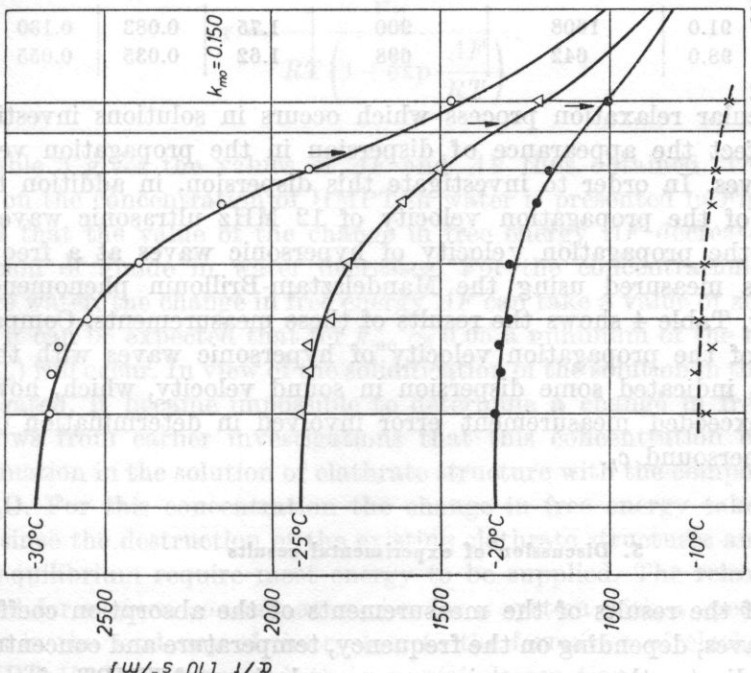

Fig. 7. The dependence of the quantity α/f^2 on the frequency of ultrasonic waves in an aqueous solution of HMPT

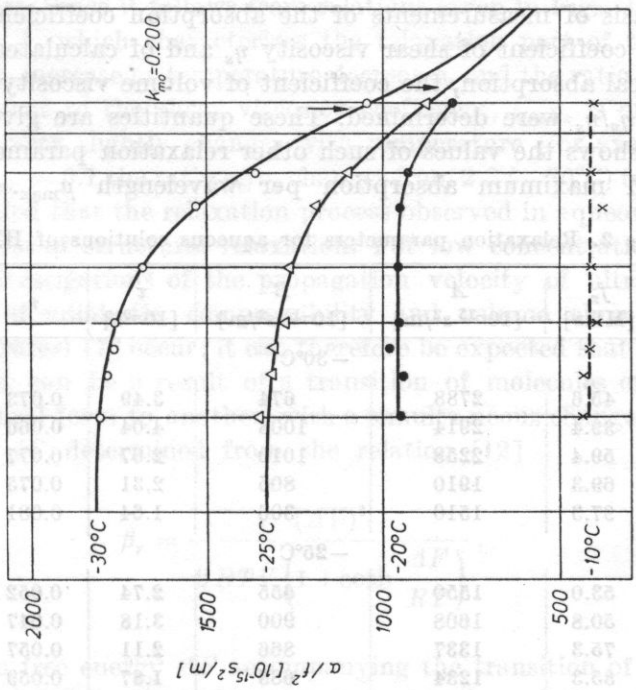

Fig. 8. The dependence of the quantity α/f^2 on the frequency of ultrasonic waves in an aqueous solution of HMPT

On the basis of measurements of the absorption coefficient of ultrasonic waves and the coefficient of shear viscosity η_s and of calculated values of the so-called classical absorption, the coefficient of volume viscosity η_v of solutions and the ratio η_v/η_s were determined. These quantities are given in Table 1, while Table 2 shows the values of such other relaxation parameters as relaxation force and maximum absorption per wavelength μ_{max}.

Table 2. Relaxation parameters for aqueous solutions of HMPT

k_{mo}	f_r [MHz]	A [10^{-15} s^2/m]	B [10^{-15} s^2/m]	τ [10^{-9}s]	r	μ_{max}
			−30°C			
0.077	45.6	2788	674	3.49	0.073	0.115
0.100	39.4	2914	1008	4.04	0.066	0.104
0.125	59.4	2258	1010	2.67	0.077	0.121
0.150	69.3	1910	805	2.31	0.075	0.117
0.200	97.3	1510	306	1.64	0.081	0.128
			−25°C			
0.077	53.0	1550	655	2.74	0.052	0.082
0.100	50.8	1608	900	3.18	0.047	0.074
0.125	75.3	1337	866	2.11	0.057	0.090
0.150	85.3	1234	683	1.87	0.059	0.093
0.200	111.0	1002	328	1.43	0.061	0.096
			−20°C			
0.100	91.0	1608	900	1.75	0.083	0.130
0.150	98.0	642	698	1.62	0.035	0.055

The molecular relaxation process which occurs in solutions investigated should also affect the appearance of dispersion in the propagation velocity of acoustic waves. In order to investigate this dispersion, in addition to the measurements of the propagation velocity of 12 MHz ultrasonic waves discussed above, the propagation velocity of hypersonic waves at a frequency of 5 GHz was measured using the Mandelsztam-Brillouin phenomenon of light scattering. Table 4 shows the results of these measurements. Comparison of the values of the propagation velocity of hypersonic waves with that of ultrasonic ones indicated some dispersion in sound velocity, which, however, only slightly exceeded measurement error involved in determination of the velocity of hypersound c_h.

5. Discussion of experimental results

Analysis of the results of the measurements of the absorption coefficient of ultrasonic waves, depending on the frequency, temperature and concentration of solutions, indicates the presence in aqueous solutions of HMPT of a single

relaxation process. Since it follows from relations given in Figs. 4-8 that values of the constant A, which characterizes the relaxation part of the absorption of acoustic wave, increase as temperature decreases, and the ratio of the volume viscosity coefficient to the shear viscosity coefficient, η_v/η_s is of the order of unity and only very slightly changes with temperature (for example, for the concentration $k_{mo} = 0.1$ the ratio η_v/η_s changes from 2.2 ($-30°C$) to 4.5 ($+15°C$); it can be concluded that the relaxation process observed in aqueous solutions of HMPT is a process of structural relaxation. For low concentrations of amides in water, the investigations of the propagation velocity of ultrasonic waves, the coefficient of adiabatic compressibility and volume show that spatial structures (clathrates) [7] occur; it can therefore be expected that the relaxation process observed can be a result of a transition of molecules of the medium from one structural form to another, with a simulta neous change in the volume of the medium ΔV determined from the relation [12]

$$\beta_r = \frac{(\Delta V)^2}{2RTV\left(1+\cosh\frac{\Delta F}{RT}\right)}, \tag{1}$$

and a change in free energy ΔF accompanying the transition of one structure into another, related to the relaxation time by the relation

$$\tau = \frac{V\eta_s}{RT\left(1+\exp\frac{\Delta F}{RT}\right)}. \tag{2}$$

Table 3 gives the values of ΔF and ΔV thus obtained. The dependence of ΔF on the concentration of HMPT in water is presented in Fig. 9. It can be noticed that the value of the change in free energy ΔF decreases as the concentration of amide in water decreases. For the concentration $k_{mo} = 0$, i.e. for pure water, the change in free energy ΔF can take a value of zero, and accordingly it can be expected that for $k_{mo} \cong 0.05$ a minimum of the relation $\Delta F = f(k_{mo})$ will occur. In view of the solidification of the solution in the temperature investigated, it became impossible to determine a change in free energy ΔF. It follows from earlier investigations that this concentration corresponds to the formation in the solution of clathrate structure with the composition HMPT·17 H_2O. For this concentration the change in free energy takes its extreme value, since the destruction of the existing clathrate structures and their return to an equilibrium require most energy to be supplied. The relaxation process observed for a given concentration, i.e. for a system with a specific structure, consists in the tendency of the system to the formation of clathrate structure of HMPT·17 H_2O type and their partial destruction.

Table 3. Results of calculation of the quantities ΔF, ΔV, β_r, β_∞ and c_∞ based on the theory of compressibility relaxation

k_{mo}	ΔF [10^6 J/kmol]	ΔV [10^{-6} m^3/mol]	β_r [10^{-12} m^2/N]	β_∞ [10^{-12} m^2/N]	c_∞ [m/s]
			−30°C		
0.077	−2.78	2.39	16.2	267	1864
0.100	−1.94	2.32	17.0	265	1863
0.125	0.60	2.22	17.0	268	1850
0.150	1.20	2.20	14.3	275	1823
0.200	1.96	2.17	10.1	292	1770
			−25°C		
0.100	−3.19	2.31	11.9	274	1836
0.125	0.19	1.98	13.6	276	1826
0.150	0.75	1.99	12.0	283	1801
0.200	1.29	1.93	8.9	298	1754
			−20°C		
0.100	−1.84	2.13	14.1	276	1831
0.150	−0.41	1.84	10.2	290	1782

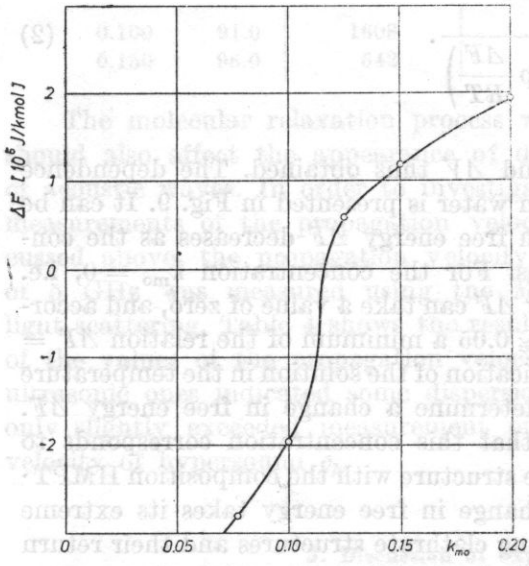

Fig. 9. The dependence of a change in free energy ΔF on concentration in aqueous solutions of HMPT for $T = -30$°C

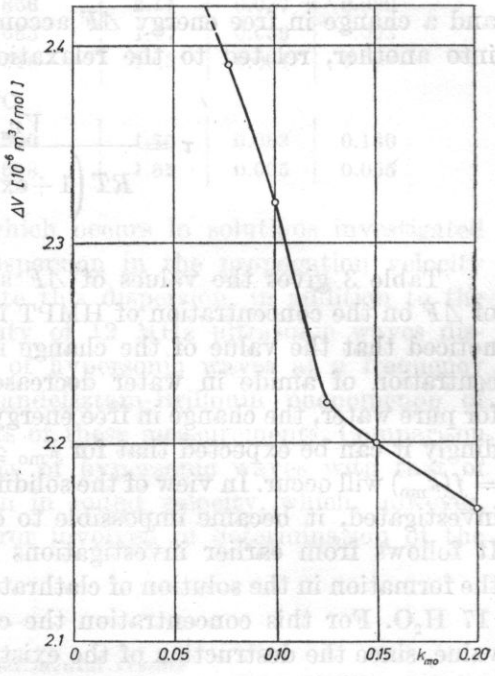

Fig. 10. The dependence of a change in volume ΔV between two structural states on concentration in aqueous solutions of HMPT for $T = -30$°C

Reaction of this type causes a change in volume of the system ΔV, whose magnitude depending on concentration is shown in Fig. 10. It follows from this dependence that for the concentration $k_{mo} \cong 0.05$ the change in volume between two states takes an extreme (maximum) value, since for $k_{mo} = 0$, i.e. for pure water, $\Delta V = 0$. Another conclusion also follows, that the relaxation process revealed consists in destruction and formation in the solution of clathrate structures with the composition HMPT·17 H_2O, since the difference in volume between the two structural states takes a maximum value for the characteristic concentration.

Analysis of results of measurements of the velocity of hypersound shows slight dispersion in the velocity of sound propagation. Similar results were, however, obtained for $T = -30°C$ on the basis of the theory of compressibility relaxation by determining the value c_∞, i.e. sound propagation velocity for

Table 4. The velocity of hypersound in aqueous solutions of HMPT. The scattering angle $\theta = 90°$, $D = 5876$ Å, $\delta\nu_L = 0.079$ cm^{-1}, $T = 15°C$

k_{mo}	$\Delta\nu$ [cm^{-1}]	n_D	f[GHz]	c_h[m/s]	c_0[m/s]	δc_h[m/s]
0.050	0.1758	1.38052	5.3	1710	1704	16
0.100	0.1807	1.40492	5.4	1727	1691	16
0.125	0.1788	1.41375	5.4	1698	1669	18
0.200	0.1735	1.42851	5.2	1630	1600	19
0.492	0.1595	1.44641	4.8	1480	1458	19
1.000	0.1437	1.45470	4.3	1326	1366	20

$f \to \infty$. Dispersion in this case does not exceed 60 m/s, i.e. 4 percent (Table 3 and 1). This agreement confirms the conclusions drawn above as to the type of relaxation occurring in aqueous solutions of HMPT. In general, for aqueous solutions of non-electrolytes the dispersion of sound velocity takes low values in view of the low value of the relaxation part of the adiabatic compressibility β_r.

6. Conclusions

Analysis of results of measurements of the absorption coefficient of ultrasonic waves and of the propagation velocity of ultra- and hypersonic waves, depending on the frequency, temperature and composition of solutions, shows the presence in aqueous solutions of HMPT of a relaxation process with a specific relaxation time, related to the formation and disintegration of strictly defined spatial structures (clathrates with composition HMPT·17 H_2O).

It was shown on the basis of the theory of compressibility relaxation that the relaxation process observed (structural relaxation) is related to a change in volume between two structural states and a change in free energy involved in the transition of one structure into another. The relaxation parameters of this molecular process were calculated.

References

[1] D. ANBANANTHAN, *Ultrasonic study of organic liquid mixtures*, Acustica, **42**, 267 (1979).

[2] J. H. ANDREAE, P. D. EDMONDS, J. F. MCKELLAR, *Ultrasonic studies of aqueous solutions of non-electrolytes*, Acustica, **15**, 74 (1965).

[3] P. ASSARSSON, F. R. EIRICH, *Properties of amides in aqueous solution*, J. Phys. Chem., **72**, 8, 2710 (1968).

[4] W. BOCH, *Absorption of ultrasonic waves in $ZnCl_2$ solutions in methanol*, Archives of Acoustics, **2**, 2, 139-147 (1977).

[5] N. INOUE, *A study on ultrasonic spectra of L-serine in aqueous solutions, using an automatic recording ultrasonic spectrometer*, Acustica, **40**, 2, 91 (1978).

[6] M. ŁABOWSKI, P. MIECZNIK, *Investigation of fluctuation kinetics of concentration in a nitrobenzene — n-heptane mixture by an acoustic method* (in Polish), Proc. XXIII Open Seminar on Acoustics, Wrocław 1975.

[7] P. MIECZNIK, *The investigation of the stabilization of the structure of aqueous solutions of hexamethylphosphortriamide using an acoustic method*, Archives of Acoustics, **5**, 4, 347 (1980).

[8] P. MIECZNIK, *Ultrasonic and hypersonic investigations of vibrational relaxation in liquid thiophene*, Archives of Acoustics, **3**, 4, 273 (1978).

[9] S. NISHIKAWA, T. YASUNAGA, K. TAKAHASHI, *Kinetic studies of fast reactions in aqueous solutions of amylamine by means of ultrasonic absorption*, Bull. Chem. Soc. Jp., **46**, 2992 (1973).

[10] J. THAMSEN, *Ultrasonic absorption in mixtures of water and 2-chloroethanol*, Acustica, **16**, 14 (1965/66).

[11] K. SESHADRI, N. P. RAO, K. C. REDDY, *Ultrasonic behaviour of binary liquid mixtures containing cyclohexane*, Z. Phys. Chem., **89**, 1-4, 108 (1974).

[12] D. SETTE, *Handbuch der Physik* (s. *Flugge*), XI/1, Berlin 1961.

[13] W. SYRBU, *Akusticheskije spektry dimetilsulfoksida, raztvorov dimetilsulfoksid — voda i ikh analiz*, Zh. Fiz., **51**, 4, 800 (1977).

[14] J. THAMSEN, *Ultrasonic absorption in mixtures of water and 2-chloroethanol*, Acustica, **16**, 14 (1965/66).

[15] K. N. THOMAS, F. B. STUMPF, *Ultrasonic studies in binary solutions of pyridine with water, methanol, ethanol*, J. Acoust. Soc. Am., **53**, 3, 714 (1973).

Received on February 19, 1982; revised version on September 1, 1982.

ARCHIVES OF ACOUSTICS
8, 1, 69-82 (1983)

DYNAMIC FOCUSING OF AN ULTRASONIC BEAM BY MEANS OF A PHASED ANNULAR ARRAY USING A PULSE TECHNIQUE

TAMARA KUJAWSKA

Department of Ultrasound, Institute of Fundamental Technological Research,
Polish Academy of Sciences
(00-049 Warsaw, ul. Świętokrzyska 21)

An approach to compute the transient radiation resulting from an impulse velocity motion of an array of annular pistons in a rigid planar infinite baffle is presented. The approach is based on developing the expression for an impulse response function, which is the time-dependent velocity potential at a spatial point resulting from an impulse velocity of a piston. The time-dependent pressure for any piston velocity motion may then be computed by a convolution of the piston velocity with the appropriate impulse response.

Numerical results of near field time-dependent radiation from annular phased array are discussed for pulsed velocity conditions. The lateral acoustical pressure distribution at different field depths is shown. The ultrasonic beamwidth as a function of the depth for every focal zone is also presented. Obtained results were compared with corresponding dependences for steady states.

Notation

a_{nw} — the internal radius of the annular piston
a_{nz} — the external radius of the annular piston
a — the radius of the circular piston
Δb — the ultrasonic beamwidth
c — wave propagation velocity
$h(\mathbf{r}, t)$ — the impulse response
$\dot{h}(\mathbf{r}, t)$ — the time derivative of the impulse response
N — the number of rings
n — ring number
p — sound pressure
r — distance from the point source
S_1 — the radiating surface
t — time

$v(\boldsymbol{r}, t)$ — the velocity motion of the radiating surface
x, x_1 } — coordinates parallel to the radiating surface
y, y_1 }
z — a coordinate perpendicular to the radiating surface
ϱ — the density of the medium
τ_0 — duration of the pulse
$\Delta\tau$ — time delay in excitation
φ — acoustic potential
ω — angular frequency

1. Introduction

The main technique in ultrasonic diagnostics has recently been the pulse technique based on echosonography with B — scanning, permitting visualization of the internal body organs and thus providing information on the dimensions, localization and character of structures under investigation. One of the fundamental problems involved in this technique is the insufficient resolution which results from the finite lateral dimensions of the ultrasonic beam radiated. Namely, information is obtained as cross-sectional image of the organ of interest and consists of a limited number of lines forming the image on the monitor. An increase in the density of these lines and a narrowing of the ultrasonic beam permit identification of internal structures in greater detail and give a more precise image of them, thus making its interpretation easier.

The lateral resolution of the equipment is defined primarily by lateral dimensions of the ultrasonic beam radiated along the whole penetration depth. The method of dynamic focusing, based on the phased array principle, is the most effective method providing minimum lateral dimensions of the ultrasonic beam along the whole space of structures examined. The phased array consists of a large number of piezoelectric transducers excited with a specified time delay, permitting focusing at a desired point on the axis. Adjusting the time delay of the excitation of each transducer with delay lines, it is possible to change the curvature of the wave front radiated and thus to move the focus along the axis. Visualization is performed by means of a mechanical sector scanning of the beam.

Considering the fact that point focusing involves a sharp narrowing of the ultrasonic beam not only in the geometrical focus but also in its direct vicinity, the whole observation depth can be divided into focal zones with a geometrical focus inside each zone. Thus, switching the focus during reception time from a closer zone into an increasingly deeper zone in succession, the ultrasonic beam is sharply focussed along the whole range of the observation depth. The speed of the switching is conditioned by the propagation velocity

of the waves in the area examined and depends on the width of focal zones. Fig. 1 shows a phased array of annular transducers with four focal zones and the corresponding fronts of the wave received. The use of annular transducers with axial symmetry permits the same lateral resolution to be obtained in all lateral directions for a given observation depth.

The previous theoretical analysis [5] performed for the dependence of the lateral resolution of a phased annular array on dimensions, configuration and excitation method was concerned only with steady states. In view of the predicted use of the system in gynaecology and obstetrics a frequency of 2.5 MHz ($\lambda = 0.6$) mm was chosen as the fundamental resonance frequency of the transducers and an observation area within 4 cm to 24 cm from the body surface [4] was used.

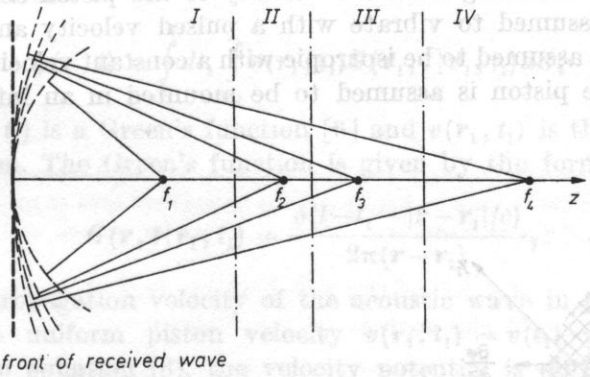

Fig. 1. The principle of the dynamic focusing system

As a result of theoretical analysis, taking into account the technological possibility of implementing the system, the degree of electronic complication of the equipment and the production cost, an annular array with a diamete of 40 mm was selected. This array consists of seven segments (six rings and a central disc) with equal surfaces, which secures a good matching with the electrical part of the equipment and effective focusing of the ultrasonic beam along the whole range of penetration depth divided into five focal zones with the geometrical focus at the distances of 4, 6, 8, 11 and 18 cm, respectively, from the radiating surface.

The aim of the present paper is to perform a theoretical analysis of the lateral resolution of a chosen phased annular array when its segments are excited by short pulses. This will permit comparison of the results obtained with the results concerning steady states and the necessary conclusions to be drawn.

2. Theoretical basis and analysis of the problem

The problem lies in calculation of the near-field transient radiation resulting from nonharmonic velocity motion of an array of annular surfaces. These surfaces are excited to vibration by signals in the form of rectangular pulsed sinusoid with time delays so selected that the beam is focused at a desired point of the field.

The theoretical method for acoustic field calculation is based on analysis of the transient radiation generated by a piston. This analysis consists in determination of the impulse response of the radiating surface at a spatial point of interest and in subsequent convolution of the piston velocity with the appropriate impulse response [8-14].

Consider the problem of determining the time-dependent pressure in half-space $z > 0$ resulting from the velocity of the piston as shown in Fig. 2. The piston is assumed to vibrate with a pulsed velocity and the medium in the half-space is assumed to be isotropic with a constant velocity of propagation. In addition, the piston is assumed to be mounted in an infinite planar rigid baffle.

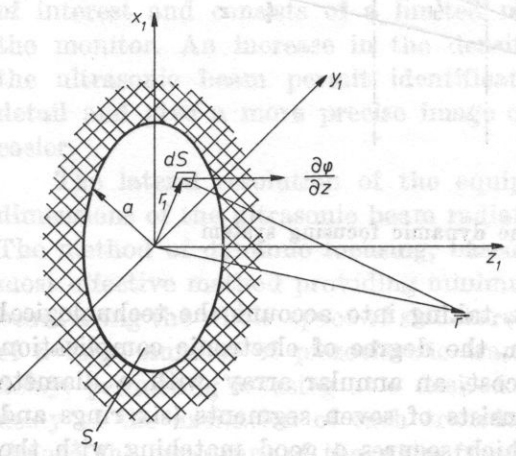

Fig. 2. A circular transducer in an infinite planar and rigid baffle

The problem of computing the pressure is formulated as a classical boundary value problem in terms of the velocity potential $\varphi(\boldsymbol{r}, t)$, where $\boldsymbol{r}$ defines the point of interest in the half-space and t is time. The pressure is obtained using the following equations:

$$p(\boldsymbol{r}, t) = \varrho \frac{\partial \varphi(\boldsymbol{r}, t)}{\partial t}, \qquad v(\boldsymbol{r}, t) = -\nabla \varphi(\boldsymbol{r}, t), \tag{1}$$

where ϱ is the density of the medium.

The mathematical specification of the boundary-value problem yields the following system of equations:

$$\begin{aligned} &\frac{1}{c^2}\frac{\partial^2\varphi}{\partial t} - \nabla^2\varphi = 0, \quad \boldsymbol{r} \in A, \\ &\frac{\partial\varphi}{\partial z} = v(\boldsymbol{r}, t), \quad \boldsymbol{r} \in S,\ t > 0, \\ &\varphi(\boldsymbol{r}, t)|_{t=0} = \frac{\partial}{\partial t}\varphi(\boldsymbol{r}, t)|_{t=0} = 0, \end{aligned} \tag{2}$$

where A is the half-space $z > 0$, S is the $z = 0$ plane and $\boldsymbol{r}$ is a point in A and S. It should be noted that $v(\boldsymbol{r}, t) = 0$ for $\boldsymbol{r}$ outside the surface of the piston.

The solution of the preceding system of equations is obtained using a Green's function development

$$\varphi(\boldsymbol{r}, t) = \int_0^t dt_1 \int_{S_1} v(\boldsymbol{r}_1, t_1) G(\boldsymbol{r}_1, t \,|\, \boldsymbol{v}_1, t_1)\, dS, \tag{3}$$

where $G(\boldsymbol{r}, t \,|\, \boldsymbol{r}_1, t_1)$ is a Green's function [6] and $v(\boldsymbol{r}_1, t_1)$ is the specified velocity of the piston. The Green's function is given by the formula [6]

$$G(\boldsymbol{r}, t \,|\, \boldsymbol{r}_1, t_1) = \frac{\delta(t - t_1 - |\boldsymbol{r} - \boldsymbol{r}_1|/c)}{2\pi(\boldsymbol{r} - \boldsymbol{r}_1)}, \tag{4}$$

where c is the propagation velocity of the acoustic wave in the medium.

Assuming a uniform piston velocity $v(\boldsymbol{r}_1, t_1) = v(t_1)$ and substituting equation (4) into equation (3), the velocity potential is obtained,

$$\varphi(\boldsymbol{r}, t) = \int_0^t v(t_1)\, dt_1 \int_{S_1} \frac{\delta(t - t_1 - |\boldsymbol{r} - r_1|/c)}{2\pi|\boldsymbol{r} - \boldsymbol{r}_1|}\, dS. \tag{5}$$

Formula (5) can be expressed as

$$\varphi(\boldsymbol{r}, t) = \int_0^t v(t_1) h(\boldsymbol{r}, t - t_1)\, dt_1, \tag{6}$$

where

$$h(\boldsymbol{r}, t - t_1) = \int_{S_1} \frac{\delta(t - t_1 - |\boldsymbol{r} - \boldsymbol{r}_1|/c}{2\pi|\boldsymbol{r} - \boldsymbol{r}_1|}\, dS. \tag{7}$$

It can be noted that equation (6) is a familiar convolution integral and may be expressed as a convoluation of two time functions

$$\varphi(\boldsymbol{r}, t) = v(t_1) * h(\boldsymbol{r}, t), \tag{8}$$

where the function $h(\boldsymbol{r}, t)$ is defined as the impulse response function of the piston to the spatial point of interest.

The attempts to determine analytically the impulse response of the piston undertaken by KHARKEVICH [1], OBERHETTINGER [7] and STEPANISHEN [10], who used different methods to solve this problem, gave the same result; namely, that the impulse response of the piston resulting from excitation by a Dirac function can be determined for two cases, shown in Figs. 3 and 4, in the following way:

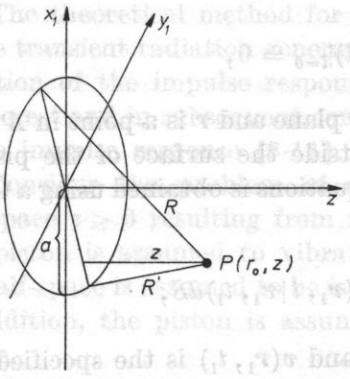

Fig. 3. The case when the observation point is within the area of the cylinder whose base is the area of the transducer

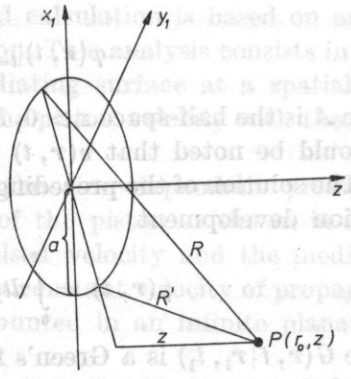

Fig. 4. The case when the observation point is outside the area of the cylinder whose base is the surface of the transducer

1. When $a > r_0$ (i.e. when the point of interest is inside the area of the cylinder whose base is the surface of the piston)

$$h(\boldsymbol{r}, t) = \begin{cases} 0, & t < \dfrac{z}{c}, \\ c, & \dfrac{z}{c} < t < \dfrac{R'}{c}, \\ \dfrac{c}{\pi} \arccos\left[\dfrac{c^2t^2 + r_0^2 - a^2 - z^2}{2r_0\sqrt{c^2t^2 - z^2}}\right], & \dfrac{R'}{c} < t < \dfrac{R}{c}, \\ 0, & t > \dfrac{R}{c}. \end{cases} \tag{9}$$

2. When $a < r_0$ (i.e. the point of interest is outside the area of the cylinder whose base is the surface of the piston)

$$h(\boldsymbol{r}, t) = \begin{cases} 0, & t < \dfrac{R'}{c}, \\ \dfrac{c}{\pi} \arccos\left[\dfrac{c^2t^2 + r_0^2 - a^2 - z^2}{2r_0\sqrt{c^2t^2 - z^2}}\right], & \dfrac{R'}{c} < t < \dfrac{R}{c}, \\ 0, & t > \dfrac{R}{c}, \end{cases} \tag{9a}$$

where $R' = \sqrt{z^2+(a-r_0)^2}$ and $R = \sqrt{z^2+(a+r_0)^2}$ are the shortest and the longest distances, respectively, from the observation point to the circumference of the piston (cf. Figs. 3 and 4).

Thus, to study the time-dependent pressure at an arbitrary near field point resulting from an impulse velocity motion of the piston, the general expression for the impulse response which is indicated in equations (9) or (9a) must be substituted into equation (6) and the resultant velocity potential substuted into equation (1). Performing the indicated substitutions and differentiation, the pressure may be evaluated from the following expression

$$p(\boldsymbol{r}, t) = \varrho \int_{-\infty}^{t} \mathring{h}(\boldsymbol{r}, t-\tau) v(\tau) d\tau, \tag{10}$$

where $\mathring{h}(\boldsymbol{r}, t)$ is the time derivative of the impulse response.

The time-dependent acoustic pressure generated by an array of annular transducers may be determined, using superposition as the sum of the pressures generated by each segment. When the system consists of a central disc with the radius a_0 and N concentric rings (Fig. 5) with the interal and external radius equal respectively to a_{nw} and a_{nz}, the summary time-dependent acoustic pressure is expressed as follows:

$$p_\Sigma(\boldsymbol{r}, t) = p_0(\boldsymbol{r}, t) + \sum_N p_n(\boldsymbol{r}, t), \tag{11}$$

where $n = 1, 2, \ldots, N$; $p_0(\boldsymbol{r}, t)$ is the time-dependent pressure resulting from the pulsed velocity of the central disk; $p_n(\boldsymbol{r}, t) = p_{nz}(\boldsymbol{r}, t) - p_{nw}(\boldsymbol{r}, t)$ is time-dependent radiation from the nth ring, $p_{nz}(\boldsymbol{r}, t)$ and $p_{nw}(\boldsymbol{r}, t)$ are time-dependent radiation from the piston with radius a_{nz} and a_{nw}, respectively.

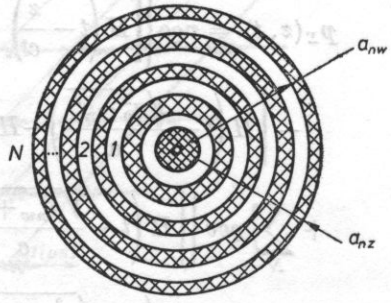

Fig. 5. The phased annular array

According to the principle of the phased array, the calculation of the field focused on axis Z at the distance f from the radiating surface requires the introduction of excitation time delays for each segment with respect to the external ring for which zero delay may be assumed.

The excitation time delay is taken into account in the following way. Assume that the segment velocity $v(t)$ is a pulsed sinusoid with a time duration τ_0 and carrier frequency equal to ω, then for the central disc

$$v_0(t) = v[H(t)-H(t-\tau_0)]\sin\omega t, \tag{12}$$

while for the nth ring of the phased array

$$v_n(t) = v[H(t+\Delta\tau_n)-H(t-\tau_0+\Delta\tau_n)]\sin\omega(t+\Delta\tau_n), \tag{13}$$

where $\Delta\tau_n = \left(\sqrt{f^2+a_n^2}-f\right)/c$ is the time delay in excitation of the nth segment (see Fig. 6).

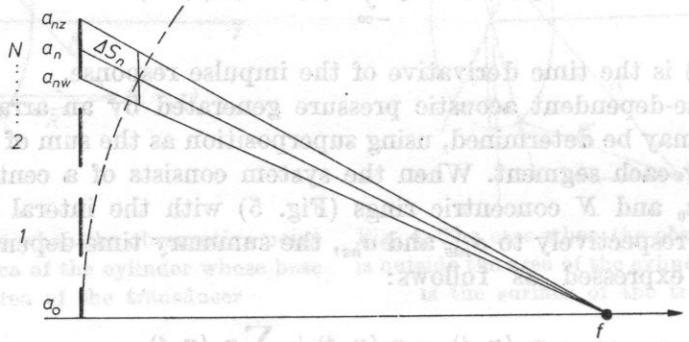

Fig. 6. The ultrasonic beam focusing by means of an annular array

Thus, according to equations (10) and (11), time-dependent pressure focused on the axis Z resulting from an impulsed velocity of annular array segments may be expressed as follows:

a) the on-axis pressure

$$p_Z(z,t) = v\varrho c\left\{\left[H\left(t-\frac{z}{c}\right)-H\left(t-\frac{z}{c}-\tau_0\right)\right]\sin\omega\left(t-\frac{z}{c}\right)-\right.$$

$$-\left[H\left(t-\frac{\sqrt{a_0^2+z^2}}{c}\right)-H\left(t-\frac{\sqrt{a_0^2+z^2}}{c}-\tau_0\right)\right]\sin\omega\left(t-\frac{\sqrt{a_0^2+z^2}}{c}\right)\Bigg\}+$$

$$+\sum_N \varrho c v\left\{\left[H\left(t-\frac{\sqrt{a_{nw}^2+z^2}}{c}+\Delta\tau_n\right)-H\left(t-\frac{\sqrt{a_{nw}^2+z^2}}{c}-\tau_0+\Delta\tau_n\right)\right]\times\right.$$

$$\times\sin\omega\left(t-\frac{\sqrt{a_{nw}^2+z^2}}{c}+\Delta\tau_n\right)-\left[H\left(t-\frac{\sqrt{a_{nz}^2+z^2}}{c}+\Delta\tau_n\right)-\right.$$

$$\left.\left.-H\left(t-\frac{\sqrt{a_{nz}^2+z^2}}{c}-\tau_0+\Delta\tau_n\right)\right]\sin\omega\left(t-\frac{\sqrt{a_{nz}^2+z^2}}{c}+\Delta\tau_n\right)\right\}, \tag{14}$$

b) the pressure at an arbitrary near-field point

$$p_{\Sigma}(\boldsymbol{r}, t) = v\varrho c\left\{\left[H\left(t-\frac{z}{c}\right)-H\left(t-\frac{z}{c}-\tau_0\right)\right]\sin\omega\left(t-\frac{z}{c}\right)-\right.$$

$$-\frac{1}{\pi}\int_{t-R_0/c_0}^{t-R_0'/c}\mathring{h}_0(\boldsymbol{r}, t-\tau)[H(\tau)-H(\tau-\tau_0)]\sin\omega\tau d\tau\Big\}+$$

$$+\sum_N\frac{v\varrho c}{\pi}\Big\{\int_{t-R_{nw}/c}^{t-R_{nw}'/c}\mathring{h}_{nw}(\boldsymbol{r}, t-\tau)[H(\tau+\Delta\tau_n)-H(\tau+\Delta\tau_n-\tau_0)]\times$$

$$\times\sin\omega(\tau+\Delta\tau_n)d\tau-\int_{t-R_{nz}/c}^{t-R_{nz}'/c}\mathring{h}_{nz}(\boldsymbol{r}, t-\tau)[H(\tau+\Delta\tau_n)-$$

$$-H(\tau+\Delta\tau_n-\tau_0)]\sin\omega(\tau+\Delta\tau_n)d\tau\Big\}. \qquad (15)$$

Equations (14) and (15) present the basic analytical expressions to compute the near field transient radiation focused at the distance f from the radiating surface of the phased annular arrary.

9. Computing results and discussion

The calculations were performed on a Cyber (IBM) computer in Fortran language. Figs. 7-11 show the transient radiation resulting from an impulse

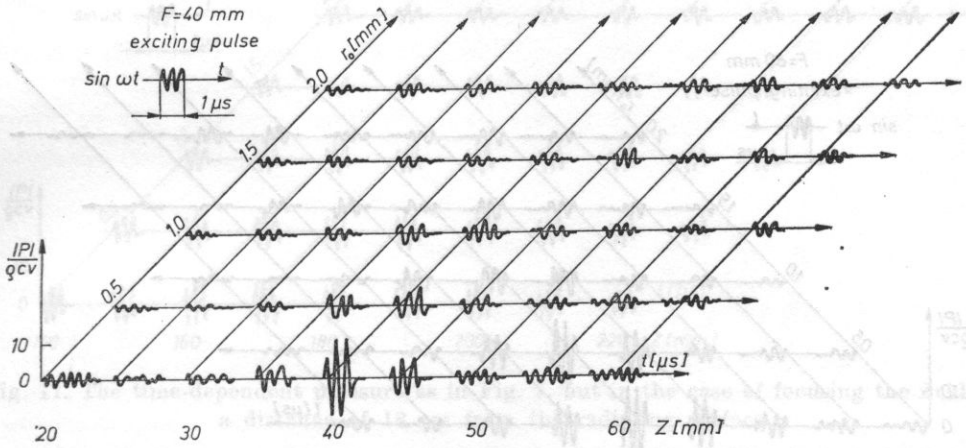

Fig. 7. The time-dependent radiation resulting from impulse velocity motion of the phased annular array in the case of focusing the field at a distance of 4 cm from the radiating surface. The segments of an array are excited by rectangular pulsed sinusoid with duration 1 μs and carrier frequency 2.5 MHz

velocity motion of the phased annular array with geometrical parameters described previously. The segments of the array are excited by rectangular pulses with duration equal to 1 μs and carrier frequency equal to 2.5 MHz. The field is focused successively in each focal zone at distnaces of 4, 6, 8, 11 and 18 cm, respectively, from the radiating surface.

On the basis of the obtained numerical data, the lateral pressure distribution at different observation depth Z, also the beam width versus observation depth for all focal zones, were determined. Fig. 12 shows the lateral pressure distribution in the focus ($F = 6$ cm) for a selected annular array excited by

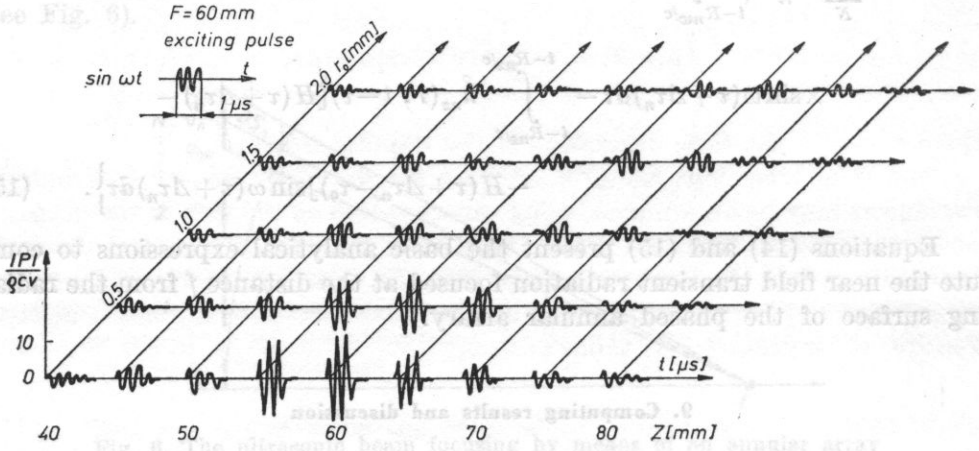

Fig. 8. The time-dependent pressure as in Fig. 7, but in the case of focusing the field at a distance of 6 cm from the radiating surface

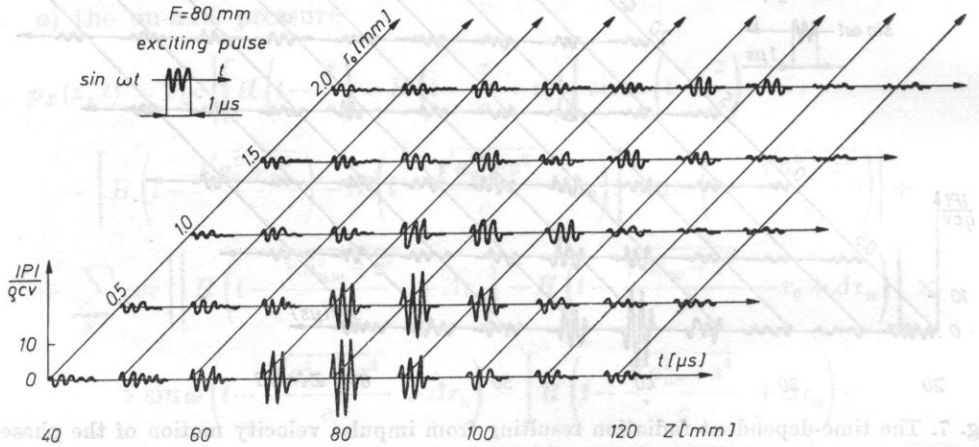

Fig. 9. The time-dependent pressure as in Fig. 7, but in the case of focusing the field at a distance of 8 cm from the radiating surface

a continuous wave (solid line) and by pulsed wave (dashed line). For comparison, the same figure shows the lateral pressure distribution calculated for a spherical transducer with the same diameter and a curvature radius of 6 cm, excited by a continuous wave [3]. It can be seen in this figure that the maximum level of the sidelobes for impulses equals — 15 dB with respect to the maximum value, for a continuous wave equals — 19 dB and for a spherical transducer is — 24 dB.

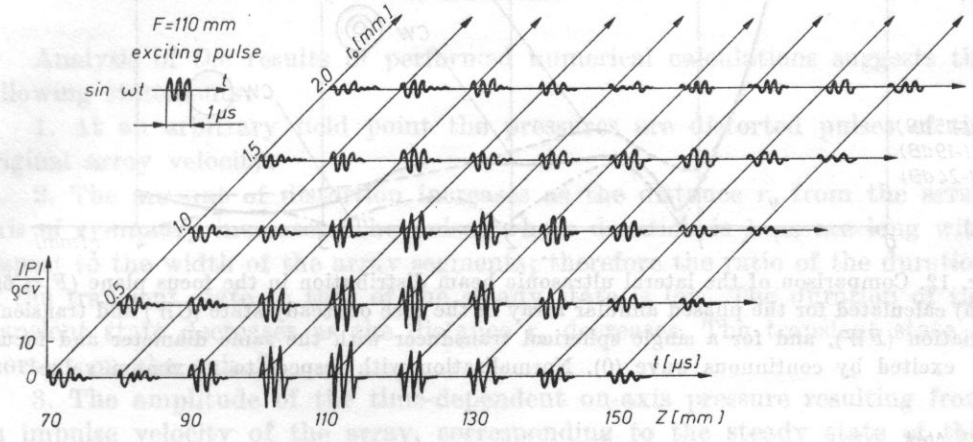

Fig. 10. The time-dependent pressure as in Fig. 7, but in the case of focusing the field at a distance of 11 cm from the radiating surface

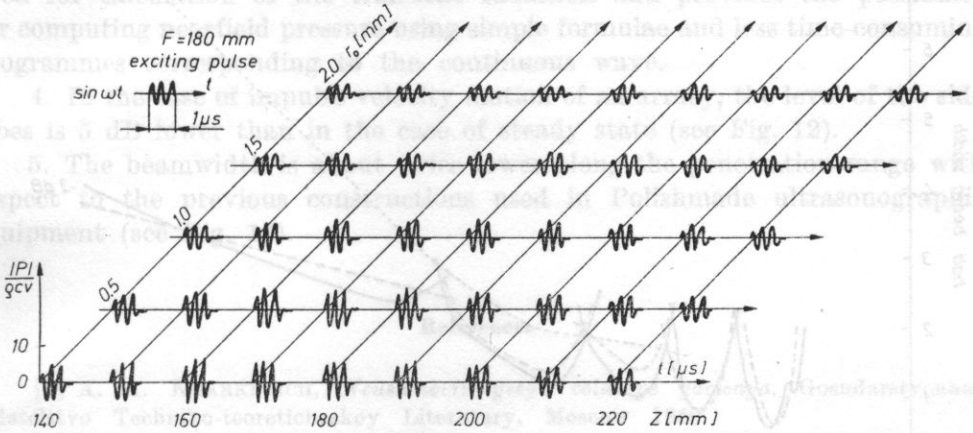

Fig. 11. The time-dependent pressure as in Fig. 7, but in the case of focusing the field at a distance of 18 cm from the radiating surface

Fig. 13 illustrates the dependence of the beamwidth generated by an annular array successively in each focal zone, on the observation depth, calculated for steady state (solid line) and for transient states (dashed line). The

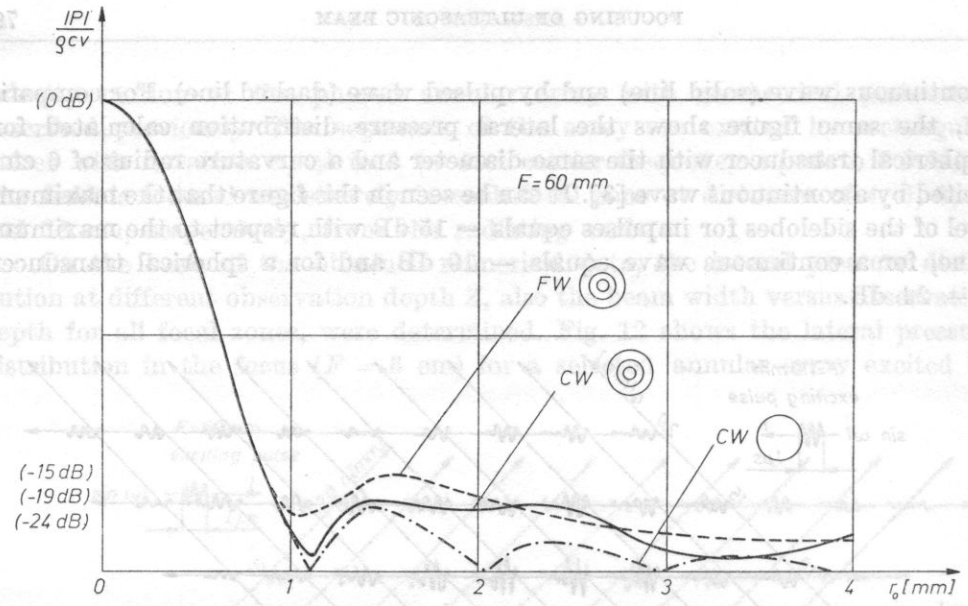

Fig. 12. Comparison of the lateral ultrasonic beam distribution in the focus plane ($F = 60$ mm) calculated for the phased annular array in the case of steady state (CW) and transient radiation (FW), and for a single spherical transducer with the same diameter and focus excited by continuous wave (0). Normalisation with respect to maximum value

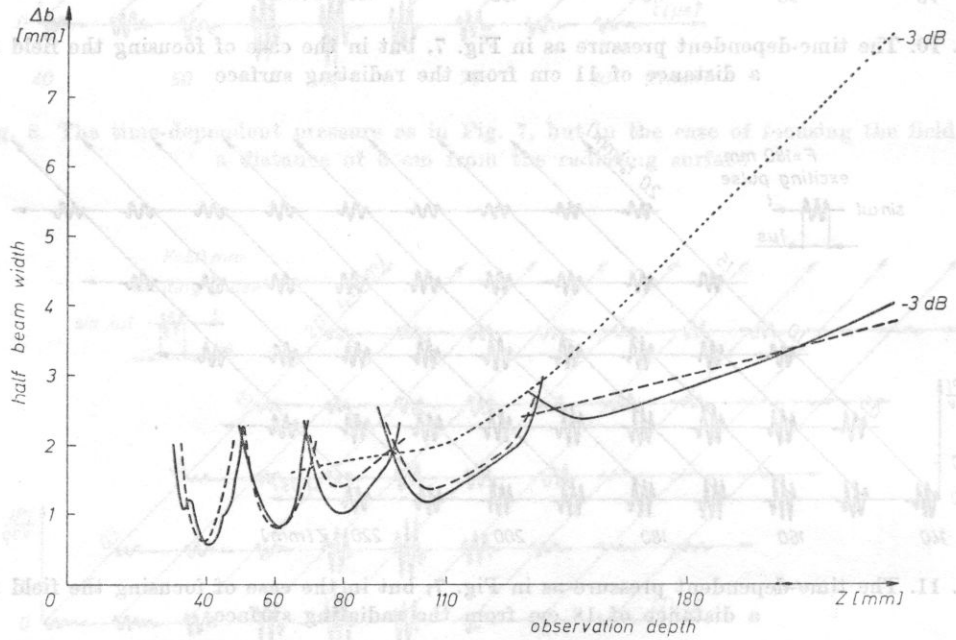

Fig. 13. The 3 dB ultrasonic beamwidth successively focussed in each focal zone, depending on the observation depth, calculated for steady state (solid line) and transient state (dashed line). This figure presents also results of measurements for a spherical transducer with 20 mm diameter and a 10 cm curvature radius (pointed line) in the case of steady state

same figure shows the results of measurements in case of a spherical transducer with a diameter of 20 mm and a curvature radius of 10 cm obtained in paper [2]. Comparison of graphs shown in Fig. 13 indicates a significant lateral resolution improvement in the case of dynamic focusing both at the beginning and at the end of the penetration range.

4. Conclusions

Analysis of the results of performed numerical calculations suggests the following statements:

1. At an arbitrary field point the pressures are distorted pulses of the original array velocity.

2. The amount of distortion increases as the distance r_0 from the array axis of symmetry increases. The pulses whose duration is 1 μs are long with respect to the width of the array segments; therefore the ratio of the duration of the transient state to that of the steady state is low. The duration of the transient state decreases as the distance r_0 decreases. The transient state is shortest on the axis Z.

3. The amplitude of the time-dependent on-axis pressure resulting from an impulse velocity of the array, corresponding to the steady state of this pressure, is the same as in the case of continuous velocity motion of the array (see Fig. 12). This indicates tne correctness of the approach and programmes used for calculation of the transient radiation and provides the possibility for computing nearfield pressure using simple formulae and less time-consuming programmes corresponding to the continuous wave.

4. In the case of impulse velocity motion of an arrary, the level of the side lobes is 5 dB lower than in the case of steady state (see Fig. 12).

5. The beamwidth is about twice lower along the penetration range with respect to the previous constructions used in Polishmade ultrasonographic equipment (see Fig. 13).

References

[1] A. A. Kharkevich, *Neustanovivshyesya volnovye yavlenya*, Gosudarstvennoe Izdatelstvo Techniko-teoreticheskoy Literatury, Moscow 1950.

[2] J. Etienne, L. Filipczyński, A. Firek, J. Groniewski, J. Kretowicz, G. Łypacewicz, J. Sałkowski, *In vivo measurements of the intensity of a focused ultrasonic beam used in ultrasonography of early pregnancy* (in Polish), Archiwum Akustyki, **11**, 1 (1976).

[3] L. Filipczyński, *Radiation of acoustic waves for pulse ultrasonic defectoscopy* (in Polish), Proc. II Conference on Ultrasound of Polish Academy of Sciences, PWN, Warsaw 1957.

[4] L. Filipczyński, I. Roszkowski, *Ultrasonic diagnostics in gynaecology and obstetrics* (in Polish), PZWL, Warsaw 1977.

[5] T. MARUK-KUJAWSKA, *Dynamic focusing of an ultrasonic beam by means of annular transducers* (in Polish), Doct. diss., Warsaw 1980.

[6] P. M. MORSE, K. U. INGARD, *Theoretical acoustics*, McGrawHill, New York 1968.

[7] F. OBERHETTINGER, *On transient solution of the baffled piston problem*, J. Res. Nat. Bur. Stand., 65b, 1961.

[8] P. R. STEPANISHEN, *The time dependent force and radiation impedance on piston in a rigid infinite planar baffle*, J. Acoust. Soc. Am., **49**, 3 (1971).

[9] P. R. STEPANISHEN, *An approach to computing time-dependent interaction forces and mutual radiation impedances between pistons in a rigid planar baffle*, J. Acoust. Soc. Am., **49**, 1 (1971).

[10] P. R. STEPANISHEN, *Transient radiation from pistons in an infinite planar baffle*, J. Acoust. Soc. Am., **49**, 5 (1971).

[11] P. R. STEPANISHEN, *The impulse response and mutual radiation impedance between a circular piston and a piston of arbitrary shape*, J. Acoust. Soc. Am., **54**, 3 (1973).

[12] P. R. STEPANISHEN, *Impulse response and radiation impedance of an annular piston*, J. Acoust. Soc. Am., **56**, 2 (1974).

[13] P. R. STEPANISHEN, *Acoustic transients in the far field of baffled circular piston using the impulse responce approach*, J. Sound Vib., **32** (1974).

[14] P. R. STEPANISHEN, *Experimental verification of the impulse response method to evaluate transient acoustic fields*, J. Acoust. Soc. Am., **69**, 6 (1981).

Received on March 19, 1982; revised version on September 22, 1982.

ARCHIVES OF ACOUSTICS
8, 1, 83-94 (1983)

ULTRASONIC CHARACTERIZATION OF TISSUES IN CARDIOLOGY*

LESZEK FILIPCZYŃSKI

Department of Ultrasound, Institute of Fundamental Technological Research,
Polish Academy of Sciences
(00-049 Warsaw, ul. Świętokrzyska 21)

In order to analyse the possibility of the determination of the properties of soft tissues using ultrasonic (noninvasive) methods, a review was made of the basic physical properties characterizing acoustic wave propagation in these tissues (propagation velocity, attenuation, scattering). In a discussion of the results of "in vitro" investigations, it was shown that investigations of backscattering can be very significant for cardiological applications; the heart muscle with scars caused by an infarct is characterized by an increased proportion of collagen-rich connective tissue which has the value of the backscattering coefficient greater by a factor of some dozens than that of normal muscle. This is related to the higher echographic visualizability of collagen than other soft tissues and suggests the practical possibility of noninvasive distinguishing of the regions of the muscle with scars caused by the infarct from normal muscle. This possibility was confirmed by "in vivo" investigations performed on dogs by the method of grey level histograms obtained from ultrasonograms of dog's hearts.

This paper has the character of a review.

1. Introduction

Information carried by ultrasonic waves penetrating the interior of the human body is encoded, in its time of passage, amplitude, frequency and phase. This information undergoes electronic processing and, when the pulse echo method is used, is displayed on the oscilloscope or kinescope screen in *A* (amplitude), — *B* (brightness) — or *M* (motion) — presentation. It is also possible to use information related to a frequency change caused by the Doppler effect

* Delivered at the International School of Ultrasonography at Erica (Sicilly) on 3 November, 1981.

[6] or ultrasonic holography. The latter method is now purely academic in significance; it has never been used practically. The recent times have seen attempts to use a method based on digital image reconstruction, as it is done in computerized *X*-ray tomography. This promising technique is now in its early development stage.

The visualization of the interior of the human body by means of ultrasound is made possible by the advantageous conditions of wave propagation in soft tissues. Wave attenuation increases in proportion to the first power of frequency. In the investigations of the organs of the pelvis, abdominal cavity and heart, ultrasonic waves of frequencies from 2 to 3 MHz cover distances of up to 25 cm, counting in one direction only. In ophthalmology, where the longest distances do not exceed 5 cm, higher frequencies, usually from 6 to 20 MHz, are used. Over this frequency range the wavelengths of ultrasound are contained within the limits 0.75-0.075 mm, which is then the resolution limit of ultrasonic diagnostic methods.

Another great advantage is the fact that the acoustic impedances of soft tissues only slightly differ from one another, mainly as a result of differences in the elastic properties of the tissues. E.g. at the interface of blood and muscle tissue only 0.1 % of the intensity of the wave incident perpendicularly on this interface is reflected. The other 99.9 % intensity penetrates deeper into the body, causing successive reflections from the increasingly deeper boundaries of tissues. Thus a large amount of information can be obtained about the successive, increasingly deeper, interior anatomical structures of the body.

The variety of the organs of the human body, the variety of their anatomical structure and physiological function causes ultrasonic diagnostic methods and ultrasonic equipment to be developed from the point of view of the specific properties of these organs. Accordingly, independent ultrasonic diagnostic equipment has been developed for the purposes of examining the organs of the pelvis and abdominal cavity, opthalmologic and cardiological problems, female breasts, peripheral circulation system etc.

2. Principle of obtaining ultrasonic images of tissue structure

There are a number of common, yet unsolved, problems which are essentially significant for further development of ultrasonic diagnostic methods. One of these is ultrasonic characterization of tissues, including a description of their properties without the necessity of using invasive investigation methods. Good results of investigations in this field can change essentially the previous significance and value of ultrasonic diagnostic methods for medicine, by permitting identification of pathological tissues discovered. However, this problem is very complex. Absorption, scattering, velocity of ultrasound, acoustic im-

pedance, its spatial distributions and frequency dependence, all affect in a variety of ways the propagation of ultrasound. As a result, the information obtained by means of ultrasonic waves "in vivo" is very complex and difficult for unambiguous interpretation.

The introduction of the grey scale into ultrasonic visualization methods was the basic condition for investigations to be initiated in the range of tissue characterization. The first ultrasonograms (ultrasonic images), obtained directly on the screens of standard oscilloscope tubes, gave highly contrasted images which showed in effect only the outline of tissue boundaries. However, soft tissues show a complex internal structure, with a large number of blood vessels with different size. Small structures, such as muscle fibres (with diameter 10-150 μm and length 1-20 mm) or small blood vessels (arterioles and capillaries with diameter 8-200 μm and length 0.1-0.2 mm) cause scattered images of ultrasonic waves [4], since their dimensions are comparable to or smaller than the wavelength.

Improvements in ultrasonic technique, such as dynamic focusing with simultaneous control of the aperture of the piezoelectric transducer, permitted high resolution to be achieved over the entire length of the ultrasonic beam and, thus, images of the internal structure of tissues to be obtained. Microprocessor-controlled digital memory, permitting storing of hundreds of thousands of data obtained ultrasonically, brought the new possibilities of using a variety of electronic signal processing techniques for the purposes of reconstruction and improvement of ultrasonic images, for seeking and calculating essential quantitative data, for determination of grey level histograms in the images of structures being identified etc. All these techniques created completely new possibilities for ultrasonic tissue characterization.

The signals obtained from the interior of tissue structures have the nature of scattered reflections propagating in all directions; their intensity decreases rapidly as the distance increases, and it increases as frequency increases.

Much more energy is carried by the echoes caused by specular reflections from flat tissue boundaries. Maximum echoes can be stronger by as much as 100 dB than the weakest echoes scattered by the internal tissue structures. In order that all these echoes may be represented on the oscilloscope or kinescope tube screens (apart from their storing in digital memory), it is necessary to compress them over the range 20-40 dB, e.g. by using logarithmic amplifiers [5]. The electronic signal pre- and post-processing prior to and after storing in memory affects to a large extent the quality of images of tissue structures.

Ultrasonic images obtained in cardiology, even when using conventional equipment based on the echo principle, permit some conclusions to be drawn about the character of tissues [17]. E.g. blood is transparent for ultrasound, giving practically no reflection, when it is investigated using the echo method. When the Doppler method for investigation of the velocity of structures is

used, blood flows cause signals which sometimes superimpose on the Doppler signals from the moving heart tissues (e.g. valves). The character of these signals, however, is completely different and distinguishable.

It is easy to detect calcification of the heart tissues, since it involves changes in their elasticity and density, and therefore in their acoustic impedance, causing an increase in the amplitude of the echoes reflected. This can be seen distinctly in the case of calcified valves, for example.

3. Velocity, attenuation and absorption of ultrasound in soft tissues

In order to analyse systematically the possibilities of ultrasonic tissue characterization in cardiology, such basic acoustic quantities as the propagation velocity, absorption coefficient and scattering of ultrasonic waves will now be discussed.

Systematic data on the propagation velocity and attenuation of ultrasonic waves were recently collected from different literature sources [9, 10]. They contain more than 800 items on the propagation velocity and more than 1000 on the attenuation of ultrasonic waves in different mammalian tissues. However, only 16 concern the velocity in the animal heart. There are no data on the human heart. The data on attenuation are more ample: 51 on the animal heart and 2 on the human heart.

Analysis of propagation velocity in different mammalian tissues indicates that it increases as the protein content increases [2]. The lowest velocity is characteristic of fat tissue, on average 1460 m/s; the highest, of tendons with 1740 m/s. The velocity in the myocardial tissue is almost equal to the mean velocity of all soft tissues, i.e. about 1580 m/s.

Apart from velocity, most information concerns attenuation measurements in mammalian tissues, while absorption measurements were not paid much attention. It is necessary to distinguish clearly between those two phenomena. Attenuation is a decrease in the amplitude of the acoustic signal as a function of the distance covered by the wave. This quantity includes all losses. In turn absorption is a phenomenon in which the energy of the acoustic wave is locally transfered to the medium where it propagates, followed subsequently by conversion of acoustic energy into heat. Attenuation is therefore a broader notion, including the phenomena of absorption, and also those of scattering, reflection, refraction and diffraction.

Attenuation in muscle tissue, collected from 65 literature items and represented as a function of frequency, shows a very large scatter of measured values. DUNN showed [2] that attenuation values arrange themselves along a straight line given by the equation

$$A = 0.140 f^{0.926}, \tag{1}$$

where A is attenuation [cm^{-1}] and f frequency [MHz]. The correlation coefficient is $R = 0.748$.

It was shown recently [8] that values of the attenuation coefficient in tissue depend to a large extent on the measurement technique used. As a result of heterogeneity of tissues the ultrasonic wave undergoes phase shifts on its path. These cause partial cancelling of the signal in the piezoelectric receiver transducer. Because of this, attenuation measurements taken by means of piezoelectric transducers give apparently higher values than those transducers which are insensitive to cancellation, such as acoustoelectric transducers [1]. It is possible to obtain a threefold difference in attenuation values, depending on the measurement method used [8]. In addition, the measured results are also affected by other factors, such as temperature, sample preparation etc. This is confirmed by the example in Fig. 1 which shows the coefficients of

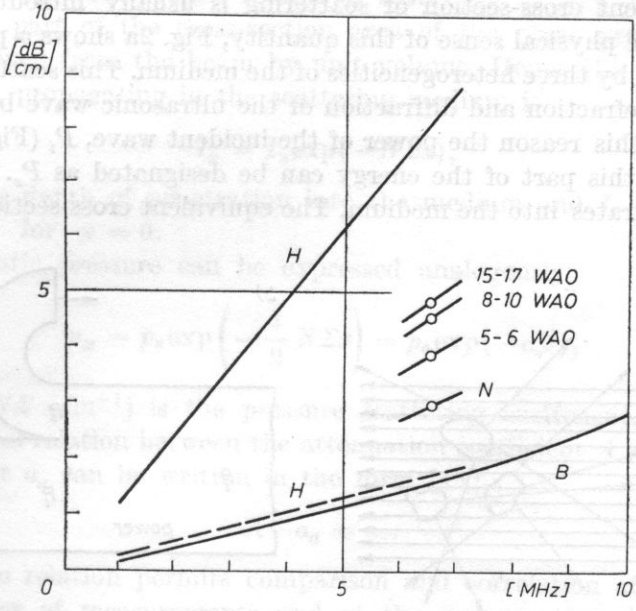

Fig. 1. The coefficients of attenuation (solid line) and absorption (dashed line) of the heart *H*, according to Goss *et al.* [8], and of blood *B*. Points mark attenuation in normal *N* and ischemic *WAO* regions of dog's hearts. In the latter case the period (from 5 to 17 weeks) following the closure of coronary circulation, acc. to O'Donnoll *et al.* [13], is given

attenuation and absorption of the heart *H* and attenuation of blood *B* as a function of frequency. These data were collected from literature and based on measurements taken mostly by means of piezoelectric receiving transducers [8-10]. Absorption was determined using the transient thermoelectric method at a temperature of 37°C [8]. In turn, the point *N* represents the attenuation coefficient obtained in the myocardium of normal dogs by means of an acoustoelectric receiving transducer [13] which eliminates the cancellation of signals with different phases on the surface of the transducer.

It can be concluded therefore that the piezoelectric technique used in conventional ultrasonic diagnostic devices cannot provide sufficiently accurate information about attenuation in soft tissues under investigation.

4. Scattering of ultrasonic waves

In contrast to the measurements of propagation velocity and attenuation, the investigations related to backscattering of ultrasound in the myocardium seem interesting and promising. These investigations were recently published by O'DONNOLL *et al.* [13].

In order to describe quantitatively the phenomenon of scattering, the notion of the equivalent cross-section of scattering is usually introduced. In order to illustrate the physical sense of this quantity, Fig. 2a shows a plane ultrasonic wave scattered by three heterogeneities of the medium. This scattering is a result of reflection, refraction and diffraction of the ultrasonic wave by these heterogeneities. For this reason the power of the incident wave, P_i (Fig. 2b), is partly scattered and this part of the energy can be designated as P_s. The remaining power P_t penetrates into the medium. The equivalent cross-section of scattering

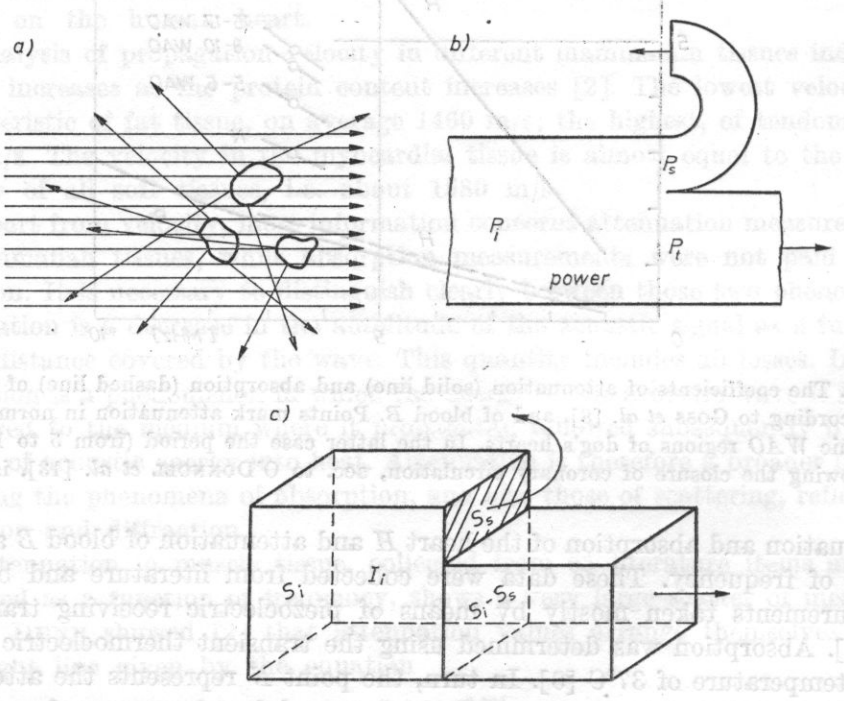

Fig. 2. Scattering of ultrasonic waves by heterogeneities in the medium (a). The division of the power P_i of the incident ultrasonic wave into the power P_s of the scattered wave and the power P_t of the wave penetrating into the medium (b). Geometrical interpretation (c)

is defined as the ratio

$$\Sigma = P_s/I_i, \tag{2}$$

where I_i is the intensity of the plane wave incident on the scattering object.

Since the scattered power $P_s = I_s S_s$,

$$\Sigma = P_s/I_i = I_i S_s/I_i = S_s \quad [\mathrm{m}^2]. \tag{3}$$

Formula (3) permits a simple, direct interpretation of the equivalent cross-section of scattering ($\Sigma = S_s$) as part of the area (S_i) of the cross-section of the plane incident wave which is removed from the beam by the scattering object (Fig. 2c).

When in a unit volume of the medium there are N (m^{-3}) scattering objects, each with the equivalent cross-section of scattering Σ (m^2), the product $N\Sigma$ (m^{-1}) is then part of the cross-section area of the plane propagating wave, which is removed from the beam by unit volume. Hence the intensity of the plane wave I_x propagating in the scattering medium is

$$I_x = I_0 \exp(-N\Sigma x), \tag{4}$$

where x is the depth of penetration into the medium and I_0 is the intensity of the wave for $x = 0$.

The acoustic pressure can be expressed analogously

$$p_x = p_0 \exp\left(-\frac{1}{2} N\Sigma x\right) = p_0 \exp(-\alpha_s x), \tag{5}$$

where $\alpha_s = \frac{1}{2} N\Sigma$ [cm^{-1}] is the pressure scattering coefficient.

The general relation between the attenuation coefficient A and the absorption coefficient α_a can be written in the form [14]

$$A - \alpha_a = \alpha_s. \tag{6}$$

The above relation permits comparison and correlation of the results of a large number of measurements and of the investigations of attenuation, absorption and scattering, which were usually obtained by different techniques. This may permit some general conclusions to be drawn about the structure and acoustic properties of soft tissues [8, 14]. In general case the phenomenon of scattering is not isotropic but depends on the direction. Therefore the differential form of the scattering coefficient per unit volume, referred to the spatial angle, is introduced. It has the shape

$$\eta = \frac{dN\Sigma}{d\Omega} = 2\frac{d\alpha_s}{d\Omega}. \tag{7}$$

The quantity η is called the differential scattering coefficient. In view of the measurement technique used, the backscattering coefficient $\eta_{180°}$ is significant. It involves the measurement of the magnitude of the wave scattered,

using the same transducer which transmits and receives at the same time [15] (see Fig. 3). However, in this case the scattering coefficient a_s cannot be determined, since the angular relation $\eta = \eta(\theta, \Phi)$ is not known. In general case, according to expression (7),

$$a_s = \frac{1}{2}\int_{\Omega} \eta(\theta, \Phi) d\Omega = \frac{1}{2}\int_0^{\Pi} \sin\theta d\theta \int_0^{2\Pi} \eta(\theta, \Phi) d\Phi, \tag{8}$$

where θ and Φ are plane angles (Fig. 3).

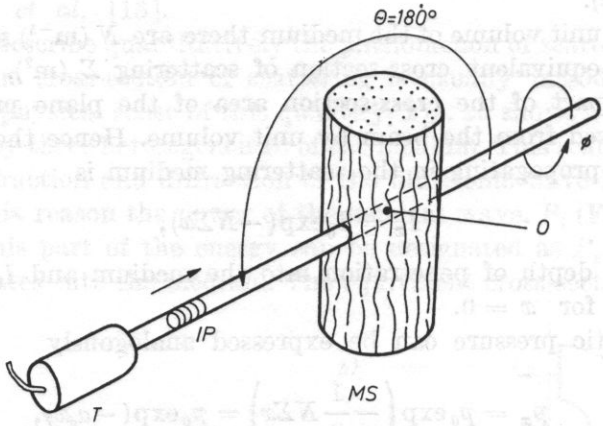

Fig. 3. The measurement of the backscattering coefficient

T – the piezoelectric transmit-receive transducer, *IP* – the pulse of the incident ultrasonic wave, *MS* – the biological sample measured; θ, Φ – plane angles

In the case of scattering objects which are very small compared to the wavelength isotropic scattering can be assumed in approximation; thus formula (8) gives directly the relation

$$a_s = 2\pi\eta_{180°} \quad [\mathrm{cm}^{-1}]. \tag{9}$$

O'DONNOLL *et al.* determined the relation between the backscattering coefficient $\eta_{180°}$ and collagen concentration in the hearts of normal dogs and those with ischemia of the myocardium caused by occulsion of the coronary vessels [13]. The aim of these investigations was to explain the mechanism of scattering of ultrasonic waves by the myocardium. The authors took "in vitro" measurements in the myocardium tissues obtained from 17 dogs subject to three different periods of ischemia of this muscle. Ischemia was caused by occlusion of the left anterior descending coronary artery. After 5, 8 or 16 weeks following the coronary occlusion the animals were killed.

The total number of ischemic regions was 18; the same number of normal regions in six hearts were examined after 5-6 weeks after the coronary occlusion. A related number of myocardial regions were examined after 8-10 and

15-17 weeks from the coronary occlusion. Fig. 4 shows the results of ten averaged measurements of each sample as a function of frequency. The change in the value of the backscattering coefficient is striking. For a frequency of 3 MHz this coefficient is greater by a factor of about 50 than in the normal myocardium.

In turn, attenuation measurements on the same samples, taken using an acoustoelectric receiving transducer, in the case of ischemia, only slightly differed from one another; it is shown in Fig. 1 by means of three points designated by the abbreviation *WAO*.

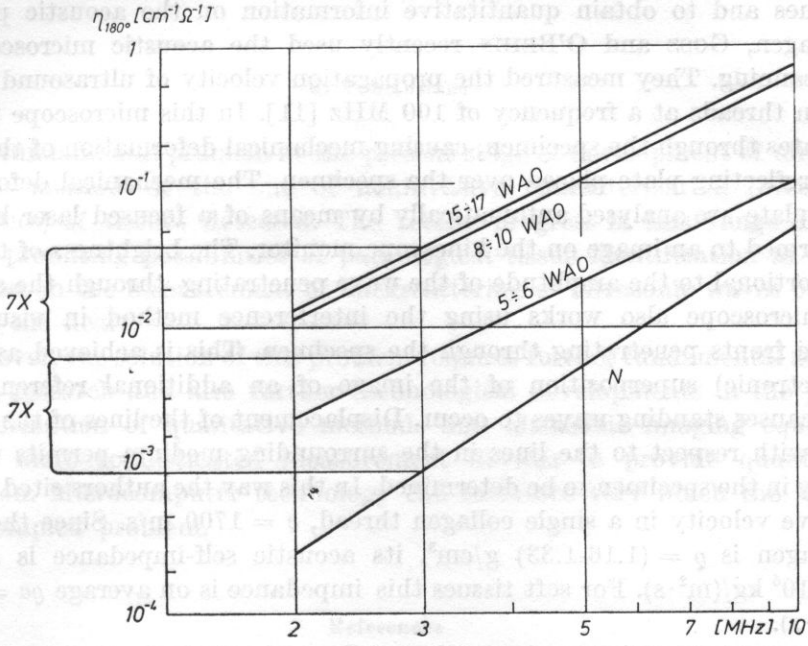

Fig. 4. The backscattering coefficient measured by O'Donnoll *et al.* as a function of frequency [13]: *N* — normal dog's myocardium, *WAO* — ischemic areas of dog's myocardium 5-17 weeks after closure of the coronary artery

In addition to changes in the backscattering coefficient, collagen concentration was estimated by a quantitative biochemical assay for hydroxyproline. The mean concentration of hydroxyproline, which is a quantitative index of the molecular content of collagen, increased ten times as much in the ischemic regions [13].

5. Discussion

The fibres of the normal myocardium are the essential object scattering ultrasonic waves over the range of a few MHz. The myocardial infarct is a dynamic process in the course of which the necrotic muscle fibres are replaced by connective tissue. It was suggested previously by Fields and Dunn [3]

that the elastic properties of connective tissue cause this tissue to be predominantly visualized in ultrasonograms. The greatest collagen concentration occurs in connective tissue. Collagen constitutes about 30 % of the total albumin amount in the system. Its composition included glycine (over 24 %), hydroxyproline (about 13 %) and a dozen or so of other amino acids in smaller proportion.

The normal myocardium show little collagen content, while the scarred myocardium contains much of it.

In order to verify the role of collagen in ultrasonographic visualization of tissues and to obtain quantitative information on the acoustic properties of collagen, Goss and O'Brien recently used the acoustic microscope with laser scanning. They measured the propagation velocity of ultrasound in single collagen threads at a frequency of 100 MHz [11]. In this microscope the wave penetrates through the specimen, causing mechanical deformation of the surface of the reflecting plate placed over the specimen. The mechanical deformations of the plate are analysed automatically by means of a focused laser beam and transformed to an image on the kinescope monitor. The brightness of the image is proportional to the amplitude of the wave penetrating through the specimen. This microscope also works using the interference method in visualization of wave fronts penetrating through the specimen. This is achieved as a result of (electronic) superposition of the image of an additional reference wave, which causes standing waves to occur. Displacement of the lines of the standing waves with respect to the lines in the surrounding medium permits the wave velocity in the specimen to be determined. In this way the authors cited obtained the wave velocity in a single collagen thread, $c = 1700$ m/s. Since the density of collagen is $\varrho = (1.16\text{-}1.33)$ g/cm^3, its accustic self-impedance is about $\varrho c = 2.1 \cdot 10^6$ kg/(m$^2 \cdot$s). For soft tissues this impedance is on average $\varrho c = 1.6 \cdot 10^6$ kg/(m$^2 \cdot$s).

These results indicate clearly that collagen is particularly strongly distinguishable in ultrasonographic images in contrast to other tissues. In view of these results it becomes clear why collagen concentration occurring in the myocardium with post-infarctional scars causes such a large increase in the backscattering coefficient.

It is interesting to note here the large potential possibilities of ultrasonic microscopy, creating a new field of biophysical investigations — sonohistology.

In cardiological terms again, it can be stated that it seems possible to distinguish between the regions of normal tissue and those pathological, on the basis of measurement of backscattering of ultrasound.

The first attempts at such a solution were published at the Sixth International Symposium on Ultrasonic Imaging and Tissue Characterization at Gaithersburg (USA) in June 1981 by Skorton *et al.* [16]. These authors investigated backscattering of ultrasound, making two dimensional ultrasonograms of hearts in awake dogs with operated (closed) chests, following circumflex coro-

nary occlusion. For the imaging of the heart they used a phase-array real-time equipment working at a frequency of 2.25 MHz. By means of an automatic digital system they determined the grey level distribution on the negatives of pictures taken of two heart regions; the interventricular septum (control region) and the posterior wall of the left ventricle (infarcted area). Grey level histograms were taken before and two days after the coronary occlusion.

The results of these preliminary investigations suggest that an acute infarct of the heart can be diagnosed from analysis of grey level distributions, comparing the regions examined with the control region separated by the ventrical cavity.

6. Conclusions

The fundamental problem at the present stage of development of ultrasonic diagnostic methods is the one of noninvasive characterization (description of properties) of tissues detected. The recent progress in this range provides the very promising possibilities of pathological tissue identification in cardiology, based on the measurement of backscattering of ultrasonic waves penetrating into the heart.

However, the solution of this problem requires further fundamental acousto-biological research and also further technological developments in the process of transformation of qualitative methods and ultrasonic imaging equipment into still more sophisticated measurement devices to provide quantitative information. Microcomputer technology can facilitate very much the solution of this complex problem.

References

[1] L. Busse *et al.*, *Phase cancellation effects*, Ultrasound in Medicine (D. White, R. Brown, eds.), Plenum Press, New York 1977, **3B**, pp. 1519-1535.

[2] F. Dunn, *Ultrasonic characterization of tissues: aspects of physical bases*, Proc. Symposium UBIOMED V, Pushchino 1981, pp. 122-123.

[3] S. Fields, F. Dunn, *Correlation of echographic visualizability of tissues with biological composition and physiological state*, J. Acoust. Soc. Am., **54**, 809-812 (1973).

[4] L. Filipczyński, *Detectability of blood vessels and flat boundaries of soft tissues in the ultrasonic pulse method*, Archives of Acoustics, Warsaw, **6**, 45-55 (1981).

[5] L. Filipczyński *et al.*, *UG-4 ultrasonograph for visualization of the organs of the abdominal cavity and its clinical application* (in Polish), Archiwum Akustyki, **10**, 111-120 (1975).

[6] L. Filipczyński, R. Herczyński, A. Nowicki, T. Powałowski, *Blood flows — hemodynamics and ultrasonic Doppler measurement methods* (in Polish), PWN, Warsaw 1980.

[7] L. Filipczyński, I. Roszkowski (eds.), *Ultrasonic diagnostics in gynaecology and obstetrics* (in Polish), PZWL, Warsaw 1977.

[8] S. Goss, L. Frizell, F. Dunn, *Ultrasonic absorption and attenuation in mammalian tissues*, Ultrasound in Med. Biol., **5**, 181-186 (1979).

[9] S. Goss, R. Johnston, F. Dunn, *Comprehensive compilation of empirical ultrasonic properties of mammalian tissue*, J. Acoust. Soc. Am., **64** (2), 423-457 (1978).

[10] S. Goss, R. Johnston, F. Dunn, *Compilation of empirical ultrasonic properties of mammalian tissues*, II, J. Acoust. Soc. Am., **68/1**, 93-108 (1980).

[11] S. Goss, W. O'Brien, *Direct ultrasonic velocity measurements of mammalian collagen threads*, J. Acoust. Soc. Am., **65/2**, 507-511 (1979).

[12] P. Morse, K. Ingard, *Theoretical acoustics*, McGraw Hill, New York 1968.

[13] M. O'Donnoll, J. Nimbs, J. Miller, *Relationship between collagen and ultrasonic backscatter in myocardial tissue*, J. Acoust. Soc. Am., **69/2**, 580-588 (1981).

[14] J. Pohlhammer, W. O'Brien, *Dependence of the ultrasonic scatter coefficient on collagen concentration in mammalian tissues*, J. Acoust. Soc. Am., **69/1**, 283-285 (1981).

[15] J. Reid, *The scattering of ultrasound by tissues*, Proc. Seminar Ultrasound Tissue Characterization, Gaithersburg 1975, pp. 29-47.

[16] B. Skorton *et al.*, *Estimation of regional ultrasonic backscatter from acutely infarcted myocardium in closed-chest dogs: feasibility and problems*, Sixth Intern. Symposium Ultrasonic Imaging and Tissue Characterization, Gaithersburg, Maryland, 1981. Abstracts, 190-191.

[17] P. Wells, *Present status of tissue identification*, Proc. 4th Symposium on Echocardiology, Martinus Nijhoff Publishers, Hague 1981, pp. 455-460.

Received on November 27, 1981; revised version on May 21, 1982.

C H R O N I C L E

VIII CONFERENCE ON THE UTILIZATION OF ULTRASONIC METHODS FOR STUDYING THE PROPERTIES OF CONDENSED MATTER

Žilina (Czechoslovakia) 1-4 September, 1982

VIII Conference on the Utilization of Ultrasonic Methods for Studying the Properties of Condensed Matter was held on 1-4 September, 1982 at Žilina (Czechoslovakia). The Conference was sponsored by the Physics Section of the Slovak Mathematicians and Physicists Association, the Acoustic Committe (Ultrasonics Subcommission) of the Czechoslovak Academy of Sciences, and organized by the Physics Department of the Technical University of Advanced Transport Engineering at Žilina, and Physics Institute of the Slovak Academy of Sciences in Bratislava. Assistant Prof. Dr. J. DURČEK was the chairman of the Organizing Committee of the Conference.

Four general lectures were delivered:

A. ZAREMBOVITVCH, *Ultrasonic investigation of molecular crystals.*

I. TUREK, I. BAJÁK, *Echo phenomena in piezoelectric powders.*

V. W. RAMPTON, *The use of high frequency phonons in studying solids.*

D. CHIPLYS, *Acoustoelectric phenomena in piezoelectric semiconductors.*

The following communications were delivered:

E. SOCZKIEWICZ, *Application of the method of quantum field theory to investigation of acoustic waves propagation in random media.*

V. HUDAIBERDYEV, *Investigation of particularities found in intermolecular interaction for glycerin solutions with ordinary and heavy water through acoustic methods.*

P. HEGEDUS, S. KOLNÍK, C. MUSIL, I. VARGA, *Determination of TOEC for NaCl and KCl by using ultrasound.*

I. BAJÁK, I. TUREK, J. VANČO, *Two pulse echo in powdered TGS in the vicinity of phase transition.*

U. STRAUBE, G. SORGE, *Investigation of properties of incommensurate $(NH_4)_2BeF_4$ by ultrasonic methods.*

MARTIN, FRANKE, WEIHNACHT, *MSC effects in apodized transducers.*

J. LISOVSKY, *Elastic properties and phase instability of doped V_2O_3.*

K. MÍŠEK, *Ultrasonic study of Nb in magnetic fields.*

J. DOMINEC, *Attenuation of ultrasound in BiSb alloys.*

J. ČÁP, S. KOLNÍK, *Polarization effects in a layer system with elastic anisotropy.*

V. GOLENISHCHEV-KUTUSOV, *Nonlinear propagation of acoustic waves in antiferromagnetics.*

M. BOUDYŠ, *Properties of elastic moduli of PZT Ceramics.*

V. ADAMAITIS, *Acoustoelectrical interaction in inhomogeneous semiconductors.*

J. BRACINÍK, J. ŠTELINA, *Quantitative study of the electric field distribution in stationary acoustoelectric domains.*

A. DAMARKAS, A. M. DIAKONOV, I. L. DRICHKO, D. KHIPLYS, *Acoustoelectric instability and acoustoelectrical interaction in indium antimonide.*

E. GARSKA, *Acoustic modulation of recombination centers.*

S. I. BEREZINA, *Measurement of acoustic wave velocity in solids by acoustical microscope.*

V. A. KRASILNIKOV, V. I. PAVLOV, J. SLABEYCIUS, *Application of Hamilton's methods in problems of interaction and radiation of waves in acoustics.*

M. KOŠEK, *Surface acoustic wave strip transducer.*

H. J. FRÖHLICH, H. J. ROHDE, *Surface acoustic wave properties of thin film CdS prepared by hot-wall technology.*

H. HOFMANN, *Signal processing by correlation with chirp and mis-matched surface acoustic waves devices.*

K. ČÁPOVÁ, *Phase sensitive optical probing of surface acoustic waves.*

M. NEVESELÝ, *Some methods for compensation of diffraction in SAW filters.*

These papers will be published in Acta Physica Slovaca.

Eugeniusz Soczkiewicz (Gliwice)

SUMMER WORKSHOP ON PSYCHOACOUSTICS OF MUSIC

Jabłonna 5-11 July, 1982

Within the series of yearly international conferences organized by the Committee on Acoustics of the Polish Academy of Sciences, the Summer Workshop on Psychoacoustics of Music took place in Jabłonna. The conference was organized by the Committee on Acoustics jointly with Frederick Chopin Academy of Music in Warsaw. There were 60 participants; among them 32 came from abroad: from Austria, West Berlin, Czechoslovakia, Holland, Canada, GDR, West Germany, Sweden, USA, Italy and Hungary — 23 lectures and reports were presented, with much time devoted to discussions. The conference language was English.

The following topics were discussed at separate sessions:

I. *Assessment of pitch*, II. *Absolute pitch*, III. *Relative pitch*, IV. *Psychoacoustic dissonance*, V. *Assessment of sound quality in musical instruments*, VI. *Assessment of concert hall acoustics.*

The lectures and reports were presented, among others, by the following foreign visitors: Dr. Judit ANGSTER (Academy of Sciences, Budapest, Hungary), Professor Dr. Frans BILSEN (Technical University, Delft, Holland), Professor Dr. Gert van den BRINK (Erasmus Universiteit, Rotterdam, Holland), Dr. Werner A. DEUTSCH (Österreichische Akademie von Wissenschaften, Wien, Austria), Professor Dr. Jurgen MEYER (Techn. Bundesanstalt, Braunschweig, West Germany), Professor Dr. Reinier PLOMP (Institute for Perception TNO, Soesterberg, Holland), Charles RAE (College of Music, Leeds, Great Britain), Dr. Peter SCHUBERT (Institut für Musikinstrumentenbau, Zwota, Vogtl, GDR), Professor Dr. Johan SUNDBERG (Royal Institute of Technology, KTH, Stockholm, Sweden), Professor Dr. Ing. Ernst TERHARDT (Institut für Elektroakustic, Technische Hochschule, München, FRG).

The Polish lecturers were the following:

Professor Dr. Gustaw BUDZYŃSKI (Technical University, Academy of Music, Gdańsk), Professor Dr. Andrzej RAKOWSKI (Laboratory of Musical Acoustics, Frederic Chopin of Music, Warsaw), Professor Dr. Stefan CZARNECKI (Institute of Fundamental Technological Research, Polish Academy of Sciences, Warsaw).

The scientific supervisor of the „Summer Workshop on Psychoacoustics of Music Jabłonna 82" was Professor Andrzej RAKOWSKI.